STRUCTURE, PROPERTIES, AND DYNAMICS OF NANOPARTICLE-TETHERED POLYMERS

A Dissertation

Presented to the Faculty of the Graduate School

of Cornell University

In Partial Fulfillment of the Requirements for the Degree of

Doctor of Philosophy

by

Sung A Kim

May 2015

STRUCTURE, PROPERTIES, AND DYNAMICS OF NANOPARTICLE-TETHERED POLYMERS

Sung A Kim, Ph. D.

Cornell University 2015

Understanding how polymer − nanoparticle interactions influences structure, dynamics, and properties of composites is of fundamental importance for both the science and technology applications of organic − inorganic hybrid materials. Great attention has been given to changes organic polymer species undergo in forming polymer nanoparticle composites. This thesis focuses on a specific type of hybrid systems created by densely grafting polymer chains onto inorganic nanoparticles to form self-suspended nanoparticle suspensions in which every polymer chain is both anchored to and confined between the surfaces of neighboring particles.

We have studied the hierarchical structure and relaxation dynamics of polymer chains in these self-suspended nanoparticle suspensions. We have investigated the conformations and thermo-physical properties of self-suspended suspensions based on polyethylene glycol (PEG) chains tethered to silica nanoparticles. It is found that the structure and crystallization of confined PEG could be very different depending on the length scale on which the structure is observed. Below the size of one hybrid unit,

particle-tethered PEG chains form more stable conformations, whereas tethered PEG is more amorphous than free chains on length scales above one hybrid unit.

We also report how tethering, crowding, and confinement by nanoparticles change the viscoelastic and dielectric relaxation dynamics of nanoparticle-tethered polymer chains. In this study, diverse molecular weights of *cis*-1,4-Polyisoprene (PI), a type A dielectric polymer, is synthesized in the spectrum from unentangled to well-entangled regime with amine end group functionality. By tethering this polymer to nanoparticles at varying grafting densities it is possible to study dynamics of polymer chains under confinement using bulk measurements. Global chain relaxation is conveniently explored since the net dipole moment of an entire chain of *cis*-1,4-PI is parallel to the end-to-end vector of the tethered molecules. We have found that tethered PI chains exhibit slower relaxation dynamics and are stretched compared to free polymers. We have studied that nanoparticles could impose topological constraints to the tubes of tethered chains when short molecular weight chains are sparsely tethered. In addition, jamming of soft glasses with increasing temperature and decreasing grafting density have been observed from dielectric spectroscopy and rheology experiments.

BIOGRAPHICAL SKETCH

Sung A Kim was born in Seoul, Korea. Shortly after her birth, her family moved to Philadelphia where she lived for 5 years while her parents were studying as graduate students at the University of Pennsylvania. Then, she grew up in Seoul with her parents and younger brother. She attended Korea University from 2004 to 2008 to pursue the Bachelor of Science in chemical and biological engineering. As an undergraduate student, she was interested in the field of polymer science. In 2008, she came to Cornell University for her Ph.D. studies in Chemical and Bimolecular Engineering to do research on structure and dynamics of polymer nanoparticle hybrid materials.

Dedicated to my parents for their unconditional love and endless support

ACKNOWLEDGMENTS

I sincerely appreciate my Ph.D. advisor, Prof. Lynden A. Archer. All of my Ph.D. works were possible because of his support and invaluable guidance. His passion for polymer science has always been inspiring me and I am truly grateful for his hands-on training and dedicated teaching.

I would like to thank my committee members, Prof. Yong L. Joo and Prof. Ulrich Wiesner, for their advice and suggestions.

I am thankful for the interactions with entire Archer group members.

I am grateful for the help from CCMR and KAUST-CU Center, including Anthony Condo, Dr. Ivan Keresztes, Dr. David Jung, Brenda Fisher, and Celia Szczepura.

I would like to thank my funding agencies, KAUST and NSF, and also the support from CCMR.

I also want to thank Shelby Clark-Shevalier, Olivia C. Cully, and Breana Nicole for their administrative help within the department.

Finally, thank you my dear friends who made my life at Cornell wonderful and joyful.

TABLE OF CONTENTS

LIST OF FIGURES

LIST OF TABLES

CHAPTER 1

INTRODUCTION[‡]

[‡] Akanksha Agrawal provided the TEM image.

1.1. POLYMER NANOCOMPOSITES

For a long time, researchers have been attracted to polymer nanocomposite materials. Diverse architectures of polymer nanocomposites are achieved by mixing polymers and particles, tethering particles to polymers, embedding particles in a polymer matrix, depositing polymers on particles and vice versa, and other approaches shown in Figure 1.1.[1] These polymer nanocomposites are attractive for practical applications such as sensors, patterning, 3D structures, photonic materials, catalysts, coatings, and so on (Figure 1.2).[2-12]

Substantial efforts have been devoted to characterizing the polymer component in polymer nanocomposite materials and to understanding how polymers change under different types of confinement. One of the confinement methods widely adopted is locating polymer chains in 2D nanolayer structures. Hiltner's group[13] reported the crystal structure of poly(ethylene glycol) (PEG) confined by the layers of poly(ethylene-*co*-acrylic acid) (EAA). Alternating layers of PEG and EAA, where PEG layer was sandwiched by EAA layers, were fabricated by layer-multiplying coextrusion method. It is known that gas molecules diffuse though amorphous phases of polymers that have higher free volume compared to the crystalline phases. It was found that the permeability of oxygen decreases as the thickness of the PEG layer reduces. It was explained that as the PEG layer becomes thinner, PEG chains are more aligned to form well stacked single crystal lamellae, compared to 3D spherulites when they are in an unconfined condition.

Mixing polymer with 2D nanolayers structures leads to different configuration of polymer chains depending on the chain concentration and the method of mixing, such as phase separated microcomposites, intercalated nanocomposites, and exfoliated nanocomposites.[14] Mijovic et al.[15] investigated the dielectric relaxation dynamics of polyisoprene (PI), a type A dielectric polymer, in 2D silicate nanolayers. They found that adding nanoclay layers to PI M_w 3,000 didn't change the relaxation dynamics of the polymer because PI M_w 3,000 was not confined at their experimental conditions where the interlayer spacing was comparable to the radius of gyration (Rg) of low M_w polymer chains. On the other hand, normal mode relaxation process became faster with increasing clay loading for PI M_w 30,000. High molecular weight PI was crammed into the interspace between clay layers which was much smaller than Rg of high M_w PI, resulting in the increased end to end distance of the chains with the addition of silicates.

Another way to confine the polymer chains is by squeezing them into 3D nanopores. Shin's group[16] studied the crystallization of polyethylene (PE) by selectively locating PE chains into uniform sized cylindrical aluminum nanopores. It was observed that the crystallinity of PE was an increasing function of nanopore diameter, implying more confined crystallization within smaller nanopores. A study on relaxation dynamics of poly(propylene glycol) (PPG) was performed by Schonhals et al.[17] by confining PPG chains into 3D glass nanopores. It was found that as the nanopore size decreased the relaxation was slower. At elevated temperature, relaxation of PPG was faster due to desorption of PPG from the surface of glass nanopores.

By studying the microphase separated materials at temperatures below the glass transition temperature of the amorphous block, confined crystallization of the semi-crystalline polymer or restricted relaxation dynamics of the other mobile block can be investigated under conditions that mimic those encountered near/between the surfaces of immobile inorganic nanoparticles. Loo et al.[18] previously reported on crystallization of polyethylene chains in polystyrene-polyethylene (PS-*b*-PE) diblock copolymers. In their study, hexagonally packed PS microdomain was macroscopically oriented by flow in the continuous matrix of PE. The authors found that polyethylene chains did not make well-defined lamella near the PS domains, but rather became organized in preferential orientation away from the PE-PS interface. Alig et al.[19] examined the dielectric relaxation dynamics of polyisoprene (PI) in polyisoprene-polystyrene (PI-*b*-PS) diblock copolymers. PI contents were varied from 27.9 to 50.4 wt% while the molecular weight of PS blocks was fixed at M_w 2830. The segmental mode relaxation of PI in block copolymers was slower compared to the bulk PI homopolymer even though the temperature dependence from Vogel-Fulcher-Tamann (VFT) analysis was similar. Likewise, the normal mode relaxation times were increased in the copolymers, but the temperature dependence of normal mode from VFT fitting was different at each molecular weight content of PI subchain.

Recently, a novel method to confine the polymer chains three dimensionally in polymer nanocomposite materials was reported.[20,21] By densely grafting polymer chains to spherical inorganic nanoparticles, polymer chains are always tethered to and confined by nanoparticles without the concern of phase separation between polymer chains and inorganic nanoparticles. As the crystallization behaviors and relaxation

dynamics of chains depend on how polymer movement is restricted in the space, studies on the concurrent effects of tethering and nanoparticle confinement on polymer chains will provide a deeper insight into the nature of polymer nanocomposite materials.

1.2. SELF-SUSPENDED NANOPARTICLE FLUIDS

Among the diverse architectures of polymer nanocomposites, this thesis focuses on a very specific type of polymer nanocomposites, where polymer chains are densely tethered to spherical nanoparticles (Figure 1.3).[20,21] By avoiding mixing of the polymer and particle components, these materials can be thought of as ideal polymer nanocomposites: One hybrid unit of nanoparticle-tethered polymer chains is already a polymer nanocomposite. Each hairy particle is then a building block for the entire polymer nanocomposite material. In addition, because the material is formed from a very large number of tethered chains, it has similarities to the super macromolecules reported by Bates et al. [22,23] and Lodge's group[24].

Various properties of these materials could be easily tuned due to the degree of freedom in selection of nanoparticles and tethered chains. For example, inorganic nanoparticles could be silica, titania, iron oxide, gold and additionally telomers, ionic liquids, copolymers could be tethered to these nanoparticles. The materials are also attractive because they exhibit fluid-like properties in the absence of any extra solvent, and hence are termed as self-suspended nanoparticle suspensions. TEM (Transmission Electron Microscopy) image provided in Figure 1.3 clearly shows that the

nanoparticles are well dispersed in the system. Therefore this self-suspended nanoparticle suspension makes it possible to use ‘‘bulk,’’ high signal-to-noise measurements to probe the dynamics and properties in very small scale.

1.3. OUTLINE OF THIS DISSERTATION

This dissertation contains my work on structure, dynamics, and properties of nanoparticle-tethered polymer chains. The goal of my studies is to understand how tethering, crowding, and confinement, imposed by nanoparticles, restrain polymer chains, and consequently affect their crystallization and relaxation.

In Chapter 2, we report the hierarchical crystal structure of nanoparticle-tethered semicrystalline polymers. For these studies, poly(ethylene glycol) (PEG) was tethered to silica nanoparticles with different grafting densities, and then the static chain configuration and structures were characterized using NMR (Nuclear Magnetic Resonance), ATR FT-IR (Attenuated Total Reflectance Fourier Transform Infrared Spectroscopy), XRD (X-Ray Diffractometer), DSC (Differential Scanning Calorimetry), and rheology. It is found that solid-state structures of nanoparticle-tethered PEG could be very different depending on the observation length scale: In particular, we find that nanoparticle-tethered chains preferred to have more energetically stable TTG (*trans trans gauche*) conformation and 3D helix crystal unit cell structure at angstrom scale and nanoscale, respectively. Our results show that at the order of 10^{-8} m, tethered chains chose to form only one type of extended crystallite, which is different from untethered chains having three different types of crystallites

such as extended, once-folded, and twice-folded. On the contrary, it is observed that polymer chains became more amorphous at bulk scale. Additionally, we report that the bulk scale thermal transition was originated from structural change in the types of crystallites at the scale of 10^{-8} m.

In Chapter 3, we investigate how tethering, crowding, and confinement imposed by nanoparticles affect the viscoelastic and dielectric relaxation dynamics of polymers. In this study, diverse molecular weight of *cis*-1,4-polyisoprene (PI) chains were tethered to silica nanoparticles with various grafting densities. From measurements of the dipole relaxation, we are able to deduce unique information about the end-to-end vector relaxation of particle-tethered chains as a function of their molecular weight, grafting density, and temperature. These measurements are augmented by rheological characterization of the bulk dynamics of silica nanoparticle-tethered PI chains. We report that tethered PI chains behaved as soft glasses and showed jamming behaviors reinforced by increasing temperature and reducing crowding, or decreasing grafting density. Our dielectric spectroscopy results show that tethering polymer chains to nanoparticles produced dramatic slowing-down in their dynamics. It is found that chains were more stretched by tethering, lowering grafting density, and increasing temperature using dielectric spectroscopy. Interestingly, we find that lowering grafting density at low molecular weight chain could lead to extreme polymer chain stretching and tremendous slow-down in relaxation behaviors, and the relaxation was dominated by confinement imposed by nanoparticles to tethered chains. Additionally, our results show that the effect of tethering and crowding was larger for short molecular weight chains. At the scale of chain segments, dielectric spectroscopy was performed to

investigate segmental mode relaxation dynamics, complemented by glass transition temperature measurement using DSC. It is observed that segmental relaxation was slower and glass transition temperature increased after tethering.

Chapter 4 concludes this dissertation and lucidly explains the differences between Chapter 2 and Chapter 3.

REFERENCES

1. Stuart, M A. C.; Huck, W. T. S.; Genzer, J.; Muller, M.; Ober, C.; Stamm, M.; Sukhorukov, G. B.; Szlerifer, I.; Tsukruk, V. V.; Urban, M.; Winnik, F.; Zauscher, S.; Luzinov, I.; Minko, S. *Nat. Mater.* **2010**, *9*, 101-113.

2. Shenhar, R.; Norsten, T. B. *Adv. Mater.* **2005**, *17*, 657-669.

3. Shipway, A. N.; Katz, E.; Willner, I. *Chem. Phys. Chem.* **2000**, *1*, 18-52.

4. Gangopadhyay, R.; De, A. *Chem. Mater.* **2000**, *12*, 608-622.

5. Trindade, T.; O'Brien, P.; Pickett, N. L. *Chem. Mater.* **2001**, *13*, 3843-3858.

6. Bauer, F.; Sauerland, V.; Glasel, H-J.; Ernst, H.; Findeisen, M.; Hartmann, E.; Langguth, H.; Marquardt, B.; Mehnert, R. *Macromol. Mater. Eng.* **2002**, *287*, 546-552.

7. Soloukhin, V. A.; Posthumus, W.; Brokken-Zijp, J. C. M.; Loos, J.; de With, G. *Polymer* **2002**, *43*, 6169-6181.

8. Daniel, M-C.; Astruc, D. *Chem. Rev.* **2004**, *104*, 293-346.

9. Bauer, F.; Flyunt, R.; Czihal, K.; Buchmeiser, M. R.; Langguth, H.; Mehnert, R. *Macromol. Mater. Eng.* **2006**, *291*, 493-498.

10. Balazs, A. C.; Emrick, T.; Russell, T. P. *Science* **2006**, *314*, 1107-1110.

11. Su, Y-L. *Rect. Funct. Polym.* **2006**, *314*, 1107-1110.

12. Zou, H.; Wu, S.; Shen, J. *Chem. Rev.* **2008**, *108*, 3893-3957.

13. Wang, H.; Keum, J. K.; Hiltner, A.; Baer, E.; Freeman, B.; Rozanski, A.; Galeski, A. *Science* **2009**, *323*, 757-760.

14. Alexandre, M.; Dubois, P. *Mater. Sci. Eng.* **2000**, *28*, 1-63.

15. Mijovic, J.; Lee, H.; Kenny, J.; Mays, J. *Macromolecules* **2006**, *39*, 2172-2182.

16. Shin, K.; Woo, E.; Jeong, Y.; Kim, C.; Huh, J.; Kim, K. *Macromolecules* **2007**, *40*, 6617-6623.

17. Schonhals, A.; Stauga, R. *J. Chem. Phys.* **1998**, *108*, 5130-5136.

18. Loo, Y.-L.; Register, R. A.; Adamson, D. H. *Macromolecules* **2000**, *33*, 8366.

19. Alig, I.; Kremer, F.; Fytas, G.; Roovers, J. *Macromolecules* **1992**, *25*, 5277-5282.

20. Rodriguez, R.; Herrera, R.; Archer, L. A.; Giannelis, E. P. *Adv. Mater.* **2008**, *20,* 4353-4358.

21. Agarwal, P.; Qi, H.; Archer, L. A. *Nano Lett.* **2010**, *10*, 111-115.

22. Won, Y-Y.; Davis, H. T.; Bates, F. S. *Science* **1999**, *283*, 960-963.

23. Bates, F. S.; Hillmyer, M. A.; Lodge, T. P.; Bates, C. M.; Delaney, K. T.; Fredrickson, G. H. *Science* **2012**, *336*, 434-440.

24. Li, Z.; Kesselman, E.; Talmon, Y.; Hillmyer, M. A.; Lodge, T. P. *Science* **2004**, *306*, 98-101.

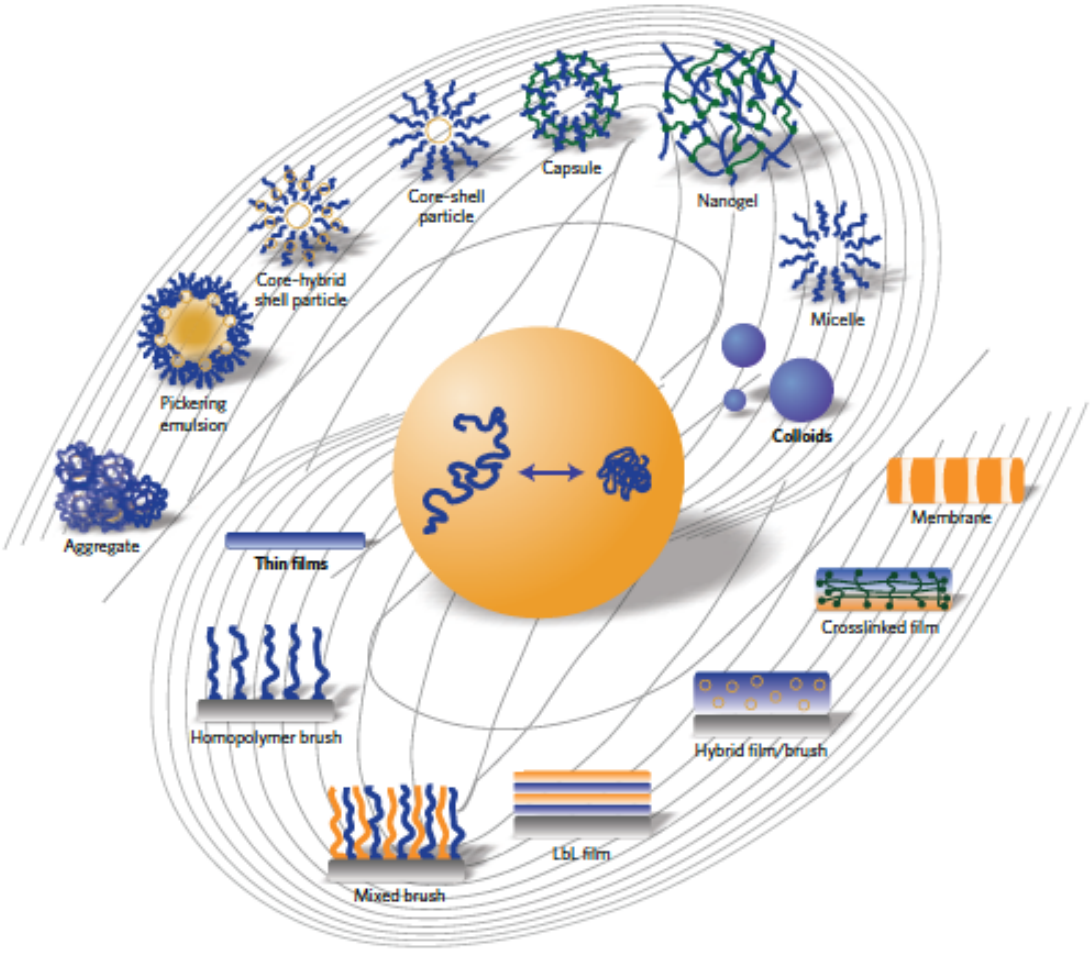

Figure 1.1. Diverse architecture of polymer nanocomposites.[1]

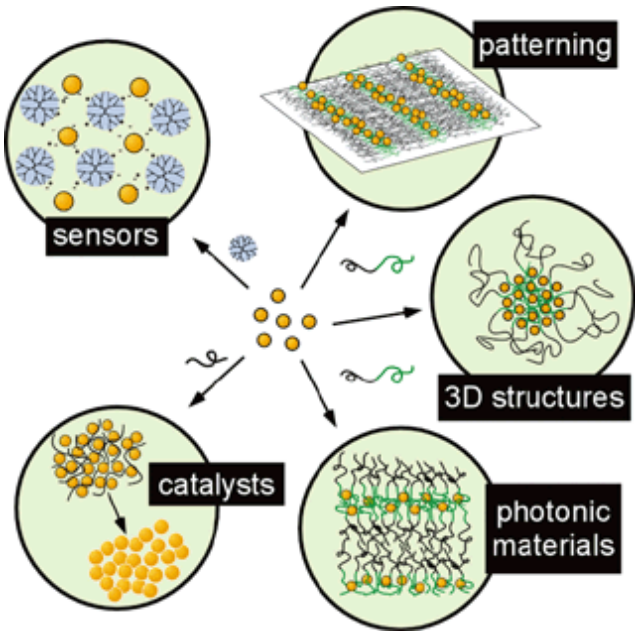

Figure 1.2. Application of polymer nanocomposites.[2]

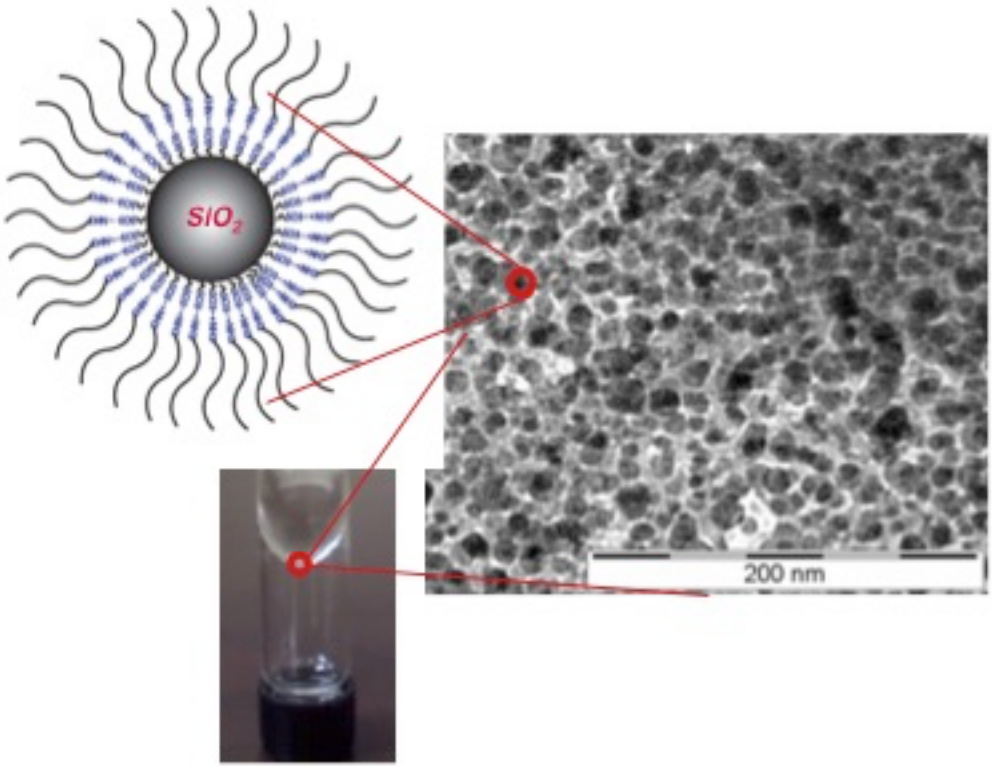

Figure 1.3. Polymer chains are densely tethered to spherical nanoparticles. [9]

CHAPTER 2

HIERARCHICAL STRUCTURE AND PROPERTIES OF NANOPARTICLE-TETHERED POLYMERS

Reprinted with permission from

Kim, S. and Archer, L. A. HIERARCHICAL STRUCTURE IN SEMICRYSTALLINE POLYMERS TETHERED TO NANOSPHERES. *MACROMOLECULES* **2014** *47*, 687-694.

ABSTRACT

We report on structural and dynamic transitions of polymers tethered to nanoparticles. In particular, we use X-ray diffraction, vibrational spectroscopy, and thermal measurements to investigate multiscale structure and dynamic transitions of poly(ethylene glycol) (PEG) chains densely grafted to SiO_2 nanoparticles. The approach used for synthesizing these hybrid particles leads to homogeneous SiO_2− PEG composites with polymer grafting densities as high as 1.5 chains/nm^2, which allows the hybrid materials to exist as self-suspended suspensions with distinct hierarchical structure and thermal properties. On angstrom and nanometer length scales, the tethered PEG chains exhibit more dominant TTG conformations and helix unit cell structure, in comparison to the untethered polymer. The nanoparticle-tethered PEG chains are also reported to form extended crystallites on tens of nanometers length scales and to exhibit more stable crystalline structure on small dimensions. On length scales comparable to the size of each hybrid SiO_2− PEG unit, the materials are amorphous presumably as a result of the difficulty fitting the nanoparticle anchors into the PEG crystal lattice. This structural change produces large effects on the thermal transitions of PEG molecules tethered to nanoparticles.

2.1. INTRODUCTION

Understanding how polymer-nanoparticle interactions influences phase behavior, structure, and properties of composites is of fundamental importance for

both the science and technology applications of organic-inorganic hybrid materials.[1] When two or more physically distinct components interact well-enough to constitute a hybrid material, at least one of the components must pass through various changes in properties to accommodate the other. Great attention has been paid to changes organic polymer species undergo in forming polymer nanoparticle composites, and the influence of well-dispersed and phase separated nanoparticles on transport and mechanical properties of polymers have been studied for a long time.[2-7] Polymer viscoelasticity, [5] diffusion,[6] global chain and segmental dynamics[7] have, for instance, all been extensively investigated by rheometry, polarimetry, and dielectric relaxation measurements. Significant efforts have also been devoted to characterizing how the melting transition,[8] crystallization,[9-11] glass transition behavior,[12-13] heat capacity,[14] degradability,[15] and ionic conductivity[16] of polymers are altered by surface adsorption to or confinement between nanoparticle surfaces.[17]

These efforts have lead to a growing knowledge set about the effects of nanoparticles on crystallization, structure, and properties of semi-crystalline polymers.[9-11] One of the most commonly adapted methods to study confined crystallization of polymers in such composites is in controlled phases, such as those formed between domains in micro-phase segregated block copolymers comprised of semi-crystalline and amorphous, glassy blocks.[18-22] By studying the microphase separated materials at temperatures below the glass transition temperature of the amorphous block, crystallization of the semi-crystalline polymer can be investigated under conditions that mimic those encountered near/between the surfaces of immobile inorganic nanoparticles. Polymers confined in thin films provide another commonly

used approach for studying how confinement effects alter chain structure and dynamics in a setting of tremendous practical importance.[23-26] Selectively locating polymer chains into nanopores with controlled surface chemistry[27-29] provides a final strategy for characterizing the effect of surface confinement on reorganization and conformational behavior of polymer chains. With the exception of approaches that take advantage of phase-separated domains in a bulk, block copolymer material to study surface and confinement behavior of polymers, all of the other approaches are challenged by the small population of the confined species and by the consequent low signal to noise associated with measurements of structural and dynamic properties of the molecules of interest.

Here we report a new approach for studying structural and dynamic transitions of confined polymers and use it to investigate the relationship between multiscale structure and thermal transitions of semi-crystalline polymer chains in nanocomposites. Specifically, by densely grafting polymer chains to inorganic nanoparticles, we create self-suspended suspensions of the particles in which every polymer chain is both anchored to and confined between the surface of neighboring particles.[30-32] A benefit of the approach is that bulk measurements reflect chain behavior under confinement in three dimensions, overcoming the poor signal to noise limitations of other approaches. Previously we showed that this approach could be employed to accurately characterize the surface relaxation behavior of *cis*-1,4-polyisoprene (PI), a type A dielectric polymer, with dipole moment parallel to its end-to-end vector.[32] Remarkably, these measurements revealed that even PI chains too-short to be considered entangled by conventional criteria, relax on the surface of

nanosized SiO_2 particles in a manner analogous to the arms of an ultra-high molecular weight, entangled polymer star. Prompted by these observations, we herein create SiO_2-polyethylene glycol (PEG) self-suspended suspensions taking advantage of the screened enthalpic interactions[33] with the particle surface to study chain conformation, reorganization, and crystallization in 3 dimensions,[34] or change their conformations.[35] We deliberately choose PEG as the semi-crystalline polymer species, because extensive studies of its conformational states have shown that, depending on the experimental conditions, PEG exhibits diverse conformations on length-scales ranging from angstroms to tens of nanometers.[36-44]

2.2. EXPERIMENTAL METHODS

2.2.1. Sample Preparation

Solution of 10nm diameter silica nanoparticles was purchased from Sigma-Aldrich. Polyethylene glycol M_W 5,000 g/mol and primary amine terminated Polyethylene glycol M_W 5,000 g/mol were purchased from Polymer Source and used as received. The synthesis method was reported elsewhere.[30,31] The final products were purified with repeated precipitation using Hexane and Methanol. Lastly, samples were dried at 65°C in convection oven overnight and in freeze dryer at least 2 days.

2.2.2. Nuclear Magnetic Resonance (NMR)

A solution of 7% (w/v) sample in water-d_2 (Cambridge Isotope Laboratories) was prepared in a standard 5mm NMR tubes. NMR spectra were collected on INOVA 600 MHz NMR operating at 599.50MHz for ^{1}H observation at 23°C. The chemical shifts were referenced to D_2O as internal standards. Self-diffusion coefficient of tethered PEG in D_2O was measured by pulse field gradient stimulated echo (PFG-SE) at 599.50MHz using INOVA 600 MHz spectrometer. DOSY Bipolar Gradient Pulse Pair double STimulated Echo (Dbppste) sequence was performed at 23°C with pulse width 6.9 ms and acquisition time of 0.6 s. The relationship between the attenuation of echo amplitude I and PFG parameters are given by the following equation;

$$\ln (I/I_o) = -Dg^2\gamma^2\delta^2\left(\Delta + \frac{4}{3}\delta + \frac{3}{2}\tau\right)$$

where D is self-diffusion coefficient, g is gradient strength in Tesla/m, γ is magnetogyric ratio, δ is gradient length (total duration of bipolar gradient pulse), Δ is diffusion delay, τ is gradient recovery delay, I_o is echo amplitude when g is zero.

2.2.3. Thermogravimetric Analysis (TGA)

The grafting densities were determined from the final weight percentage of TGA Q1000 (TA Instruments) scanning with 5°C/min from 20°C to 600°C under nitrogen atmosphere.

2.2.4. Attenuated Total Reflectance Fourier Transform Infrared Spectroscopy (ATR FT-IR)

The conformation states of PEG chains were characterized at 298K using Nicolet iS10 (Thermo Fisher Scientific) equipped with deuterated triglycine sulfate (DTGS) detector and SMART iTR diamond ATR accessory. Background was scanned with the resolution of 4 cm^{-1} for sample scan for background correction purpose. Each spectrum was fitted with numbers of Gaussian functions for intensity and width.

2.2.5. Differential Scanning Calorimetry (DSC)

Melting transition behaviors were studied using DSC Q2000 (TA Instruments). For melting temperature measurement and crystallinity calculation, samples were heated to 100°C for 10 min to erase previous thermal history, then cooled down to 0°C with 2°C /min, and finally heated up to 100°C with the rate of 2°C /min under nitrogen flow. The melting peaks of second heating cycle were recorded.

For crystallization kinetics study, samples were heated at 100°C for 10mins and cooled down with different cooling rates to 0°C (2, 5, 10, 15, 20, 30°C/min). Relative crystallinity was obtained as the function of crystallization time after the onset of crystallization at this cooling cycle.

2.2.6. Rheology

Intrinsic viscosity was characterized from self-suspended nanoparticles diluted in a low molecular weight polyethylene glycol dimethyl ether host at 65°C through

steady shear measurements using Rheometrics Scientific ARES rheometers outfitted with cone and plate fixture.

2.2.7. X-Ray Diffraction (XRD) Analysis

Crystal structures were investigated with Rigaku SmartLab X-rady Diffractometer with Anton Paar domed hot stage accessory. To compare with DSC experiment results, XRD operating sequences were mimicked the heat/cool/heat cycle of DSC measurements; samples were heated to and kept at 100°C for 10min, cooled with 2°C /min, and heated again with 2°C /min under inert gas. At the second heating cycle, samples were scanned from 1.5° to 30° with wavelength 1.54 Å.

2.3. RESULTS AND DISCUSSION

Nuclear magnetic resonance (NMR) measurements were performed on self-suspended SiO_2-PEG nanocomposites and untethered/free PEG to characterize the effects of surface attachment. As shown in Figure S1, the proton NMR spectrum of the free polymer is consistent with usual chemical shifts for polyethylene glycol. Figure 2.1 shows that when PEG chains are tethered to silica nanoparticles, chemical shifts from the polymer repeating unit are identical to the untethered case, while new peaks from short ligands attached to silica nanoparticles are observed, as expected. Because of the proximity to the strong electron withdrawing group on the particle surface, peak d downfields compared to the free polymer (Supporting Information Figure S2), implying that a bond between the polymer and ligand is formed. Additionally, new

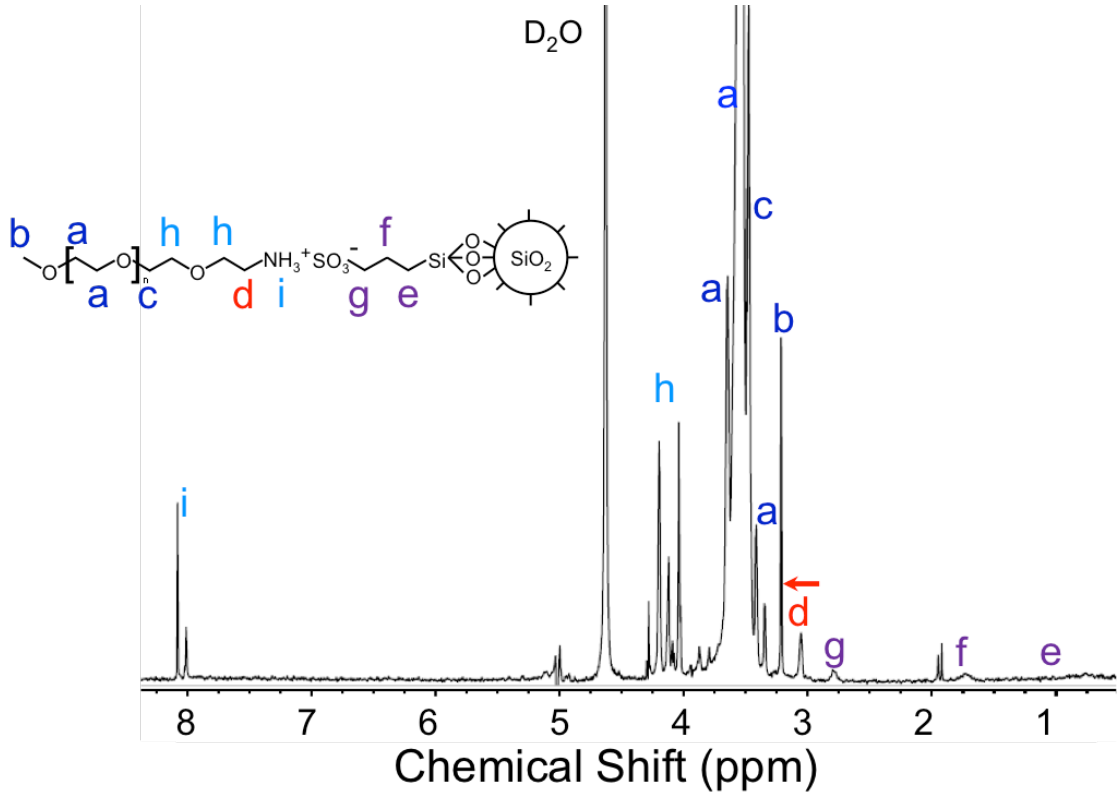

Figure 2.1. ^{1}H NMR spectrum of tethered PEG (M_w 5,000) on silica nanoparticles. Chemical shifts from PEG repeating unit and bonds right next to the repeating unit don't change after tethering, shown in blue color (a, b, c). After tethering, short ligand peaks (purple: e, f, g) and peaks in the vicinity of bonding group (light blue: h, i) appear, and also peak d (red) downfields due to strong electron withdrawing group.

peaks around 8ppm and 4ppm are observed, which are believed to originate from protons near the bonding group (peaks h) and protons at the bonding group (peaks i).

Finer insights into the origin of peaks h and i can be achieved by means of Diffusion-Ordered SpectroscopY (DOSY) experiments. ^{1}H DOSY has recently received considerable attention due to its convenience and sensitivity.[45] In this study, the bipolar gradient pulse double stimulated echo sequence approach was utilized to measure the self-diffusion coefficient.[46] The results from two dimensional DOSY experiments (Figure S3) shows that the diffusion coefficient of each component (y axis) depends on the component size, whereas the x axis represents the usual chemical shift information. Except for the D_2O peak, all other peaks observed in the measurement are seen to have the same diffusion coefficient, indicating that on the time-scales of these measurements, the polymer and particles in the SiO_2-PEG hybrids are completely coupled.

To determine how the attachment of PEG chains onto SiO_2 nanoparticles affects the structure of the polymer chains, we employed measurement techniques capable of interrogating chain structure and conformation on length scales ranging from angstrom to bulk. The angstrom scale molecular structure was studied using Attenuated Total Refection Fourier Transform Infrared Spectroscopy (ATR FT-IR).[47] This approach avoids limitations with traditional FT-IR stemming from the KBr sample preparation method, which has the potential to hinder the PEG crystalline structure due to hygroscopic KBr.[37] It has been well-known that the most stable conformation of PEG backbone is TTG (-O-CH_2-CH_2), *trans-trans-gauche*, and the second most stable

conformation as TTT (-O-CH_2-CH_2), *trans-trans-trans*, each of which is the building block for the crystal unit cell, Helix and Planar Zigzag, respectively.[37,39,40,44] FT-IR bands of free PEG with vibrational assignment and conformational states have been reported in the literature.[37,39,40,42]

Figure 2.2 presents ATR FT-IR spectra for free PEG and the SiO_2-PEG composites. Absorption bands in the range of 800-1500 cm^{-1} of greatest interest for studying the chain conformation are assigned by vibrational mode, conformation, and crystal unit cell type in Table 2.1. Absorption bands between 1800-2300 cm^{-1} are intrinsic to the ATR diamond crystal and absorbance in range of 2800-3000 cm^{-1} are due to CH_2 groups from the polymer repeating unit.[48]

The total absorbance of an *N*-component mixture can be estimated using the Bouger-Lambert-Beer law (Beer's law):

$$\mathrm{A}(\nu) = \sum_{i=1}^{N} [a_i(\nu) b c_i]$$

where $a_i(\nu)$ is the absorbance of each component i in the unit of (concentration•path length)$^{-1}$, b is light path length, and c is the concentration of the component i.[47]

As the silica particles used in this study scatters some light, characteristic absorbance peaks from the amorphous inorganic nanoparticles are not observed. Consequently, the total absorbance mainly originates from the organic species and the intensities decrease as the inorganic content of the hybrids increase. Some of the IR bands observed for the free polymer are clearly not visible when the inorganic content

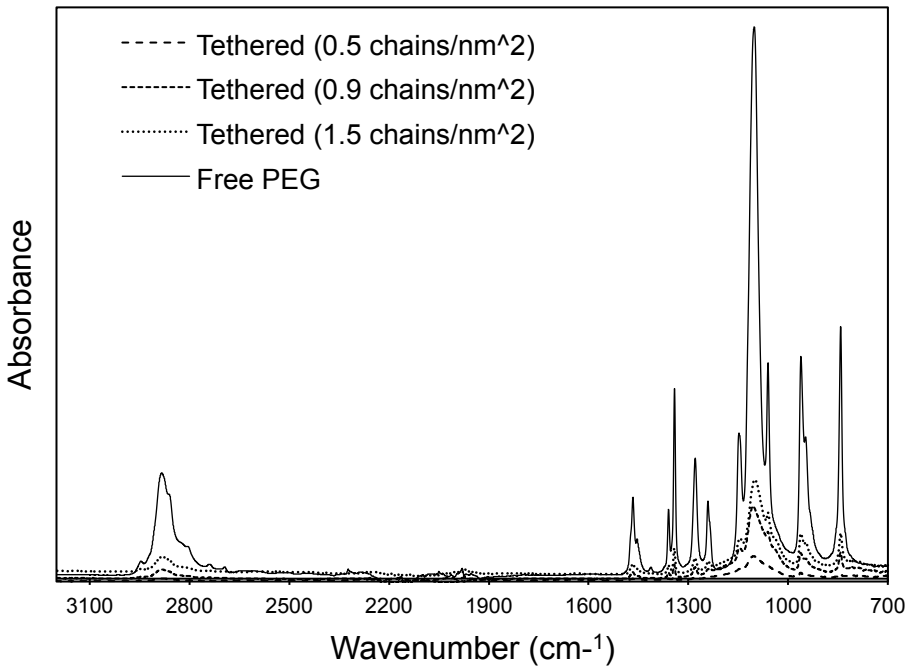

Figure 2.2. FT-IR spectra of PEG and tethered PEG with different grafting densities in parenthesis.

Table 2.1. Assignment of FT-IR bands for PEG

Peak position (cm^{-1})		Vibrational Assignment	Conformations	Crystal Unit Cell
Free PEG	Tethered PEG (1.5 chins/nm^2)			
842	842	C-O stretch, CH_2 rock	mostly C-C gauche, C-C trans	Helix
949	949	C-O stretch, CH_2 rock	C-C gauche, C-O trans	Helix
962	962	C-O stretch, CH_2 rock		Zigzag
1061	1060	C-O stretch, C-C stretch, CH_2 rock		Helix
1103	1009	C-O stretch, C-C stretch		
1147	1146	C-O stretch, C-C stretch		
1234	1234	CH_2 twist (antisymmetric)	C-O trans	Helix
1241	1241	CH_2 twist (antisymmetric)	C-O trans	Zigzag
1280	1280	CH_2 twist (symmetric)	C-O gauche	Helix
1342	1342	CH_2 wag (antisymmetric)	C-C trans	Zigzag
1360	1359	CH_2 wag (antisymmetric)	C-C gauche	Helix
1454	1454	CH_2 scissor		Helix
1466	1466	CH_2 scissor		Zigzag

exceeds a certain value. Additionally, the absence of intramolecular bonded OH bands in the 3200-3600 cm^{-1} range signify that there is little if any physical adsorption between polymer chains and the nanoparticles, consistent with expectations based on the high polymer surface coverage. Finally, but for the small peak at 2735 cm^{-1} associated with the $–CH_2NH_2$ terminal group, which disappears after tethering, all of the peaks for the free polymer chains observed for the hybrids maintaining their positions. This means that the types of conformations adopted by the tethered polymer backbone are more or less the same as those for the free polymer.

The relative intensities of FT-IR peaks within a given spectra for a polymer can be used to provide information about the chain conformations. The ratio of *gauche* and *trans* states for C-C or C-O bonds within the same vibrational mode can be utilized provide insight about the chain conformations. Only one pair of *trans*/*gauche* states are found for our materials that satisfies these requirements, C-C *trans*/*gauche* of CH_2 wagging vibration region (1342-1360 cm^{-1}) of the spectra (Table 2.1). Figure 2.3a shows that *gauche* conformations are more abundant for the tethered polymer. As the *gauche* conformation of the C-C bond is reported to have lower energy than the *trans* conformation,[37,49,50] tethering at lower grafting densities yields PEG chains in more energetically stable states at the angstrom scale.

Structure of the tethered PEG chains on nanometer length scales can be characterized by counting the helix and zigzag contents. Free PEG possesses both helix and zigzag unit cell structures (Table 2.1 and Figure 2.2).[37,40,42] When polymers are anchored, they are able to maintain both structures, but the proportion is changed.

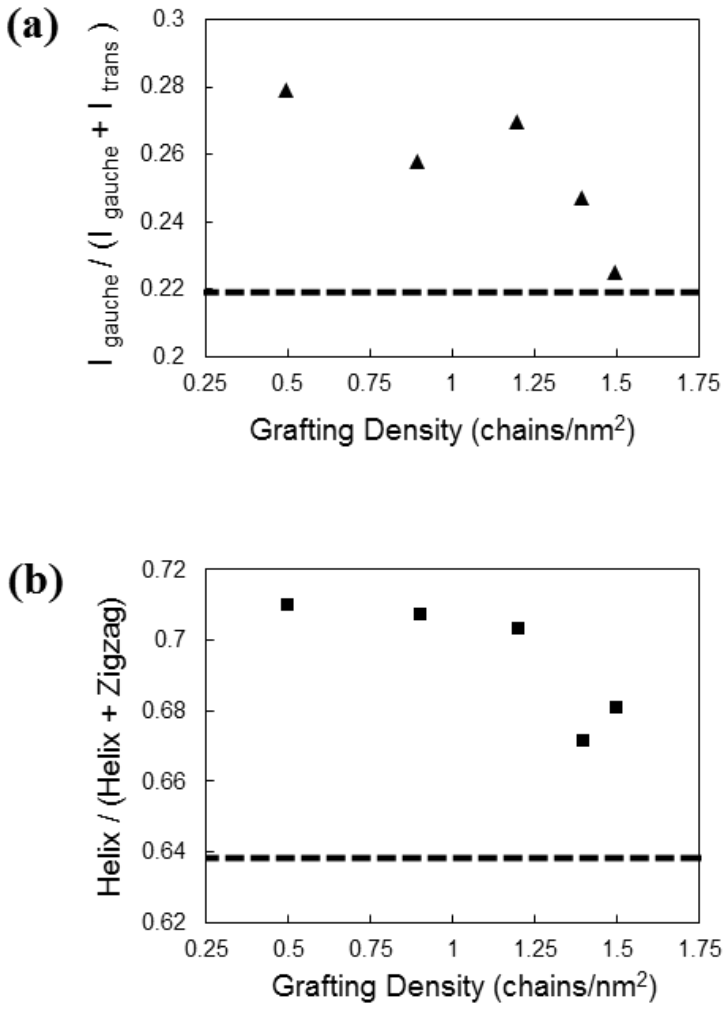

Figure 2.3. (a) Intensity ratio between gauche (I^{1359}) and trans (I^{1342}) conformations of C-C bonds of tethered (black triangle) and free (dashed horizontal line) PEG. (b) Intensity ratio between helix and zigzag structures of tethered (black square) and free (dashed horizontal line) PEG.

Helix and zigzag populations were computed by adding up the intensity of each assignment deduced by fitting the FTIR spectra to a Gaussian function (Supporting Information Figure S4). The results are reported in Figure 2.3b indicating that the helix population increases as a function of SiO_2 content (lower PEG grafting density) in the SiO_2-PEG hybrids. Since the helix unit cell is more stable than the planar zigzag unit cell,[37] tethering again is found to result in more stable chain structures on nanometer length scales.

The melting transition reflects changes in the crystal structure of semi-crystalline polymers on length scales of 10^{-8} m and larger. Figure 2.4 reports results from differential scanning calorimetry (DSC) measurements for free PEG (dashed line) and SiO_2-PEG hybrids (continuous line). The figure shows that the untethered PEG displays three different melting peaks, each representing the various types of chain packing possible in PEG crystallite - extended, once-folded, and twice folded from high to low temperature. Qiu et al. reported that depending on the polymer molecular weight, PEG chains show a hierarchy of extended, once, twice, trice, folded chain packing configurations in its crystallites.[36] The results observed here for our untethered chains are in excellent agreement with the results reported by Wunderlich et. al. for comparable PEG molecular weights. The Thompson-Gibbs equation can be used to relate the melting temperature, T_m , and the crystal thickness L_c:

$$T_m = T_m^o \left(1 - 2\sigma / L_c \rho_c \Delta h\right)$$

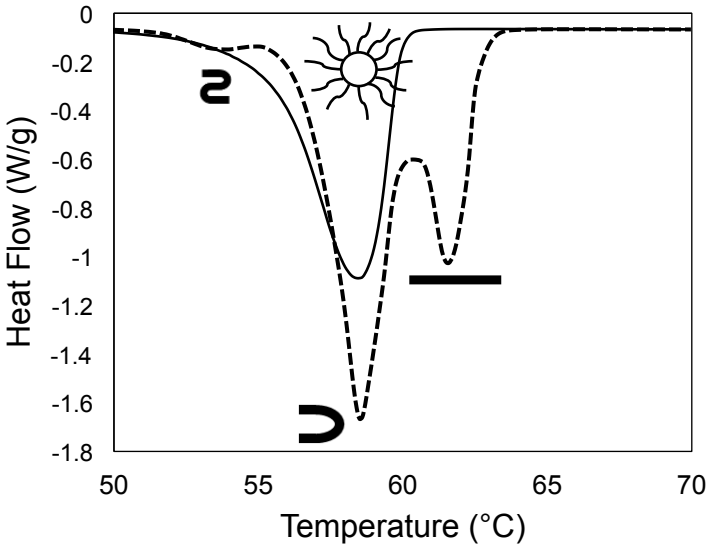

Figure 2.4. DSC thermograms for free chains (dashed line) and tethered chains (continuous line) of grafting density 0.9 chains/nm^2. All other tethered PEG chains with different grafting densities have similar thermograms as this tethered one. Free PEG chains have 3 types of crystallites-extended, once folded, and twice folded from high to low temperature, whereas tethered PEG chains have only one crystallite type-extended.

where T_m^o is equilibrium melting temperature, σ is the fold surface free energy, ρ_c is the crystal phase density, and Δh is the heat of fusion[51]. The melting temperature and crystal thickness of 3 types of crystallites are plotted in Figure S5.

The corresponding results for the SiO_2-PEG hybrids are shown as the continuous line in Figure 2.4. In contrast to the free chains, the tethered PEG displays only one melting peak, indicating that only one kind of crystallite structure exists. We assign this one melting peak to the extended type of crystallite for the following reasons: First, the lateral spacing between polymer chains on the nanoparticle surface is less than 0.5nm, i.e. below the Kuhn step length of 1.1 nm, and considering the particle curvature, the inter chain spacing only becomes comparable to the Kuhn step length at a distance $l \approx R(b_K \Sigma^{1/2} - 1)$, which at all grafting densities Σ studied here is of the order of the mean square end-to-end distance of the short PEG chains studied here. This means that the chains will form an extended brush on the particle surface.[32] Second, the polymer brush height deduced from intrinsic viscosity experiments is 10~12 nm (Figure 2.5), i.e. about 10-times the root-mean-squared end-to-end distance for a random coil chain of the same molecular weight and about 0.4 times the fully extended length of the chain. These findings are consistent with our recent report showing the *cis*-1,4-polyisoprene chains of comparable molecular weight also form an extended brush when tethered to SiO_2 nanoparticles.[32] The observed brush heights for the single polymer molecular weight studied here are also roughly consistent with the prediction $H \sim N^{4/5} b$, as proposed by Dukes et al.[52] and Ohno et al.[53] irrespective of

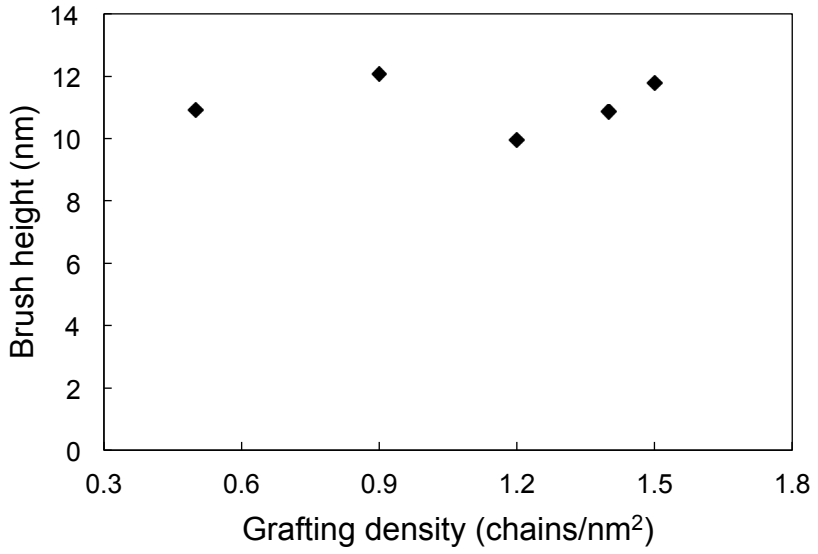

Figure 2.5. Polymer brush height obtained from intrinsic viscosity experiments.

the polymer chain grafting density. Lastly, because the polymer chains appear unable to stack together to form well-developed spherulitic crystals, but rather appear to crystallize around the nanospheres, the brush height of tethered polymer provides a crude estimate for the thickness of crystallites comprised of extended chains. Figure S5 shows that results for the tethered PEGs all lie between T_m and L_c of once and twice folded free chains.

This finding has some support from a recent theory for self-suspended nanoparticle fluids such as the SiO_2-PEG used in this study. This theory posits that in order to fill the inter-particle space, particularly in the most difficult-to-reach locations between particles, tethered chains in a self-suspended suspension must on average extend away from the particle surface.[54] The DSC experiments, therefore, support the results that the tethered polymer chains manifest more stable structures compared to free polymer on length scales O (10^{-8} m), as the tethered PEG has extended crystallite. At lower grafting densities, the tethered polymers exist more in a 3-dimensional helix unit cell structure which possesses larger unit cell volume than 2-dimensional zigzag structure (Figure 2.6). Thus, by changing the grafting density, the effect which polymer chains are experiencing from a nanosphere can be controlled and ultimately molecular level structures can be manipulated gradually.

At larger length scales, around the size of one SiO_2-PEG hybrid unit, XRD experiments provide additional information about PEG crystallization. Figure 2.7 is the stacked XRD diffractograms for free and SiO_2-tethered PEG over a range of polymer grafting densities from 0.2 to 1.5 chains/nm^2. At high grafting densities (i.e.

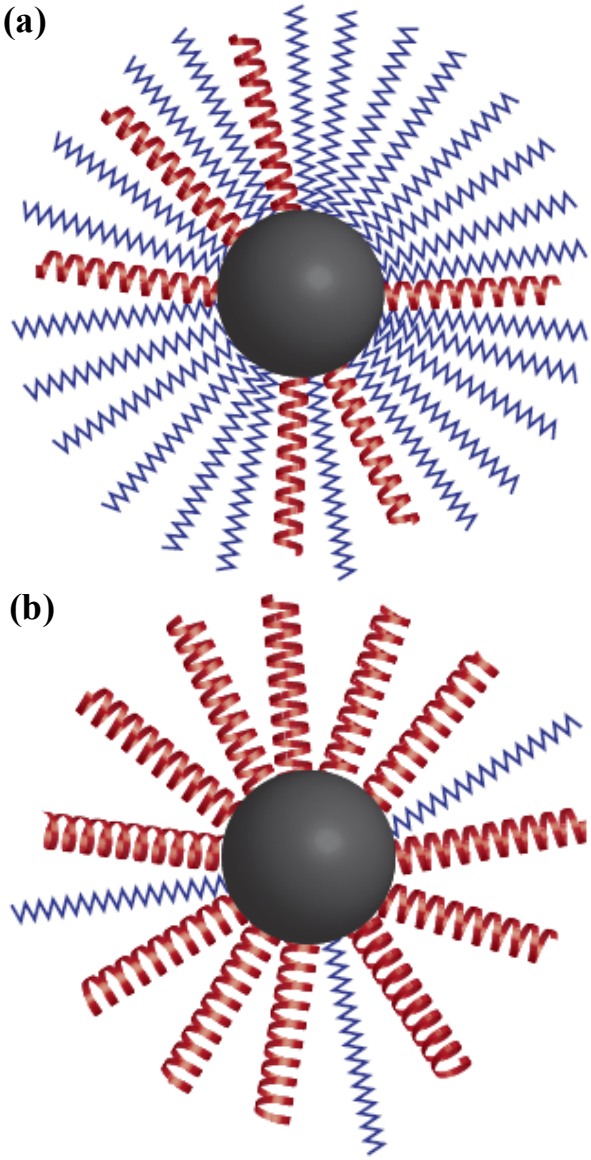

Figure 2.6. Space filling constraint. (a) Densely grafted. 2 dimensional zigzag is more effective to be squeezed into confined space than helix does. (b) Sparsely grafted. Chains have enough space to be developed as 3-dimensional helix. The structures of the order of O ($^{-9}$m) have been exaggerated to show helix and zigzag unit cells.

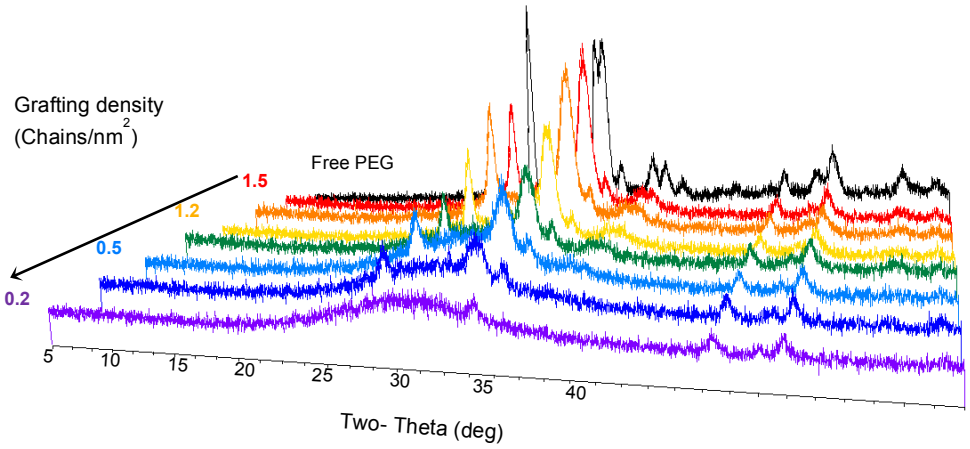

Figure 2.7. XRD spectra of free (black) and tethered PEG with different grafting densities. Spectra slowly lose crystalline characteristics as less polymer chains are tethered and the material is completely amorphous halo at a grafting density of 0.2 chains/nm^2.

low SiO_2 content), the XRD pattern for the particle-tethered PEG appears quite similar to that of free PEG with slightly reduced intensities. As grafting density reduces, scattering due to PEG crystallites falls gradually at all diffraction angles, θ, and for SiO_2 PEG hybrids with the lowest grafting density (i.e. highest SiO_2 contents), well defined diffraction peaks associated with PEG crystallites are no longer seen. They are instead replaced by a broad halo characteristic of an amorphous material.

To understand these observations of reduced crystallinity for lower grafting density PEG, one can compute and compare the crystal sizes for each lattice direction. Each peak of diffraction angle, θ , can be converted to the its characteristic lattice spacing, d, using Bragg's law:

$$n\lambda = 2d \sin\theta$$

where n is integer, λ is the wavelength.[55] Since the inorganic components are 3D nanospheres, the d spacing is not as straightforward to interpret. However, information on the size of crystals from each lattice plane, which has the same d spacing, can be used provide an indirect inference. Scherrer's equation shows that the size of crystal, D is in inverse proportion to FWHM (Full Width Half Maximum), β;

$$D = k\,\lambda/\beta\,cos\theta$$

where k is a crystal shape related constant ~1, λ is the wavelength, and θ is the Bragg angle.[55] The crystal size for each peak, i.e. each lattice direction, has been plotted in Figure S6 and values are summarized in Table 2.2. It is remarkable that despite the visual similarities of the XRD patterns for the untethered and tethered PEG at high

Table 2.2. X-ray diffraction data of free and tethered PEG

Free PEG			Tethered PEG (1.5 chins/nm^2)				
2θ	FWHM	Crystal size (nm)	2θ	FWHM	Crystal size (nm)	hkl	d (Å)
19.09	0.27	65.2	19.12	0.46	25.5	120	4.65
22.08	0.16	27.16				023	4.05
22.97	0.41	29.3	23.12	5.19	1.6	112	3.88
23.43	0.59	17.8	23.30	0.75	13.2	032	3.78
24.19	0.34	38.4	24.29	0.25	65.6	130	3.66
26.13	0.43	26.8	26.34	1.08	8.5	033	3.40
26.84	0.41	28.5	26.72	0.92	10.2	131	3.32
27.83	0.27	54.6				200	3.20

coverage, the PEG-SiO_2 hybrids generally form noticeably smaller crystals at all grafting densities. This indicates that the hybrids are more amorphous on length scales bigger than one unit. Only crystals corresponding to a 2 θ value of ~24° appear to become larger as a result of tethering the PEG to SiO_2 and confining it between particles. A straightforward explanation for this observation is that because silica nanoparticle diffraction overlaps with that from the PEG crystallites at this angle, the crystal size deduced from the data is a composite value and thus less trustworthy.

The effect of tethering on crystallization seen at different dimension might at first seem counterintuitive. However, if one again considers the requirement that the tethered polymer in a self-suspended suspension fully fill the interparticle space, it becomes clear that the particle constraints on any particular chain become greater the fewer the number of polymer chains available on each particle to fill the interparticle space. In other words, by immobilizing one end, tethered polymer has to be aligned to form polymer brush resulting in more ordered states. Importantly, the reduction of the interparticle space that occurs at higher particle contents (lower grafting density) that may be thought to weaken this constraint at larger scale, leads to an additional effect – confinement, which also would interfere with polymer crystallization and lower crystallite size; perhaps explaining the remarkable effect of the SiO_2 particles on PEG crystallization at all grafting densities.

Finally, we consider the effect of tethering PEG to SiO_2 on bulk crystallinity and morphology of PEG crystalline domains. The fractional crystallinity can calculated by dividing crystalline peak area into overall peak area from XRD

diffractograms, where results were plotted in Figure 2.8. Crystallinity can be also calculated from DSC results using the following well-known formula:

$$X_c(\%) = (\Delta H_m / \Delta H_m^o) \times 100$$

where X_c is percent crystallinity, ΔH_m is the heat of melting observed, and ΔH^o_m is the heat of melting for an ideal 100% crystalline PEG. It is significant that results from both approaches agree to within the error size. A strong conclusion can also be made from the results in Figure 2.8: the crystalline is a decreasing function of the polymer grafting density.

Loo et al.[56] previously reported on crystallization of polyethylene chains in polystyrene-polyethylene diblock copolymers. The authors found that polyethylene chains do not make well defined lamella near the PS domains, but rather become organized in preferential orientation away from the PE-PS interface. One might intuitively anticipate similar physics in the present case to lead to amorphous PEG regions near the curved particle surfaces and crystallization away from the interface. Based on the preceding discussion, this is apparently not the case for short PEG chains densely grafted to particles. In particular, the densely tethered PEG chains near the surface are thought to be so crowded that any given chain segment will have plenty of neighboring segments which can pack to form 3-d lamellar-like structures conformal with the anchoring particles. Because the chain spacing grows in proportion to distance from the particle surface, for densely grafted chains the thickness *l* of the

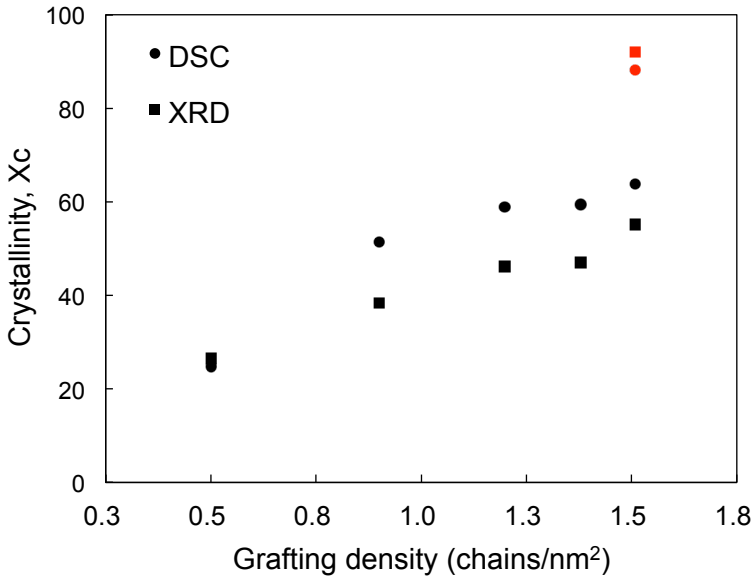

Figure 2.8. Degree of crystallinity as a function of grafting density. Red circle and red square indicate the crystallinity of free PEG obtained from DSC and XRD measurements, respectively.

pseudo-lamellar brush would be at least, $l \approx R(b_K\Sigma^{1/2} - 1)$ where R is the nanoparticle radius and b_K is the Kuhn step length.For a typical PEG grafting density of 1.5 chains/nm^2, l is about $R/3$, which is close to the rms end-to-end length of the PEG chains. On length scales much larger than l, i.e. far away from the particle surfaces, chain segments are free to explore space and crystallize much as they would in the untethered polymer. Thus, two zones of crystallization are expected around densely grafted particles: an inner zone conformal to the particle surface where crystallization results from chain crowding and a region far from the particles where crystallization occurs by chain folding and stacking. For the short, densely grafted chains studied here, the inner conformal zone comprised of extended chain crystallites is expected to dominate. For sparsely tethered, long PEG chains, l is small, and the outer section would dominate and produce crystallization behavior analogous to what has been observed for PS-b-PE copolymers.

Taken together, our results show that even though nanospheres act as immovable, stabilizing platforms that allow tethered polymer chains to develop more stable structures on small length scales O (10^{-10}~10^{-8} m), on scales larger than the size of a single SiO_2-PEG unit, the particles impede the polymer chains from forming the lamellae stacks characteristic of PEG crystallization, and instead appear to restrict crystallization to a narrow region around the nanospheres. Studies of the non-isothermal crystallization kinetics provide powerful support for this point.

To this end, we characterized the crystallization kinetics of free and SiO_2-tethered PEG chains within the framework of the classic Avrami plot.[57] The method

credited to Ozawa[58] is usually used to interpret non-isothermal crystallization kinetics, but the chain fold-temperature factor was ignored in this method, which reduces its utility for the present systems. In the Avrami approach the time-dependence of the relative crystallinity X_{rc} can be described using the following formula:

$$\ln \{ -\ln[1-X_{rc} (t)] \} = \ln k + n \ln t$$

where k is the crystallization rate constant, n is the Avrami index, and t is the crystallization time (Supporting Information S7). The Avrami index is known to sensitively reflect the macroscopic geometry of crystal growth and n values between 3 and 4 imply are characteristic of 3-dimensional spherulitic growth.[51] Figure 2.9a report the Avrami indices for free and SiO_2-tethered PEG. The figure shows that for either material, Avrami index is in fact between 3 and 4, consistent with spherulitic. Considering the spherical symmetric geometry of the SiO_2-tethered PEG hybrid materials this observation is perhaps unsurprising. Figure 2.9b reports the crystallization rates for free and SiO_2-tethered PEG with two grafting densities. Remarkably, we find that the crystallization kinetics of the most sparsely grafted particles (materials with the highest SiO_2 content) are closest to those of the untethered PEG chains at all cooling rates. These materials are thought to be the most geometrically confined between nanoparticles and results presented earlier showed that they form among the smallest crystallites. Conversely, the most densely grafted SiO_2-PEG hybrids exhibit slower crystallization kinetics and the weakest dependence of crystallization rate on the cooling temperature. These results imply that molecular

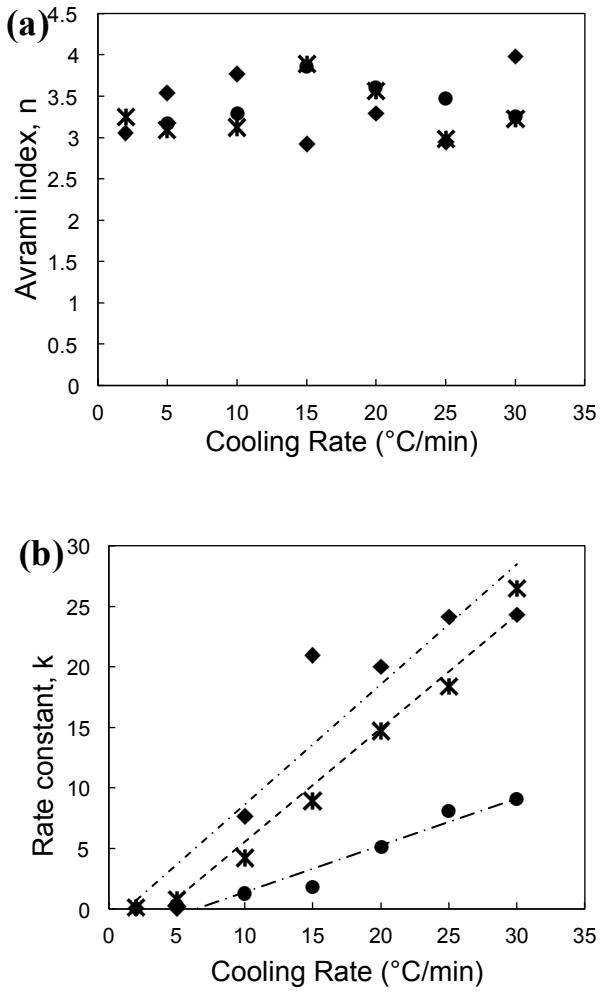

Figure 2.9. (a) Avrami index, n. (b) Crystallization rate constant, k. Diamonds correspond to free polymer, circles to silica nanoparticle-tethered PEG chains with fixed grafting density of 1.5 chains/nm^2, and stars to silica nanoparticle-tethered PEG chains with fixed grafting density of 0.5 chains/nm^2. The lines through the data are the best fitted straight lines.

motions, which are more restricted in the densely tethered case,[32] may play the decisive role in setting the crystallization rate.

Kissinger[57] proposed that the activation energy for crystallization could be calculated as follows:

$$\frac{d\left[\ln\left(a/T_p^2\right)\right]}{d\left(1/T_p\right)} = \frac{-E_a}{R}$$

where a is the cooling rate, T_p is peak of crystallization transition, R is the gas constant. The calculated crystallization activation energy is reported in Figure S8. These results can be interpreted as follows: When polymer chains are densely tethered, they are readily stacked around the nanoparticles due to crowding by their neighbors, which facilitates crystallization. When they are sparsely tethered, polymer chains require more energy to activate stacking with other polymers on the other nanoparticles. This explanation also implies that because the length-scales on which the stacking must occur in the most densely grafted SiO_2-PEG systems is smaller, crystallization is least sensitive to the rate at which the materials are cooled.

2.4. CONCLUSIONS

We have demonstrated that tethering of semi-crystalline polyethylene glycol (PEG) chains to nanoparticles to form densely grafted, self-suspended nanoparticle fluids generates conflicting structures at different length scales. The size of one unit of the hybrid SiO_2-PEG nanostructures is about 30nm. Below this size, we have shown

that tethered polymer chains are more stable than the free polymer because one end is localized in a densely grafted brush layer near the particle surface. Vibrational spectroscopy measurements further show that TTG conformations and the helix unit cell moiety are more abundant at sub-nano and nanometer dimensions in SiO_2-PEG. Tethered chains are found by means of DSC and intrinsic viscosity measurements, to form extended chain crystallites. This structural change significantly alters the melting transition of the tethered polymer chains. In contrast, on length-scales larger than that of a single hybrid SiO_2-PEG unit, the materials are more amorphous than the untethered PEG chains, exhibit smaller crystallite size for each lattice direction, and manifest lower bulk crystallinity. This feature of the materials is thought to arise because particles hinder crystallization to a narrow region around the nanospheres, which leads to overall failure of the material in forming the spherulites characteristic of PEG. Figure S9 summarizes Chapter 2.

ACKNOWLEDGMENTS

This work was supported by the National Science Foundation, Award No. DMR-1006323 and by Award No. KUS-C1-018-02, made by King Abdullah University of Science and Technology (KAUST). Facilities available though the Cornell Center for Materials Research (CCMR) were used for this study (DMR-1120296). The authors thank Dr. Ivan Keresztes for the help with the NMR experiment.

REFERENCES

1. Shenhar, R.; Norsten, T. B.; Rotello, V. M. *Adv. Mater.* **2005**, *17*, 657-669.

2. Einstein, A. *Ann. Phys. (Weinheim, Ger.)* **1905**, *17*, 549-560.

3. Einstein, A. *Ann. Phys. (Weinheim, Ger.)* **1906**, *17*, 289-306.

4. Batchelor, G. K. *Fluid Mech.* **1977**, *83*, 97-117

5. Suhr, J.; Koratkar, N.; Keblinski, P.; Ajayan, P. *Nat. Mater.* **2004**, *4*, 134-137.

6. Oh, H.; Green, P. F. *Nat. Mater.* **2009**, *8*, 139-143.

7. Tuteja, A.; Mackay, M. E.; Narayanan, S.; Asokan, S.; Wong, M.S. *Nano Lett.* **2007**, *7*, 1276-1281.

8. Wang, Y.; Rafailovich, M.; Sokolov, J.; Gersappe, D.; Araki, T.; Zou, Y.; Kilcoyne, A. D. L.; Ade, H.; Marom, G.; Lustiger, *Phys. Rev. Lett.* **2006**, *20*, 028303.

9. Lemstra, P. J. *Science*, **2009**, *323*, 725-726.

10. Baer, E.; Hiltner, A.; Keith, H. D. *Science*, **1987**, *235*, 1015-1022.

11. Huang, X. D.; Goh, S. H. *Macromolecules*, **2001**, *34*, 3302-3307.

12. Kropka, J. M.; Pryamitsyn, V.; Ganesan, V. *Phys. Rev. Lett.* **2008**, *101*, 075702.

13. Forrest, J. A.; Dalnoki-Veress, K.; Stevens, J. R.; Dutcher, J. R. *Phys. Rev. Lett.* **1996**, *77*, 2002.

14. Ruggerone, R.; Geiser, V.; Vacche, S. D.; Leterrier, Y.; Manson, J. E. *Macromolecules*, **2010**, *43*, 10490-10497.

15. Zanetti, M.; Camino, G.; Reichert, P.; Mulhaupt, R. *Macromol. Rapid Commun*. **2001**, *22*, 176–180.

16. Schaefer, J. L.; Moganty, S. S.; Archer, L. A. *Adv. Mater.* **2010**, *22*, 3677–3680; Srivastava, S.S.; Schaefer, J.L.; Yang, Z.; Tu, Z.; Archer L.A. *Adv. Mater.* **2013**, *26*, 201-233.
17. Richman, E. K.; Hutchison, J. E. *ACS Nano*, **2009**, *3*, 2441-2446.
18. Loo, Y.; Register, R. A.; Ryan, A. J.; Dee, G. T. *Macromolecules*, **2001**, *34*, 8958-8977.
19. Loo, Y.; Register, R. A.; Ryan, A. J. *Phys. Rev. Lett.* **2000**, *84*, 4120-4123.
20. Chian, Y.; Ho, R.; Thomas, E. L.; Burger, C.; Hsiao, B. S. *Adv. Funct. Mater.* **2009**, *19*, 448-459.
21. Reiter, G.; Castelein, G.; Sommer, J.; Rottele, A.; Thurn-Albrecht, T. *Phys. Rev. Lett.* **2001**, *87*, 226101.
22. Zhu, L.; Cheng, S. Z. D.; Calhoun, B. H.; Ge, Q.; Quirk, R. P.; Thomas, E. L.; Hsiao, B. S.; Yeh, F.; Lotz, B. *J. Am. Chem. Soc.* **2000**, *122*, 5957-5967.
23. Frank, C. W.; Rao, V.; Despotopoulou, M. M.; Pease, R. F. W.; Hinsberg, W. D.; Miller, R. D.; Rabolt, J. F. *Science*, **1996**, *273*, 912-915.
24. Hu, Z.; Baralia, G.; Bayot, V.; Gohy, J.; Jonas, A. M. *Nano Lett.* **2005**, *5*, 1738-1743.
25. Wang, H.; Keum, J. K.; Hiltner, A.; Baer, E.; Freeman, B.; Rozanski, A.; Galeski, A. *Science*, **2009**, *323*, 757-760.
26. Reiter, G.; Sommer, J. *Phys. Rev. Lett.* **1998**, *80*, 3771.
27. Duran, H.; Steinhart, M.; Butt, H.; Floudas, G. *Nano Lett.* **2011**, *11*, 1671-1675.
28. Woo, E.; Huh, J.; Jeong, Y. G.; Shin, K. *Phys. Rev. Lett.* **2007**, *98*, 136103.

29. Nojima, S.; Ohguma, Y.; Namiki, S.; Ishizone, T.; Yamaguchi, K. *Macromolecules*, **2008**, *41*, 1915-1918.

30. Rodriguez, R.; Herrera, R.; Archer, L. A.; Giannelis, E. P. *Adv. Mater.* **2008**, *20,* 4353-4358.

31. Agarwal, P.; Qi, H.; Archer, L. A. *Nano Lett.* **2010**, *10*, 111-115.

32. Agarwal, P.; Kim, S.; Archer, L.A. *Phys. Rev. Lett.* **2012**, *109*, 258301.

33. Schadler, L. *Nat. Mater*. **2007**, *6*, 257-258.

34. Khan, J.; Harton, S. E.; Akcora, P.; Benicewicz, B. C.; Kumar, S. K. *Macromolecules*, **2009**, *42*, 5741-5744.

35. Naito, M.; Nobusawa, K.; Onouchi, H.; Nakamura, M.; Yasui, K.; Ikeda, A.; Fugiki, M. *J. Am. Chem. Soc.* **2008**, *130*, 166797-16703.

36. Qiu, W.; Pyda, M.; Nowak-Pyda, E.; Habenschuss, A.; Wunderlich, B. *Macromolecules* **2005**, *38*, 8454-8467.

37. Chrissopoulou, K.; Andrikopoulos, K. S.; Fotiadou, S.; Bollas, S.; Karageorgaki, C.; Christofilos, D.; Voyiatzis, G.A.; Anastasiadis, S.H. *Macromolecules* **2011**, *44*, 9710-9722.

38. Maxfield, J.; Shepherd, I.W. *Polymer* **1975**, *16*, 505-509.

39. Matsuura, H.; Fukuhara, K. *J. Polym. Sci., Part B: Polym. Phys.* **1986**, *24*, 1383-1400.

40. Deng, Y.; Dixon, J. B.; White, G**. N.** *Colloid. Polym. Sci*. **2006**, *284*, 347-356.

41. Koenig, J.L.; Angood, A.C. *J. Polym. Sci., Part A-2* **1970**, *8*, 1787-1796.

42. Marcos, J.I.; Orlandi, E.; Zerbi, G. *Polymer* **1990**, *31*, 1899-1903.

43. Shimanouchi, T.; Mizushima, S. *J. Chem. Phys.* **1955**, *23*, 707-711.

44. Takahashi, Y.; Sumita,; I. Tadokoro, H. *J. Polym. Sci.:Polymer Physics Edition* **1973**, *11*, 2113-2122.

45. Wu, D.; Chen, A.; Johnson, C. S. *J. Magn. Reson. Ser. A.* **1995**, *115*, 260-264.

46. Jerschow, A.; Muller, N. *J. Magn. Reson.* **1997**, *125*, 372-375.

47. Griffiths, P. R.; de Haseth, J. A. *Fourier Transform Infrared Spectrometry,* 2nd ed.; Wiley-Interscience: Hoboken, NJ, 2007.

48. Socrates, G. *Infrared and Raman Characteristic Group Frequencies: Tables and Charts,* 3rd ed.; John Wiley & Sons: Chichester, England, 2001.

49. Mark, J. E.; Flory, P. J. *J. Am. Chem. Soc.* **1965**, *87*, 1415-1423.

50. Mark, J. E.; Flory, P. J. *J. Am. Chem. Soc.* **1966**, *88*, 3702-3707.

51. Gedde, U. W. In *Polymer Physics;* Kluwer Academic Publishers: Norwell, MA, 2001; p144.

52. Dukes, D.; Li, Y.; Lewis, S.; Benicewicz, B.; Schadler, L; Kumar, S. K. *Macromolecules* **2010**, *43*, 1564.

53. Ohno, K.; Morinaga, T.; Takeno, S.; Tsujii, Y.; Fukuda, T. *Macromolecules* **2007**, *40*, 9143.

54. Yu, H.; Koch, D. L. *Langmuir* **2010**, *26*, 16801-16811.

55. Suryanarayana, C.; Grant Norton, M. In *X-Ray Diffraction: A Practical Approach;* Plenum Press: New York, 1998; p50-53, p212-213.

56. Loo, Y.-L.; Register, R. A.; Adamson, D. H. *Macromolecules* **2000**, *33*, 8361-8366.

57. Lorenzo, M.L.; Silvestre, C. *Prof. Polym. Sci.* **1999**, *24*, 917-650.

58. Ozawa, T. *Polymer* **1971**, *12*, 150-158.

APPENDIX: Supporting Information for Chapter 2

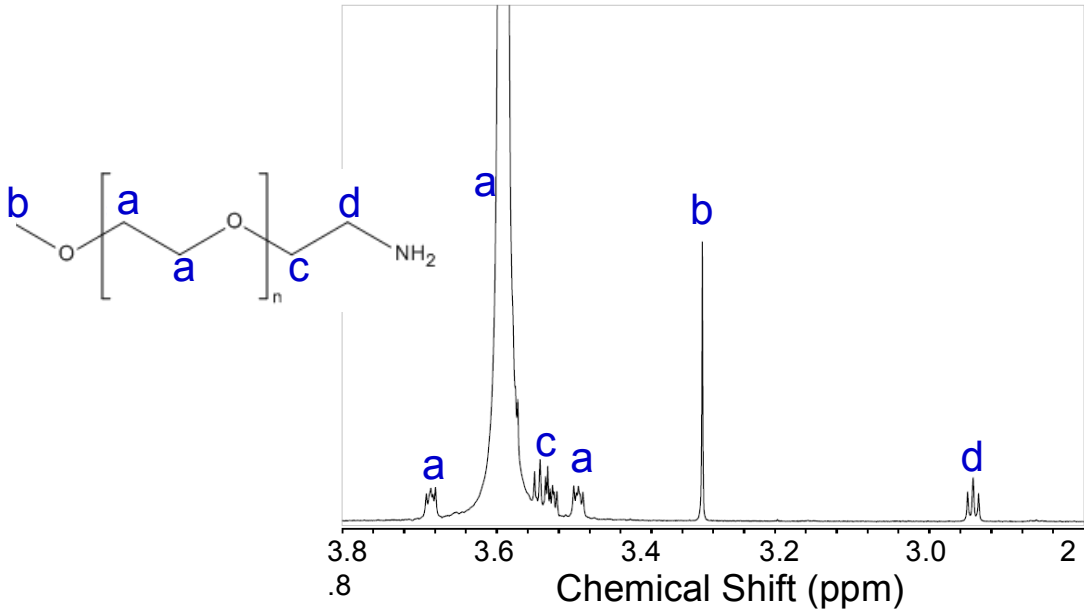

Figure S1. ^{1}H NMR spectrum of free PEG (M_w 5,000).

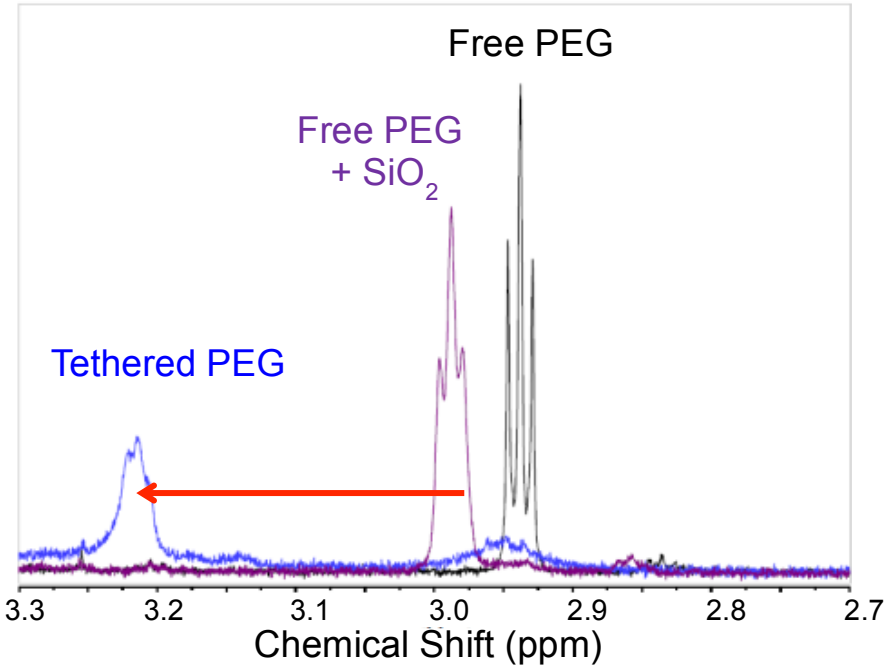

Figure S2. Downfield of peak d after tethering.

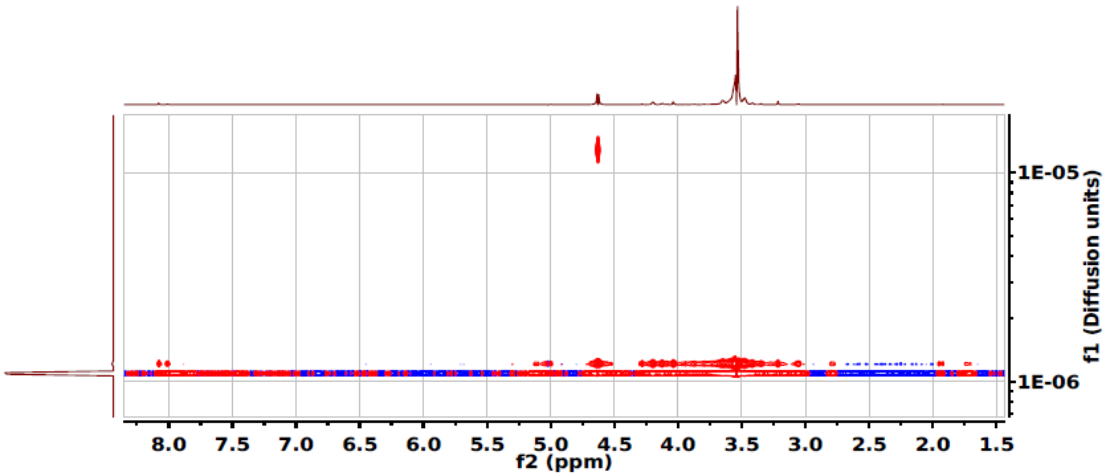

Figure S3. DOSY NMR of tethered polymers.

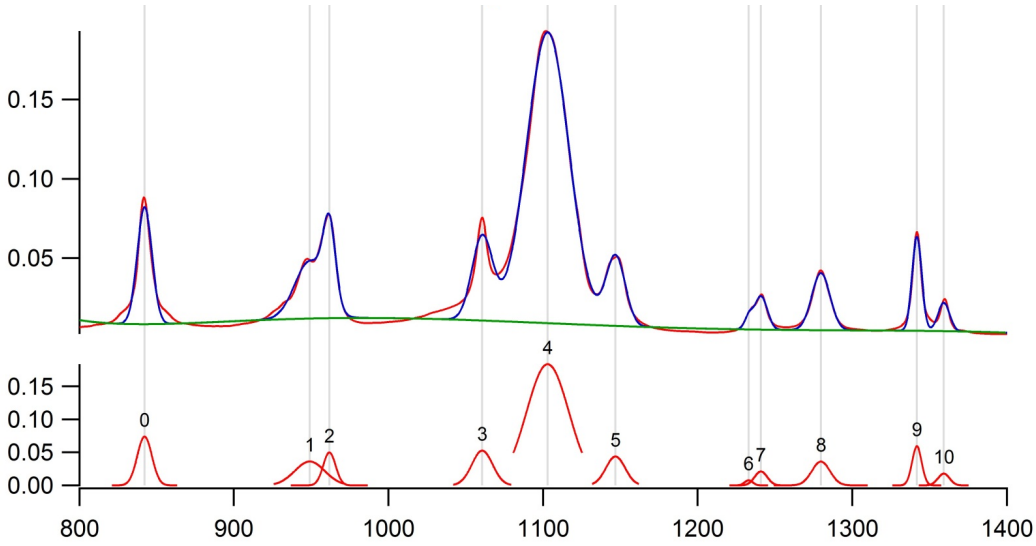

Figure S4. Gaussian function fitting for free PEG.

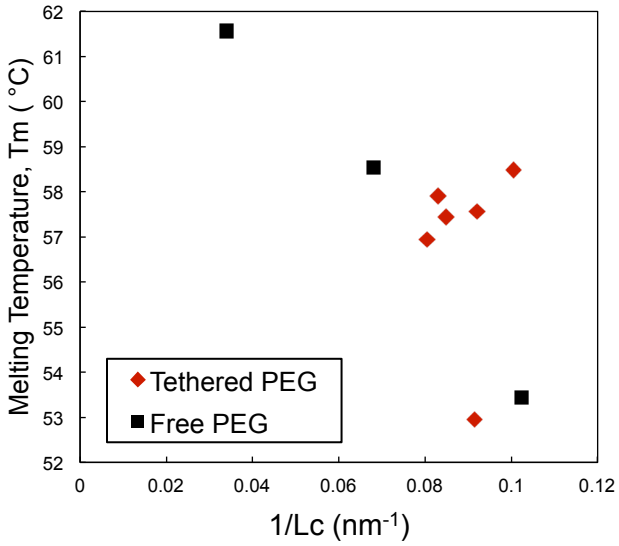

Figure S5. Melting temperature vs. 1/Lc of free and tethered PEG.

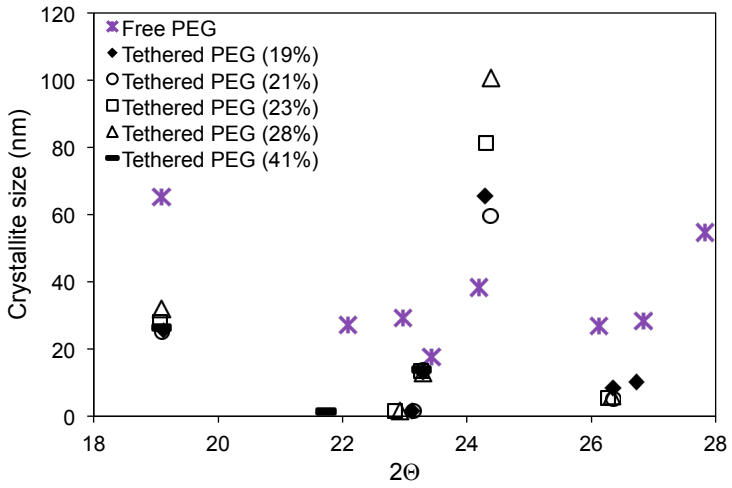

Figure S6. Crystal size for each plane facing specific miller index lattice direction.

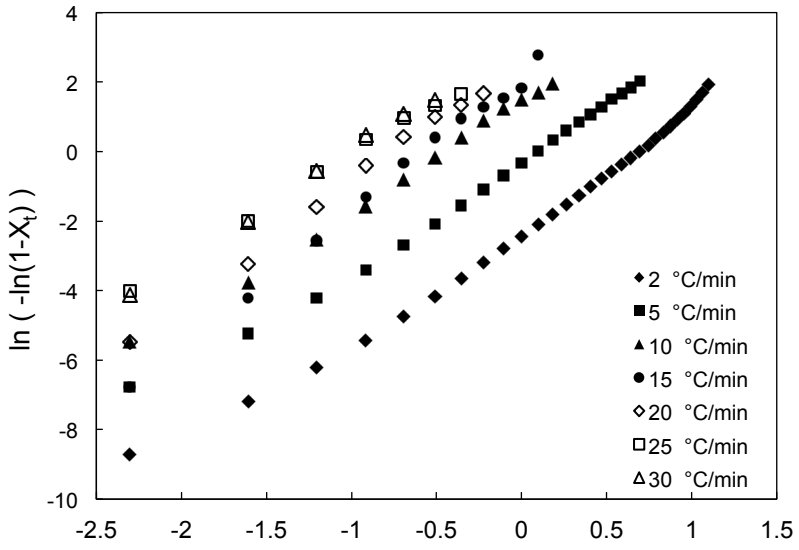

Figure S7. Avrami plot of tethered polymers having grafting density 0.5 chains/nm^2.

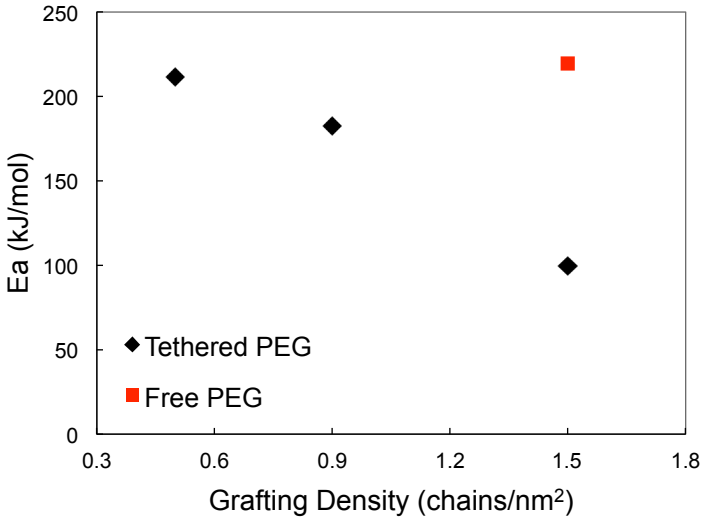

Figure S8. Activation energy for crystallization.

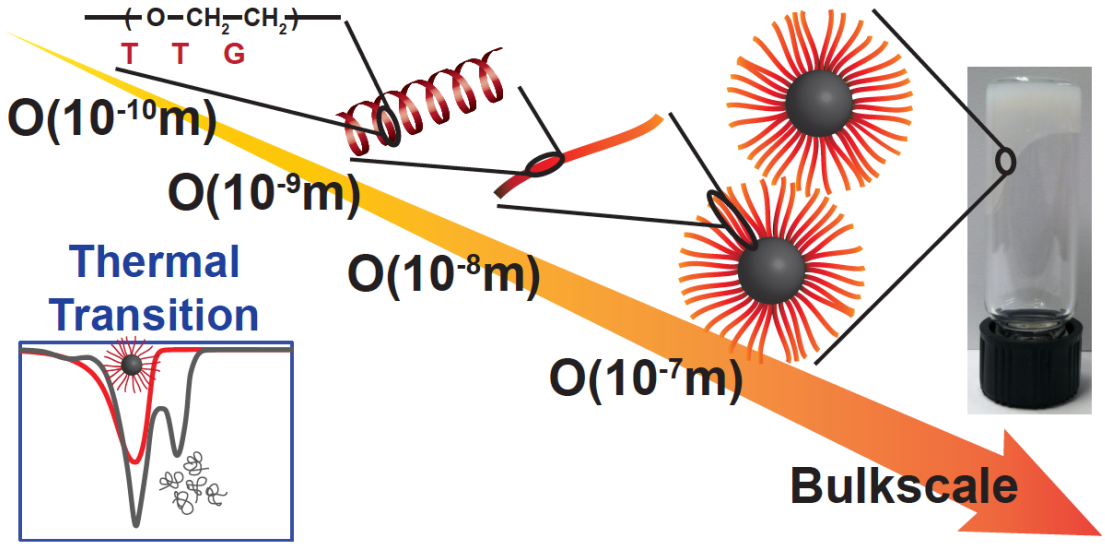

Figure S9. Summary of Chapter 2.

CHAPTER 3

RELAXATION DYNAMICS OF NANOPARTICLE-TETHERED POLYMERS[§]

[§] Rahul Mangal carried out Small Angle X-ray Scattering experiments.

ABSTRACT

The viscoelastic and dielectric relaxation dynamics of nanoparticle-tethered polymer chains are investigated. By grafting polymer chains to spherical nanoparticles, effects of tethering, crowding, and confinement imposed by nanoparticles are studied as a function of molecular weight, grafting density, and temperature. Tethering is shown to lead to tremendous changes in rheological properties of polymers at bulk scale. A transition from simple fluid behavior to rheological characteristics of soft glasses is observed. Novel phenomena such as jamming, yielding and enhanced glassy behaviors by increasing temperature and decreasing grafting density are reported. Dielectric spectroscopy experiments show that tethered polymer chains relax remarkably slower than their untethered counterparts on nanometer length scale. We report the relationships among relaxation time, chain stretching, and molecular weights of tethered chains. Shorter molecular weight polymer chains are more stretched when they are tethered, resulting in more drastic slow-down in chain relaxation, while the chain stretching and change in relaxation speed is trivial for very high molecular weight. We have studied the crowding effect controlled by grafting density of polymer chains to nanoparticle. Interestingly, we have found that lowering grafting density at low molecular weight chain could produce extreme polymer chain stretching and subsequently extraordinarily impeded relaxation behavior and that nanoparticles could impose another confinement effect on tethered chains at this condition. At the scale smaller than the size of one global chain, dielectric spectroscopy is performed to investigate segmental mode relaxation dynamics, complemented by glass transition measurement

using Differential Scanning Calorimetry (DSC). Relaxation time of chain segments is also increased and higher glass transition time is observed after tethering polymer chains to nanoparticles.

3.1. INTRODUCTION

Understanding the behaviors of polymer chains has always been a challenging problem in both soft matter and condensed matter physics. Movement of short linear polymer can be described using models for Brownian motion of beads linked by harmonic springs, or the Rouse model.[1-3] If the molecular weight of polymer chains is long enough, individual chains entangle to create topological constraints to adjacent chains, and polymers diffuse through the confined tubes, formed by neighboring chains, with a snake-like process termed reptation. Thus, above the entanglement molecular weight, the dynamics of linear polymers is usually explained with the Reptation model,[4-10] proposed by de Gennes,[4] Edward,[5] and Doi.[7] When polymers have more complicated architectures, such as star polymers, h-polymers, and combs, entanglements produce more complex changes in their dynamics, and the concepts of arm retraction and hierarchical relaxation play a crucial role in understanding the overall rheological response.[11-14]

Dynamics of entangled polymers, either linear, star, combs, h-polymers, or dendrimers, have been studied empirically with diverse approaches from NMR,[15-17] neutron scattering,[18-20] rheology,[15,17-23] dielectric spectroscopy,[17-20,24-69] and others.

Among these techniques, dielectric spectroscopy is advantageous especially when materials possess a net dipole moment on length scales comparable to the polymer end-to-end vector. In a dielectric spectrometer, a sinusoidal voltage is applied to sample electrodes and consequently in-phase and out-of-phase responses from electrodes are recorded to determine impedance, permittivity, resistance, capacitance, phase angle, and conductivity of sample materials.[24] As the dipoles of materials between the electrodes align with the direction of external electric field, these polarization responses correspond to relaxation of polymer bonds, segments, and chains.

It is known that there are three different types of dipoles in polymeric materials; type A, type B, and type C, which were first suggested by Stockmayer.[25] Type A dipoles are parallel to the chain backbone and type B dipoles are perpendicular to the backbone, while type C dipoles are attached onto side group on the backbone.[26] Therefore, by employing type A dielectric polymers, dielectric relaxation allows global chain, or normal mode, relaxation of the end-to-end vector of polymers to be investigated.

There are a large number of studies conducted to understand the global chain and segmental relaxation of polymers in various systems. With type A polymers, such as *cis*-1,4-polyisoprene (PI) and poly(propylene glycol) (PPG), the normal mode and segmental mode relaxation dynamics of simple linear homopolymer systems,[27-36] linear chains in dilute, semidilute, and concentration solution[37-40] systems using good

solvent and Θ solvent, and linear chains in homopolymer blend[40-43] and copolymer blend[17] systems have been examined.

In detail, on the subject of linear homopolymers, Adachi's group[27-28] and Boese et al.[29] empirically showed that the dielectric relaxation time of linear PI followed the Rouse theory below critical molecular weight, M_c (10,000 g/mol for PI), while the relaxation time obeyed the reptation theory above M_c. Adachi et al.[30] reported that the dielectric normal mode relaxation times approximately coincided with viscoelastic relaxation times of PI. Roland and Ngai[31] found that the widths of segmental mode relaxation from dielectric loss spectra of polybutadiene (PBD) depended on the varying vinyl contents of PBD and also on the molecular structure by comparing PBD with PI. Rossler's group[32] performed the study on a wide range of molecular weight from 652 to 436,000 g/mol of PI and found the relationship between the ratio of the normal mode to the segmental mode relaxation time and molecular weight, and observed the evolution of normal mode relaxation spectrum over a vast spectrum of frequency. Stockmayer and coworker[33] first reported the normal mode relaxation of PPG, and Ngai et al.[34] found that hydrogen bonding of the OH end group of PPG led to coupling between chains, resulting in stronger dependence of normal mode relaxation time on molecular weight than predicted by the Rouse theory. Kaminski and coworkers[35] controlled the coupling between PPG chains by adopting two different PPG end groups of OH and NH_2 units. Mijovic et al.[36] investigated the relaxation dynamics of linear PPG chains with symmetrically inverted dipoles.

To understand the behaviors of linear polymers in solutions and blends, Adachi et al.[37-39] and Patel et al.[40] carried out the investigation into the normal mode relaxation of different molecular weights of PI in a good solvent, moderately good solvent, and theta solvent from dilute, semidilute, to concentrated solutions to find that the Rouse-Zimm theory explained the relaxation in the diluted concentration while at high concentration the dielectric loss spectrums were broader than predicted by the Rouse-Zimm model. Adachi and coworkers[41-42] conducted the dielectric relaxation measurements to understand the relaxation time and the end-to-end vector of high molecular weight test chain in low molecular weight matrix and vice versa in the binary blends of PI. van Ruymbeke et al.[43] and Watanabe et al.[44] used the concept of dynamic tube dilution (DTD) to explain the binary blends of PI which describes that the slower component has a dilated tube, or the increased tube diameter, for relaxation after the faster component in the blends relax beforehand. Lodge, Ediger, Mijovic, and coworkers[17] reported the monomer friction coefficients using rheology, pulse field-gradient NMR, and dielectric spectroscopy and then compared with the theoretical values from Lodge-McLeish model in polyisoprene/poly(vinylethylene) blends.

By synthesizing diblock[45-48] and triblock[49-50] copolymers where one block is a type A polymer and others are non type A, global chain and segmental relaxation dynamics of polymers restricted by nanodomains of other blocks have been studied. Alig et al.[45] examined the dielectric relaxation dynamics of polyisoprene (PI) in polyisoprene-polystyrene (PI-*b*-PS) diblock copolymers. Both the normal mode and the segmental mode relaxation of PI in block copolymers were slower with respect to the bulk PI homopolymer. Stuhn et al.[46] observed the broadened relaxation spectrum

in dielectric loss of diblock copolymers compared to the homopolymers. Floudas and coworkers[47] reported on the dynamics of PI in symmetric PI-*b*-PS diblock copolymers, finding the dynamics of both the homopolymer PI and PI subchain in diblock copolymer was changed in the blends which could be qualitatively explained by the reptation and the arm retraction model, respectively. Watanabe's group[48] observed the thermo-rheological complexity of the dielectric and viscoelastic data in diblock copolymers of polyisoprene and poly(*p*-*tert*-butylstyrene) (PtBS) in comparison with PI/PtBS blends. This was because the PI block was forced to relax slower anchored by the less movable PtBS block at low temperature, whereas at high temperature the difference in their relaxation speed reduced. Floudas and coworkers[49] suggested that the dielectric spectroscopy could be utilized as a dynamic probe of the interface in ordered triblock copolymers, showing the new chain dynamics related to the mobility of the junction points at the interface. Watanabe et al.[50] studied the dielectric behavior in relation to nanodomain morphology of PS-*b*-PI (SI) diblock and PS-*b*-PI-PI-*b*-PS (SIIS) triblock copolymers which has the head-to-head dimer of isoprene block creating the dipole inversion at the midpoint of the middle II block.

Expanding the dimensions of polymer architectures from simple linear chains to more elaborate designs such as stars,[51-52] branched polymers,[53] dendrimers,[54] and nanonetworks[55-56] is another effective way to produce confinement effects. Boese, Kremer, and Fetters[51] studied that the relaxation time of a tethered chain of star polymers was approximately four times of the relaxation time for a free chain of the same length, regardless of the number of star arms and the molecular weight of each arm. Watanabe et al.[52] reported that the DTD molecular picture couldn't explain the

dynamics of star PI because the star polymers had broad distribution of relaxation. Mijovic and coworkers[53] carried out the study on the dynamics of multigraft copolymers, such as comb-, centipede-, and barbwire-shaped copolymers, of PI and PS. In their study, PI backbone was restricted by PS grafts, leading to the slower PI relaxation in multigraft copolymers than its untethered counterpart. Watanabe et al.[54] evaluated the validity of DTD in an entangled Cayley-tree-type polyisoprene, a three-arm star where each arm carries two outer arms to ultimately form two layers of inner arms, near the core, and the outer arms. Mijovic et al.[55-56] performed the studies on the dielectric and viscoelastic relaxation of the nanocomposites, based on polyhedral oligomeric silsesquioxane (POSS) and PPG, and also the nanonetworks of POSS and PPG. Intriguingly, the authors found that the normal mode and segmental mode processes were faster in the nanocomposites with increasing POSS concentration because POSS reduced the interactions among the PPG chains. On the other hand, both relaxation modes became slower and broader as the reaction between POSS and PPG proceeded to form the nanonetworks.

In addition to these methods, other approaches have been investigated to confine polymers and to delineate its consequences on relaxation dynamics of polymers. Thin films on substrates with controlled film thickness,[57-58] locating polymer chains between two dimensional nanolayers changing interlayer space[59-61] or into 3 dimensional nanopores altering pore size,[62-63] and placing nanoparticle fillers into polymer matrix without any interactions between nanoparticles and polymers[64] have all been used to produce the steady confinement effects on polymer conformation and dynamics.

Specifically, Serghei et al. found[57] the new relaxation mode in thin films of PI induced by the immobilization of chain segments at an interface but the changes in the segmental and normal mode were not shown. Mapesa et al.[58] also investigated the PI thin film structure and observed large changes in normal mode relaxation above the critical molecular weight of PI. It is surmised that the differences in the results between two studies arise from the different thin film preparation and loading methods.

On the topic of chains in 2D nanolayers and 3D nanopores, Mijovic et al.[59] reported that the relationship between the radius of gyration (Rg) of PI and the interlayer spacing of silicate plates determined the dielectric relaxation dynamics of PI. If the Rg of PI was longer than the interlayer spacing, the end-to-end vector of PI chains was extended and, in consequence, exhibited longer relaxation time. Hernandez et al.[60] observed the Maxwell-Wagner-Sillars effect in dielectric loss spectra which was attributed to interfacial polarization at the interface between nanolayers and polymers in natural rubber and silicate nanocomposites. Schonhals and coworkers[61] investigated the segmental mode relaxation dynamics of the nanocomposites composed of polypropylene (PP) and layered double hydroxides. Archer's group[62] controlled the degree of confinement in glass nanopore by coating with a monolayer of oligomers. In the study, the pore size of porous glass was comparable to the PI random coil size. After the coating deactivated the adsorbable sites of the surface, the slowing down of global chain relaxation disappeared. Floudas et al.[63] observed the broadened spectrum of the normal mode and the segmental mode in dielectric loss data of unentangled PI within the nanoporous alumina, indicating the wide distribution of

relaxation events within the nanoporous alumina. Ding and coworkers[64] studied that the segmental mode was slowed down to some extent and the normal mode relaxation was slightly slower by adding C_{60} nanoparticles to PI. Thus, it is speculated that the insertion of nanoparticles into polymeric matrix, without any interactions between them, affects the relaxation dynamics mostly at the scale of polymer segments.

More efficient method to control the dielectric relaxation of chains in the composites of nanoparticle fillers and polymer matrix is tuning the interaction between polymers and nanoparticles. With the adsorption to particle surface, several studies reported the segmental relaxation of immobilized polymers on silica particles.[65-68] Kirst et al.[65] studied the segmental mode relaxation of poly(dimethylsiloxane) (PDMS) adsorbed on hydrophobic and hydrophilic fumed silica. The authors observed that the PDMS chain segments in the adsorption layer were more movable in the hydrophobic fumed silica compared to the hydrophilic one. Roland and coworkers[66] investigated the segmental dynamics in the nanocomposites of poly(vinyl acetate) (PVA) and silica nanoparticles. It was shown that the segmental mode relaxation speed in the nanocomposites remained same in comparison with that of bulk PVA whereas the dielectric intensities of segmental mode relaxation in dielectric loss spectra reduced in the nanocomposites. Kumar, Mijovic, Gidley, and coworkers[67] immobilized poly(2-vinylpyridine) (P2VP) on silica nanoparticles and found that the nanoparticle fillers marginally slowed down the segmental dynamics. Schonhals's group[68] studied PVA adsorbed on silica nanoparticles and two different segmental mode relaxations were detected: one related to chain motions near the particle surface and the other associated with the motion of bulk-like chains. They also found that glass transition

temperature increased because of reduced chain mobility. It is conjectured that the contradictory results in the similar material system of polymers adsorbed on nanoparicles is originated from the sample preparation methods, including annealing condition.

Previously, we proposed that the normal mode relaxation of silica nanoparticle (SiO_2) tethered *cis*-1,4-polyisoprene could be explained using an arm retraction model similar to that used to explain the relaxation of the entangled star polymers.[69] This SiO_2-PI system is unique since every polymer chain is tethered to and confined by nanoparticles. In particular, without any extra solvent, this material exhibits fluid-like properties, and thus is termed as self-suspended nanoparticle suspension. Since every polymer is tethered to nanoparticle and there is no free polymer, one hybrid unit of nanoparticle-tethered polymer is polymer nanocomposite itself and is the building block of whole polymer nanocomposite system. Therefore, this material system makes it possible to employ high signal-to-noise measurements in bulk scale to examine the nanoscale dynamics of polymer chains.

In this study, by deliberately attaching polymer chains to spherical nanoparticles with controlled grafting density, we are particularly interested in how tethering, crowding, and confinement by nanoparticles change the dielectric and viscoelastic relaxation of nanoparticle-tethered PI, encompassing the complete molecular weight regime from unentangled to well-entangled range. We find that tethering restricts the relaxation of chains in all molecular weight ranges studied and also makes the end-to-end distance of chains stretched. As the lessened grafting density produces the

diminished chain crowding on particles and the strengthened confinement between particles, these systematic studies of SiO_2-PI with varying grafting density will allow us to isolate and understand how crowding and confinement affect chain dynamics. We report that it is possible to tailor the degree of entanglement by controlling the grafting densities of polymer chains to nanoparticles.

3.2. EXPERIMENTAL METHODS

3.2.1. Polymerization and Polymer End-Functionalization

Methyl and secondary amine terminated polyisoprene[70] were synthesized with anionic living polymerization. After purification with n-butyl lithium, cyclohexane was distilled and stored on a vacuum line. Isoprene monomer, purified with n-butyl lithium, was added, followed by addition of sec-butyl lithium in cyclohexane as initiator at room temperature. As the polymerization was propagated, the color change in the reaction solution to orange was observed. For baseline methyl terminated polyisoprene, the polyisoprenyl lithium solution was terminated with isopropanol and precipitated with excess methanol. To create secondary amine terminated PI, N-benzylidene methylamine (Sigma-Aldrich) was added for functionalization, and later followed by termination with isopropanol and precipitation with excess methanol.

3.2.2. Preparation of Nanoparticle-Tethered Polymers

The method of preparing sulfonic acid functionalized silica nanoparticles was described previously.[71,72] Briefly, silica nanoparticles were functionalized with sulfonic acid ligands and then purified extensively by dialysis to remove unattached ligands. Secondary amine terminated polyisoprene was dissolved in THF and this PI solution was added slowly to sulfonic acid functionalized silica nanoparticle aqueous solution in a media bottle. When the solution in the bottle starts to become milky, indicating phase separation, addition of PI solution was stopped but instead pure THF solvent was added until the solution became transparent again. This step of alternately adding PI in THF and pure THF was repeated until the targeted amount of PI was introduced to the reactor. By varying the amount of PI below the amount set by the stoichiometric ratio to sulfonic acid groups on silica, it was possible to manipulate the grafting density over a rather wide range. After about 5 days of reaction at room temperature while the reactor was covered by aluminum foil to avoid sunlight, water and THF was dried at room temperature, generating the mixture of nanoparticle-tethered polyisoprene and untethered polyisoprene. Untethered polyisoprene was removed with repeated precipitation (usually 6-7 times) using toluene and methanol. Finally, nanoparticle-tethered PI was dried in vacuum oven at room temperature about 5 days and stored in vacuum oven while vials were always covered by aluminum foil.

3.2.3. Gel Permeation Chromatography (GPC)

Molecular weights (M_n and M_w) and polydispersities (M_w/M_n) were determined by Waters ambient temperature GPC equipped with a Waters 410 refractive index

detector and 486 UV-Vis detector. Polyisoprene was dissolved in THF with the concentration of 1mg/ml.

3.2.4. Thermogravimetric Analysis (TGA)

The grafting densities of PI chains to silica nanoparticles were determined using thermal gravimetric analysis TGA Q1000 (TA Instruments). A fixed temperature scan rate of 5 °C/min was used to ramp the materials from 20 to 600 °C under a nitrogen atmosphere, and the total mass of inorganic and organic polymer was determined.

3.2.5. Differential Scanning Calorimetry (DSC)

Glass transition behaviors were studied using a DSC Q2000 (TA Instruments). Samples were heated to 100 °C, then cooled to -100 °C at a fixed rate of 2 °C/min, and finally heated up to 100 °C at 2 °C/min under nitrogen flow. The glass transition step change was recorded from the second heating cycle.

3.2.6. Small Angle X-ray Scattering (SAXS) Measurements

Examination of the static structure factor $S(q) = I(q) / \lim_{\phi \to 0} I(q)$ obtained from SAXS measurements. Experiments were carried out at Sector 12–ID–B of the Advanced Photon Source (APS) at the Argonne National Laboratory with extremely small exposure time (0.2 s), providing insight into the degree to which the particles are correlated.

3.2.7. Dielectric Spectroscopy

Frequency dependent dielectric loss and dielectric constant were measured using Novocontrol Broadband Dielectric Spectrometer with Quatro temperature control. Isothermal frequency sweep experiments were carried out in the wide range of temperature above the glass transition temperature. Samples were loaded to the inner area of Teflon ring spacer, sandwiched between the gold plated copper electrodes.

3.2.8. Mechanical Rheometry

Frequency-dependent and strain-dependent oscillatory shear measurements were performed using stress controlled Rheometer, Anton Paar MCR 301, outfitted with cone and plate fixtures at various temperatures. First, samples were presheared to erase previous history until the strain sweep data were reproducible. Data were collected following the sufficient waiting time. Strain sweep measurements were performed at a fixed shear frequency, ω =10 rad s^{-1}, and frequency sweep experiments were executed at a strain within the linear viscoelastic regime for each material.

To construct Time Temperature Superposition (TTS) plots, frequency sweep rheology experiments were performed from 0.1 to 10 rad/s at each temperature for 3 samples. Then, moduli data at different temperatures were shifted vertically and horizontally with the reference of 30°C moduli data for each sample.

3.3. RESULTS AND DISCUSSION

3.3.1. Structural Characterization

It is found that polyisoprene chains, which are synthesized with anionic living polymerization, have low polydispersity index (PDI) in Table 3.1. Entanglement molecular weight (M_e) of *cis*-1,4-PI is known to be ~5,000 g/mol and critical molecular weight (M_c) is twice M_e, ~10,000 g/mol.[32] Thus, by employing the molecular weight from 3.2K to 25.1K Da, the full spectrum of chain configuration from unentangled to well entangled regime is covered in this study.

To understand the effect of grafting density in the different molecular weight regime on the relaxation dynamics of tethered polymer chains, one molecular weight below M_c and the other above M_c are chosen to be grafted to the nanoparticle surface with the broad range of grafting densities from densely tethered to sparsely tethered. The limit of the lowest grafting density of polymer chains is determined at the extent where the polymer chains are still crowded enough so that none of chain backbone segment folds backwards to adsorb on the nanoparticle surface, determined from the theoretical calculation of chain configuration near the nanoparticle surface.

Figure 3.1 shows the scattering intensity from Small Angle X-ray Scattering (SAXS) experiments for nanoparticle-tethered PI 25.1K Da with different grafting densities. At the low q regime, the upturn in *I(q)* is not observed but scattering intensity has a plateau value, meaning there is no large scale particle aggregate within the system and the nanoparticles and well dispersed.

In the absence of a suspending fluid, nanoparticle-tethered polymers are subject to a space-filling constraint, which leads to extension of the chains away from the surface of particles.[72] These physics have been shown to lead to soft glassy rheology even in the limit of moderate particle loadings ($\phi \sim 10\%$)[69,73,74] and to an increased degree of correlation among the particles. Results reported in Figure 3.2 and Figure 3.3 show that the arrangement of nanoparticles in single-component fluids are quite different from those typically seen in the suspensions of hard spheres (HS) at comparable particle volume fractions (shown in dashed lines in the figures), for which a molecular solvent fills the inter–particle space. The strong deviation of the measured *S(q)* from the structure factor values of HS suspensions in the low *q* region and the enhanced correlation peaks are consistent with these expectations[74] and in accord with expected results for an incompressible molecular fluid in which all elements are identical. These self-suspended systems can therefore be employed as model systems to examine the relaxation dynamics of nanoparticle-tethered chains.

3.3.2. Viscoelastic Relaxation

Figure 3.4 illustrates the soft-glassy behavior of nanoparticle-tethered polyisoprene of molecular weight 7.2K Da with the grafting density of 1.21 chains/nm^2. Soft glasses, proposed by Sollich et al.,[75,76] are the colloidal glasses which exist in the metastable energy states where particles are trapped in tight cages formed by potential energy wells. In Figure 3.4, three distinct flow regimes are observed: (i) at low shear strains, strain independent linear viscoelastic regime, where G' is larger than

G", (ii) at intermediate shear strains, a nonlinear viscoelastic regime, where G" increases, and (iii) at high strains, a strain softening liquid regime where the loss modulus is larger than the storage modulus and both moduli are decreasing functions of the shear strain. One distinct feature of soft glasses, different from free polymers, is the maximum of loss modulus when the storage modulus reduces.[73]

Since the maximum in G" is originated from the energy dissipated during the cage breaking of soft glasses,[77] the relative size of loss maximum compared to G" in the linear viscoelastic regime at low shear strains reflects the measure of jamming within the system.[73] It is shown in Figure 3.5a that the normalized loss maximum is increasing with temperature, which indicates that materials are more jammed at higher temperature. Loss tangent, G"/G', decreases in the linear regime with increasing temperature in Figure 3.5b, implying more solid-like or more jammed system at elevated temperature. Noise temperature signifies the activation energy available for hopping of particles to escape the cages and has the following relationship with phase lag, δ;[73]

$$X = 1 + \frac{2}{\pi}\delta$$

As temperature increases, noise temperature monotonically decreases, which suggests that the energy, which is required to escape out of the cages, is less available within the system (Figure 3.5c). This jamming behavior with raised temperature was formerly reported for the nanoparticle-tethered polymers with different polymer chemistries or different molecular weights under the critical molecular weight of each

polymer chemistry.[73] It was demonstrated that low molecular weight polymer chains interpenetrate each other more intensely at the elevated temperature when tethered to nanoparticles, called thermal jamming.

Another jamming behavior is observed for SiO_2-PI in this study by changing the grafting density of polymer chains. It is plotted in Figure 3.6a, b, and c that the relative size of loss maximum increases, tan δ decreases, and noise temperature decreases as the grafting density of 7.2K PI chains decreases, meaning that lower grafting density leads to more jammed or more solid-like system. Therefore, like thermal jamming, jamming could be induced by lowering grafting density of nanoparticle-tethered polymer chains. It is thought that when low molecular weight polymers are sparsely attached to nanoparticles, the number of grafted polymer chains to the number of nanoparticle anchors is small and hence, each chain has to stretch further to fill the space, compared to the densely tethered polymer chains do. When stretched longer, chains are more interpenetrated each other, creating deeper energy potential wells in the energy landscape of the materials (Figure 3.7).

While jamming with higher temperature and lower grafting density is clearly shown for low M_w polymers below the M_c, high M_w polymers such as 25.1K PI chains don't exhibit thermal jamming and additionally grafting density induced jamming is weak. For nanoparticle-tethered 25.1K Da PI with grafting density of 1.91 chains/nm^2 (Figure S1), the normalized loss maximum is more or less same, loss tangent increases, and noise temperature also increases with elevated temperature, which are the usual characteristics of viscoelastic materials. Hence, when the molecular weight is

larger than M_c and polymers are well entangled, increasing temperature could not produce jamming. Figure S2a, b, and c present the subtle jamming caused by lowering the grafting densities for nanoparticle tethered 25.1K PI. Increased relative size of loss maximum is observed by reducing the grafting densities in Figure S2a, indicating the lessened number of chains generates jamming, similar to the short chains. However, the trends in loss tangent and noise temperature are somewhat unclear. Indeed noise temperature and tan δ are gradually increasing function of grafting densities, implying that nanoparticle-tethered high M_w polymers are more jammed with decreasing the numbers of the tethered chains. However, tan δ and noise temperature of free polymer are smaller than those of tethered polymers, which means that tethering rather make the system more fluidic from more solid-like highly entangled polymers. It is conjectured that when 2Rg of free polymer is comparable to or larger than the size of nanoparticles, tethering to nanoparticles could probably disentangle the highly entangled free polymer chains and raising temperature doesn't lead to jamming of the system.

Time Temperature Superposition (TTS)[3,78] presents the mechanical properties of materials in the wide frequency spectrum, or longer windows of time scales. Instead of performing one frequency sweep measurement from extremely low to very high frequency, which would take enormous period of time to finish for low frequency range and also would be inaccurate for very high frequency region due to the inertia of motor, several short frequency window experiments are usually executed in the range of 0.1 to 10 rad/s. Subsequently, storage and loss moduli data from 0.1 to 10 rad/s at each temperature are simultaneously shifted in accordance with reference moduli data

at a reference temperature, resulting in TTS master curve in the wide range of frequency. The horizontal and vertical shift factors of untethered and tethered PI 7.2K are shown in Figure S3.

While the crossover points at TTS of free polymers are known to be Kuhn monomer relaxation time, Rouse time of entanglement strand, Rouse time of the chain, and reptation time depending on the molecular weight, polymer chemistry, and frequency range,[3] the crossover point between storage and loss modulus in TTS (Figure 3.8) of nanoparticle-tethered PI 7.2K is the cage breaking time of the jammed material. The cage breaking time of sparsely tethered polymer with 1.21 chains/nm^2 grafting density is ~460,000 times longer than that of densely tethered polymer of 1.68 chains/nm^2. It is because more stretched and thus more interpenetrated chains form excessively tighter cages when sparsely tethered. For the lowest grafting density of 0.84 chains/nm^2, cages are exceedingly rigid at every temperature in Figure S4 and could not be broken apart in these experimental conditions.

TTS for untethered and tethered 25.1K PI is shown in Figure S5. The plot for free polymer is expected: the slope of loss modulus at low frequency range is -1 and the slope of storage modulus is -2. On the other hand, TTS of tethered 25.1K shows the complicated flow behaviors, which are very similar to the TTS of multi-arm polymers.[23] It is speculated that the trade-off between the disentanglement by tethering M_w chains and jamming by lowering grafting density makes the energy landscapes of these nanoparticle-tethered high M_w chains extraordinarily intricate, leading to the broad overlap regime between both moduli.

From the rheology experiments, bulk scale dynamics of nanoparticle-tethered polymers in unentangled and well-entangled regime is studied. It is demonstrated that tethering to nanoparticles transform unentangled polymers into soft glasses, while highly entangled polymers experience disentanglement by tethering. At higher temperature, short chains are more jammed while long tethered chains become more liquid-like.

The grafting density onto nanoparticle surface is reflected as the extent of crowding of chains. Whether the molecular weight is low or high, less crowded chains will experience more jamming in comparison with polymers surrounded by a multitude of neighbors. If the grafting density is low, each chain has to stretch longer compared to crowded chains, leading to more interpenetration of polymer chains. Jamming with lower grafting density is significant for short chain, creating strikingly long cage breaking time whereas disentanglement by tethering of highly entangled chains makes the jamming with lower grafting density tricky.

3.3.3. Global Chain Relaxation Dynamics

Dielectric spectroscopy provides the information about the global chain dynamics from the responses of the end-to-end vector of type A dielectric polymer chains. Typical dielectric loss (ε") spectra of untethered and tethered PI with low molecular weight are shown in Figure 3.9 for PI 3.2K Da. First of all, the peak locations of dielectric loss have shifted dramatically to the lower frequency at each

temperature. The peak location is converted to the relaxation time by the following equation;

$$\tau = 1/2\pi\omega_p$$

where ω_p is the frequency of dielectric loss peak. Thus, tethered polymers have significantly longer relaxation time at each temperature. Secondly, the peak width has been broadened after tethering at each temperature. Thirdly, the peak intensity and peak area of dielectric loss are stronger and larger as tethered.

Likewise, when the molecular weight of polyisoprene is higher than critical molecular weight, broadened width, higher intensity, and larger peak area are observed (Figure S6). However, it is found that the relaxation time of high M_w PI is more or less same after tethering.

One important remark should be clearly made about the difference between the relaxation times determined from rheology and dielectric spectroscopy. Watanabe et al.[44, 79-81] reported that the crossover point of storage and loss moduli in frequency sweep rheology results occurs two time faster than the relaxation peak of ε" in dielectric spectroscopy measurements of polymer systems. It was explained that while the correlated orientation of end-to-end vector is recorded by dielectric spectrometer, rheometer reads the shear dependent orientation of polymer molecules. In this study, the crossover of mechanical moduli is found at the lower frequency than the peak location of ε" for tethered polymers with the several order magnitude separation. It is because the crossover of moduli for nanoparticle-tethered polymers is the cage

breaking time of soft glasses, which is much slower than the relaxation of polymer chains. Consequently, it is regarded that rheology shows the bulk scale relaxation, whereas dielectric spectroscopy probes the nanoscale global chain relaxation of nanoparticle-tethered polymers.

To completely understand the changes in spectra, all dielectric loss data are fitted with a model function. Unlike Debye model, which assumes all energy potential wells are symmetric, Havriliak-Negami (H-N) model describes that there are multiple asymmetric energy potentials within the system.[24] Debye equation expresses the ideal ε" relaxation spectrum when Cole-Cole equation presents the symmetric broadening of the ε" peak and Cole-Davison model reflects the asymmetric broadening.[24] Because H-N model is the most generalized expression from Debye, Cole-Cole, and Cole-Davidson models, H-N theory is thought to be the most appropriate model to describe nanoparticle-tethered polymers with the complicated energy landscapes. The H-N function for the frequency dependent permittivity $\varepsilon^*(\omega)$ is given by

$$\varepsilon^*(\omega) = \varepsilon_\infty + \frac{\Delta\varepsilon}{(1 + (i\omega\tau_{HN})^\beta)^\gamma} = \varepsilon'(\omega) - i\varepsilon''(\omega)$$

where β (0<β) describes symmetric broadening, γ (βγ≤1) for asymmetric broadening, τ_{HN} for H-N relaxation time, ω for frequency, ε_∞ the dielectric constant (ε') at high frequency limit, and Δε the dielectric strength.[24] Dielectric intensity at ε' plot is calculated with $\Delta\varepsilon = \varepsilon_s - \varepsilon_\infty$ where ε_S the dielectric constant (ε') at low frequency

limit. At the same time, dielectric strength could be determined from ε" spectra by integrating the area under ε" peaks;

$$\Delta\varepsilon = (\pi/2)\int \varepsilon''(\omega)\, d\, ln\omega$$

All of the dielectric loss data are fitted with following function,[24] which is the imaginary part of ε*.

$$\varepsilon''(\omega) = \Delta\varepsilon \left[1 + 2(\omega\tau_{HN})^{\beta}\cos\left(\frac{\beta\pi}{2}\right) + (\omega\tau_{HN})^{2\beta}\right]^{-\gamma/2} sin\left\{\gamma\, arctan\left[\frac{sin(\beta\pi/2)}{(\omega\tau_{HN})^{-\beta} + cos(\beta\pi/2)}\right]\right\}$$

It is known that fitting experimental ε' data to the H-N function of the real part of ε* produces the same results as performing analysis with empirical ε" to the H-N function of the imaginary part of ε*. As one of our interests is to decide the relaxation time, which is the peak of ε", ε" data are chosen for fitting. From H-N fitting, four parameters are determined, τ_{HN}, Δε, β, and γ. Figure S7 and Figure S8 show that the ε" equation from H-N model fits well to the empirical data either at low or high temperature. In comparison with Figure S9 of relaxation times calculated from the peak values of raw ε" data, it could be concluded from Figure 3.10 that H-N function provides reliable fitting for all molecular weight range and also the relaxation time is not model dependent but is the inherent feature of untethered and tethered polymers.

Among these four parameters from H-N fitting, it is found that relaxation time exhibits the most pronounced change by tethering. In Figure 3.10, the relaxation time,

τ_{HN}, of untethered and densely tethered PI is plotted for diverse molecular weights from unentangled to well-entangled regime. It is obviously presented that once polymers are tethered, the relaxation time of polymer chains becomes longer.

Interestingly, higher the molecular weight of polymer chains, the difference between the relaxation times of untethered and densely tethered is smaller in Figure 3.10. The ratio between the relaxation time of densely tethered to untethered is plotted in Figure 3.11. When the molecular weight is below the critical molecular weight, this time ratio is over 10^4. For PI of molecular weight 3.2K Da, tethered chains relax about $2*10^4$ times slower than untethered chains do. As the molecular weight of polymer chains is longer, the time ratio reduces sharply. When the molecular weight is higher than the critical molecular weight of PI, this time ratio is independent on molecular weight but rather ranges between 2-4.

Boese et al.[29] reported that the relaxation time of star polymer is 4 times of that of linear counterparts regardless of the number of arms and the molecular weight of each arm. Surprisingly, the relaxation time ratio of nanoparticle-tethered to untethered chains for high M_w is close to the ratio of star to free polymer. Previously, we reported that the relaxation time of nanoparticle-tethered polymers could be predicted with arm retraction model for star polymers since nanoparticle-tethered polymer system resembles the structure of star polymers apart from the size difference between nanoparticles and linkers of star polymers.[69]

When polymer chains are tethered to the surface of nanoparticles, the one end of chain is immobilized to the surface. If polymer chains are densely grafted, not only the

end points of chains but also some chain length near the surface is "immobilized" due to the crowded neighbor chains. The length of this restricted chain by crowding is stem length (l), which is determined with the equation;[71]

$$l \approx R\left(b_K \Sigma^{1/2} - 1\right)$$

where R is radius of nanoparticle, b_K Kuhn monomer length of PI, and Σ the grafting density. The stem lengths for nanoparticle-tethered chains are calculated in Table 3.1. As shown in the equation, the stem length is determined only by the grafting density not by the molecular weight of the whole chain, even though longer molecular weight chains will tend to have lower grafting density compared to short M_w chains because of the steric hindrance during grafting-to synthesis method to nanoparticles. The rest of a chain above the stem length would be less restricted regarding their degree of freedom to move, and the magnitude of restriction to a segment decreases, as the chain segment is farther away from the surface.

Figure 3.12a and b illustrate the polymer chain configuration around the nanoparticles for low and high M_w chains, respectively. It is assumed that the grafting density of low and high M_w chains is same and very dense. The degree of restriction being imposed to chain segments is expressed by the intensity of colored line in the figure. Red color indicates the most extreme restriction and yellow signifies the minimal confinement like the condition of free polymers. The portion of stem length in a chain would be much larger for shorter chain. If the chain is extremely short so that every segment of a chain is in the stem length region as in Figure 3.12a, then chains would relax significantly slow, like short chains densely tethered to the flat

surface relaxing though the confined tubes with very narrow diameter. On the contrary, for very long chains (Figure 3.12b), the fraction of stem length in a chain would be trivial, and thus chains would be immobilized only in the vicinity of nanoparticles while the chain segments near the open ends feel like they are free polymer, far away from the surface. Since anyway one end of this long chain is anchored, they would relax by mimicking the arm retraction mechanism of stars. Therefore, the relaxation time ratio of tethered to untethered in Figure 3.11 is thought to be close to the ratio for star to linear polymer at very high M_w while the time ratio is substantially high for short M_w chains.

The second parameter from H-N fitting, which has another noticeable changes by tethering, is dielectric strength or dielectric intensity, Δε. Figure 3.13 shows the dielectric strength (left Y-axis), obtained from H-N fitting, versus temperature for diverse molecular weights. Dielectric intensity is related to the mean end-to-end distance r with the following relationship;[79]

$$\Delta\varepsilon_n = \frac{4\pi N_A {\mu_p}^2 F_{onsager}}{3k_B TM}\langle r\rangle^2$$

with N_A Avogadro number, μ_p dipole moment, $F_{onsager}$ Onsager correction factor, k_B Boltzmann constant, T absolute temperature, M molecular weight, r the mean end-to-end distance of polymer chains. The ideal free polymer should have the value of 1.22 for $\langle r^2\rangle^{\frac{1}{2}}/2R_g$ where the mean end-to-end distance r is divided by 2Rg. Thus, $\langle r^2\rangle^{\frac{1}{2}}/2R_g$ of untethered polymers from H-N fitted Δε at 293.15K is taken as

reference, and then corrected to 1.22 with a correction factor α. Same value of correction factor α is applied to the calculated $\langle r^2 \rangle^{\frac{1}{2}} / 2R_g$ of tethered polymers at each molecular weight. Subsequently, right Y-axis is the characteristic dimensionless length, describing how much chains are stretched or collapsed compared to the ideal chain value of 1.22.

In all molecular weight regimes, dielectric intensity and the characteristic dimensionless length increase after tethering, which indicates that tethering to nanoparticles makes polymer chains stretched. For lowest M_w 3.2K, this chain stretching is most dramatic: polymer chains are stretched about 7 times compared to free polymer in Figure 3.13a. This stretching by tethering is less effective as the molecular weight increases and for 25.1K, stretching of the most densely tethered chains is less than 1.5 times.

Moreover, it is found that the characteristic length of tethered polymers is increasing function with temperature while the characteristic length is weak-decreasing function for free polymer. The characteristic length of free polymer decreases because Hookean constant reduces with temperature. For nanoparticle-tethered chains, thermal jamming of nanoparticle-tethered polymers, where chains are more stretched and interpenetrated at higher temperature, could support the stretching of tethered polymer chains with temperature measured by dielectric spectrometer.

Another chain stretching is noticed when the grafting density reduces for 7.2K and 25.1K Da (Figure 3.13b and d, respectively). At 7.2K M_w, sparsely tethered

polymers have more stretched chains compared to densely tethered polymers. The most sparsely tethered 7.2K PI is about 4-5 times longer than densely tethered 7.2K PI. Sparsely tethered 25.1K chains also show stretching in comparison with densely tethered 25.1K, but the ratio is much smaller than that of 7.2K. This chain stretching with lowering grafting density could be complemented by jamming of less crowded chains. As chains are more stretched and more interpenetrated at lower grafting density, they exhibit jamming behavior demonstrated by strain sweep rheology experiments.

To further understand the effect of crowding to the relaxation dynamics, the relaxation times of untethered and tethered 7.2K PI with different grafting densities are plotted in Figure 3.14. The relaxation times of densely tethered polymers at the grafting density of 1.68 chains/nm^2 are only ~2-4 times longer than those of untethered polymers. As M_w 7.2K is close to the critical molecular weight, it is predicted that the ratio between relaxation time of tethered to untethered PI is small, close to the ratio of star polymers. However, it is not expected that sparsely tethered polymers relax considerably slower than densely tethered polymers.

When the lateral spacing (ξ), the distance between the nearest chains onto the nanoparticle surface, is longer, the restriction due to crowding is weaker. If the lateral spacing is larger than Kuhn monomer length, 0.84nm for PI, then it is expected that polymer chains are not crowded at the nanoparticle surface. As summarized in Table 3.1, sparsely tethered PI 7.2K of 1.21 chains/nm^2 and 0.84 chains/nm^2 are anticipated to have lengthy lateral spacing and even stem length is calculated to be 0.

As we reported previously,[69] polymer chains have to retract down near the nanoparticle surface, then restretch again to find new configuration along the narrow tubes, formed by neighbor polymer chains, when polymer chains relax. Based on this hypothesis for the relaxation mechanism for tethered polymer chains, it is predicted that the relaxation time of these sparsely tethered PI is a little bit shorter than that of the most densely tethered but longer than that of untethered PI. Since it is anchored, they relax slower compared to free polymer. At the same time, they are not crowded as densely tethered polymers of 1.68 chains/nm^2, and subsequently it is guessed that they would relax faster in comparison with densely tethered ones due to the limited crowding.

However, the results from dielectric spectrometer in Figure 3.14 show that sparsely tethered polymers exhibit substantially slower relaxation behaviors compared with either free or densely tethered. This implies that there is another confinement effect being applied to this system, leading to further slower motion. In Table 3.2, the interparticle distance, the distance from the center of one particle to the center of another one, is calculated with the following equation, assuming the system is hard sphere suspension of silica nanoparticle in polyisoprene;[82]

$$\lambda = d\left(\frac{0.63}{\phi}\right)^{1/3}$$

where d is particle diameter and ϕ is silica nanoparticle volume fraction. Furthermore, the distance from surface of one nanoparticle to surface of another nanoparticle is calculated by subtracting silica nanoparticle diameter, d from interparticle distance.

From Figure 3.13, it is observed that polymer chains stretch as they are tethered to nanoparticles, whereas free polymers have coiled conformation. The Rg of 7.2K PI is 2.66nm and the contour length Nb is 50.4 nm. When densely tethered with the grafting density of 1.68 chains/nm^2, the $\langle r^2 \rangle^{1/2}$, or polymer brush height is about 10nm while the surface-to-surface distance is about 14.7nm. For 1.21 chains/nm^2 grafting density polymer chains, surface-to-surface distance is ~12.3nm whereas chains are stretched about 40nm. This indicates that polymer chains of 1.21 chains/nm^2 are stretched over 1 polymer-tethered nanoparticle distance (brush + core + brush,12.3 + 10 + 12.3 nm). When polymer chains are most sparsely tethered with grafting density of 0.84 chains/nm^2, tethered polymer chains have brush height extended to ~50nm over 9.9nm of surface-to-surface nanoparticle distance, which implies that chains are stretched over 2 polymer-tethered nanoparticle distance. More sparsely tethered polymer has more stretched chain while the surface-to-surface distance is shorter because nanoparticle content increases relative to the amount of polymer chains in the system.

This more coiled or more stretched configuration of chains is depicted in Figure 3.15. Free polymer has usual coiled conformation as in Figure 3.15a. When they are tethered and crowded enough, only chain segments near the nanoparticle surface are extended and as the distance from the surface is longer, they have more room to be coiled as shown in Figure 3.15b. At high grafting density, polymer arms are less likely to be stretched over another nanoparticle distance and the arm retraction model could predict their relaxation speed. On the other hand, Figure 3.15c describes that the

nanoparticles act like obstacles to polymer chains when chains retract down near the particle and restretch as they relax. Hard inorganic nanoparticles could impose further entanglement effect on the tubes of tethered chains and this new confinement by nanoparticles determines the relaxation time of sparsely tethered polymers. This jamming, resulted from reducing grafting density observed from dielectric spectrometer results, could be complementarily supported by rheology experiments, where jamming with lowering grafting density and longer cage breaking time are found.

It was previously reported that the grafting density didn't affect the relaxation time for nanoparticle-tethered PI of M_w 5K.[69] The lateral spacing of these materials is calculated to be always smaller than Kuhn monomer length, meaning they were all densely tethered. Thus, the nominal change in relaxation time with different grafting densities was resulted from the grafting density within the bounds of densely tethering.

The crowding effect on the relaxation time of high molecular weight chains is shown in Figure S10. Tethered chains have similar relaxation speed compared to each other regardless of the grafting density. Even the most sparsely tethered PI 25.1K with the grafting density of 0.91 chains/nm^2 exhibit the relaxation time similar to that of densely tethered 25.1K, although it has similar grafting density to the most sparsely tethered PI 7.2K with 0.84 chains/nm^2 showing dramatic slow-down. For very high molecular weight, nanoparticle volume fraction is very small because the molecular weight of polymer is high. This means that the surface-to-surface distance of the nanoparticles would be long. In addition, it is shown in Figure 3.13 that chain

stretching of tethered PI 25.1K is weak. Therefore, it is thought that arm retraction model dominates the relaxation mechanism for high molecular weight.

Finally, another 2 parameters from H-N fitting are β and γ. β describes the symmetric broadening of relaxation spectrum, whereas γ presents the asymmetric broadening above the peak frequency in dielectric loss spectra (Figure 3.16a). Once polymer chains are tethered to nanoparticles, they always exhibit lower value of β and βγ in Figure 3.16b, meaning that material system deviates from ideal Debye model after tethering.

Activation energy could be derived from fitting relaxation time to Vogel-Fulcher-Tamman (VFT) equation;[71,83]

$$\log(\tau) = A + \left(\frac{B}{T - C}\right)$$

where A is the high temperature limit of the relaxation time, B is the activation energy, T is the absolute temperature, and C is Vogel temperature. Figure 3.17 shows the activation energy of untethered and tethered PI with diverse molecular weights versus core volume fraction. As the grafting density decreases, the silica nanoparticle core volume fraction increases. It is found that once polymer chains are tethered to nanoparticles and also the grafting density reduces, they always need higher activation energy for polarization under the external electric field in dielectric spectrometer, which is in good agreement with other data.

After tethering, global chains relax through the arm retraction mechanism that is slower compared to free polymer. In addition, tethered chains are more stretched and the relaxation spectrum is broadened. Smaller the molecular weight of chains, more considerable the slow-down effect is for nanoparticle-tethered with dense grafting density since more portion of a polymer chain is immobilized.

The degree of crowding is crucial when molecular weight of tethered chains is short. By reducing crowding of chains, chain stretching and slower chain relaxation could be reinforced. It is because fewer numbers of chains have to stretch more to fill the space, also shown by jamming with lower grafting density from rheology experiments.

Nanoparticle could impose another confinement, or entanglement effect to the system when polymer chain is short and tethered sparsely so that chains have to travel over another polymer-tethered nanoparticle distance when they relax. Like entangled free polymer, nanoparticles could impose topological constraints to the tubes of tethered chains. The critical condition for this nanoparticle entanglement is determined by polymer chain molecular weight, grafting density, degree of chain stretching, and the nanoparticle concentration.

3.3.4. Segmental Mode Relaxation Dynamics and Glass Transition

It is found that tethering and crowding effects on segmental relaxation dynamics are similar to those on global chain dynamics. Figure 3.18 shows the segmental mode

relaxation time of untethered and tethered PI M_w 3,200 and 25,100, where the segmental relaxation times of different grafting densities of 25.1K Da are plotted. While segmental mode relaxation time for 25.1K remains similar regardless of tethering and crowding, segmental relaxation time of 3.2K becomes ~2500 times slower by tethering. After tethering, segmental mode relaxation is slower at low M_w, but the extent of slowing down in segmental mode relaxation is relatively minuscule compared to that of global chain relaxation.

Kirkwood and Frohlich proposed the equation for the intensity of segmental mode relaxation peaks as following;[64, 84]

$$\Delta\varepsilon_{\text{seg}} = \text{g}\frac{4\pi FN\rho\mu^2}{3k_BT}$$

here, $\Delta\varepsilon_{seg}$ is dielectric intensity of segmental mode relaxation peak in ε", F is local field correction, and g is Kirkwood Frohlich correlation factor measuring the correlation between dipole moments in neighboring units. Tethering enhances $\Delta\varepsilon_{seg}$ of 3.2K, which means that g becomes larger and subsequently there are stronger intermolecular interaction leading to the decrease in relaxation rate of segmental mode. On the other hand, noticeable change in $\Delta\varepsilon_{seg}$ is not observed for 25.1K. As depicted in Figure 3.12, when the whole chain is more restricted in low molecular weight, also the local movement of chain segments is more confined for densely tethered short chains. On the contrary, local motion of chain segments in the free polymer-like region of high molecular weight would have the unrestricted local

motion. Analogous to normal mode relaxation, the grafting density at high molecular weight doesn't change the speed of segmental mode relaxation speed.

Glass transition temperature is the temperature at which the segmental motion can occur but energy is not enough for global chain motion.[3] By tethering polymers to nanoparticles, polymers lose mobility at one end, therefore the glass transition temperature goes higher as shown in Figure 3.19. Considering that the Tg difference of 3.2K after tethering is only 5°C, the effect of slow-down in segmental relaxation of ~2500 times is indeed tremendous. The glass transition temperature difference is smaller for higher molecular weight, analogous to the global chain relaxation time ratio of tethered to untethered in Figure 3.11. It is found that glass transition temperature is independent on the grafting densities in all molecular weight ranges.

3.4. CONCLUSIONS

The viscoelastic and dielectric relaxation dynamics of the material system where polymer chains are anchored to and confined by nanoparticles are studied. By attaching polymer chains to the spherical nanoparticles with changing grafting densities, effects of tethering, crowding, and confinement by nanoparticles are demonstrated.

After tethering, polymers change to soft glassy materials, showing enhanced jamming behaviors by increasing temperature from rheology. Dielectric spectroscopy experiments show that tethered polymer chains relax through arm retraction model,

and they have broader spectrum of relaxation. Chain stretching after tethering leads to longer relaxation time, and this chain stretching and slower relaxation time is more effective for shorter polymer chains.

Crowding, controlled by grafting density of polymer chains to nanoparticles, also plays an important role when molecular weight is short enough. Like jamming with temperature, another jamming and tighter cages could be induced with lowering grafting density, resulting in longer chain stretching and global chain relaxation time.

Nanoparticles could exert another confinement effect on polymer chains, when the molecular weight of tethered chains is short and they are sparsely tethered. Under this condition, nanoparticles impose topological constraints to the tubes of polymers. As polymers relax through the long tubes, nanoparticles act like obstacles.

Tethering and crowding are also influential on segmental mode relaxation dynamics, but the degree of effects is smaller because segmental mode relaxation is local motion.

ACKNOWLEDGMENTS

This work was supported by the National Science Foundation, Award No. DMR-1006323 and by Award No. KUS-C1-018-02, made by King Abdullah University of Science and Technology (KAUST). Facilities available though the Cornell Center for Materials Research (CCMR) were used for this study (DMR-1120296).

REFERENCES

1. Rouse, P. E. *J. Chem. Phys.* **1953**, *21*, 1272-1280.

2. de Gennes, P. G. *Macromolecules* **1976**, *9*, 587-593.

3. Rubinstein, M.; Colby, R. H. *Polymer Physics*; Oxford University Press: New York, 2003.

4. de Gennes, P. G. *J. Chem. Phys.* **1971**, *55*, 572-579.

5. Edwards, S. F.; Grant, J. W. V. *J. Phys. A: Math., Nucl. Gen.* **1973**, *6*, 1169-1185.

6. Klein, J. *Nature* **1978**, *271*, 143-145.

7. Doi, M.; Edwards, S. F. *Theory of Polymer Dynamics*; Oxford University Press: New York, 1988.

8. Kas, J.; Strey, H.; Sackmann, E. *Nature* **1994**, *368*, 226-229.

9. Perkins, T. T.; Smith, D. E.; Chu, S. *Science* **1994**, *264*, 819-822.

10. Russell, T. P.; Deline, V. R.; Dozier, W. D.; Felcher, G. P.; Agrawal, G.; Wool, R. P.; Mays, J. W. *Nature* **1993**, *365*, 235-237.

11. Kapnistos, M.; Lang, M.; Vlassopoulos, D.; Pyckhout-Hintzen, W.; Richter, D.; Cho, D.; Chang, T.; Rubinstein, M. *Nat. Mater.* **2008**, *7*, 997-1002.

12. Read, D. J.; Auhl, D.; Das, C.; den Doelder, J.; Kapnistos, M.; Vittorias, L.; McLeish, T. C.B. *Science* **2011**, *333*, 1871-1874.

13. de Gennes, P.G. *J. Phys*. **1975**, *36*, 1199-1203.

14. Milner, S. T.; McLeish, T. C. B. *Macromolecules* **1997**, *30*, 2159-2166.

15. Pearson, D. S.; Fetters, L. J.; Graessley, W. W.; Strate, G. V.; von Meerwall, E. *Macromolecules* **1994**, *27*, 711-719.

16. Graf, R.; Heuer, A.; Spiess, H. W. *Phys. Rev. Lett.* **1998**, *80*, 5738-5741.

17. Haley, J. C.; Lodge, T. P.; He, Y.; Ediger, M. D.; von Meerwall, E. D.; Mijovic, J. *Macromolecules* **2003**, *36*, 6142-6151.

18. McLeish, T. C. B; Allgaier, J.; Bick, D. K.; Bishko, G.; Biswas, P.; Blackwell, R.; Blottiere, B.; Clarke, N.; Gibbs, B.; Groves, D. J.; Hakiki, A.; Heenan, R. K.; Johnson, J. M.; Kant, R.; Read, D. J.; Young, R. N. *Macromolecules* **1999**, *32*, 6734-6758.

19. Bent, J.; Hutchings, L. R.; Richards, R. W.; Gough, T.; Spares, R.; Coates, P. D.; Grillo, I.; Harlen, O. G.; Read, D. J.; Graham, R. S.; Likhtman, A. E.; Groves, D. J.; Nicholson, T. M.; McLeish, T. C. B. *Science* **2003**, *301*, 1691-1695.

20. Likhtman, A. E. *Macromolecules* **2005**, *38*, 6128-6139.

21. Fetters, L. J.; Kiss, A. D.; Person, D. S.; Quack, G. F.; Vitus, F. J. *Macromolecules* **1993**, *26*, 647-654.

22. Archer, L. A.; Sanchez-Reyes, J.; Juliani. *Macromolecules* **2002**, *35*, 10216-10224.

23. Archer, L. A.; Juliani. *Macromolecules* **2004**, *37*, 1076-1088.

24. Kremer, F.; Schonhals, A. Broadband Dielectric Spectroscopy; Springer, 2003.

25. Stockmayer, W. H. *Pure Appl. Chem.* **1967**, *15*, 539-554.

26. Watanabe, H. *Macromol. Rapid Commun.* **2001**, *22*, 127-175.

27. Adachi, K.; Kotaka, T. *Macromolecules* **1984**, *17*, 120-122.

28. Adachi, K.; Kotaka, T. *Macromolecules* **1985**, *18*, 466-472.

29. Boese, D.; Kremer, F. *Macromolecules* **1990**, *23*, 829-835.

30. Adachi, K.; Yoshida, H.; Fukui, F.; Kotaka, T. *Macromolecules* **1990**, *23*, 3138-3144.

31. Roland, C. M.; Ngai, K. L. *Macromolecules* **1991**, *24*, 5315-5319.

32. Abou Elfadl, A.; Kahlau, R.; Herrmann, A.; Novikov, V. N.; Roossler, E. A. *Macromolecules* **2010**, *43*, 3340-3351.

33. Baur, M. E.; Stockmayer, W. H. *J. Chem. Phys.* **1965**, *43*, 4319-4325.

34. Ngai, K. L.; Schonhals, A.; Schlosser, E. *Macromolecules* **1992**, *25*, 3340-3351.

35. Kaminski, K.; Kipnusu, W. K.; Adrjanowicz, K.; Mapesa, E. U.; Iacob, C.; Jasiurkowska, M; Wlodarczyk, P.; Grzybowska, K.; Paluch, M.; Kermer, F. *Macromolecules* **2013**, *46*, 1973-1980.

36. Mijovic, J.; Sun, M.; Han, Y. *Macromolecules* **2002**, *35*, 6417-6425.

37. Adachi, K.; Okazaki, H.; Kotaka, T. *Macromolecules* **1985**, *18*, 1687-1692.

38. Adachi, K.; Kotaka, T. *Macromolecules* **1987**, *20*, 2018-2023.

39. Adachi, K.; Kotaka, T. *Macromolecules* **1988**, *21*, 157-164.

40. Patel, S. S.; Takahashi, K. M. *Macromolecules* **1992**, *25*, 4382-4391.

41. Adachi, K.; Nishi, I.; Itoh, S.; Kotaka, T. *Macromolecules* **1990**, *23*, 2550-2554.

42. Adachi, K.; Itoh, S.; Nishi, I.; Kotaka, T. *Macromolecules* **1990**, *23*, 2554-2559.

43. van Ruymbeke, E.; Masubuchi, Y.; Watanabe, H. *Macromolecules* **2012**, *45*, 2085-2098.

44. Matsumiya, Y.; Kumazawa, K.; Nagao, M.; Urakawa, O.; Watanabe, H. *Macromolecules* **2013**, *46*, 6067-6080.

45. Alig, I.; Kremer, F.; Fytas, G.; Roovers, J. *Macromolecules* **1992**, *25*, 5277-5282.

46. Stuhn, B.; Stickel, F. *Macromolecules* **1992**, *25*, 5306-5312.

47. Floudas, G.; Meramveliotaki, K.; Hadjichristidis, N. *Macromolecules* **1999**, *32*, 7496-7503.

48. Chen, Q.; Matsumiya, Y.; Masubuchi, Y.; Watanabe, H. *Macromolecules* **2011**, *44*, 1585-1602.

49. Alig, I.; Floudas, G.; Avgeropoulos, A.; Hadjichristidis, N. *Macromolecules* **1997**, *30*, 5004-5011.

50. Matsumiya, Y.; Chen, Q.; Uno, A.; Watanabe, H. *Macromolecules* **2012**, *45*, 7050-7060.

51. Boese, D.; Kremer, F.; Fetters, L. J. *Macromolecules* **1990**, *23*, 1826-1830.

52. Matsumiya, Y.; Watanabe, H. *Macromolecules* **2001**, *34*, 5702-5710.

53. Mijovic, J.; Sun, M.; Pejanovic, S.; Mays, J. W. *Macromolecules* **2003**, *36*, 7640-7651.

54. Watanabe, H.; Matsumiya, Y.; van Ruymbeke, E.; Vlassopoulos, D.; Hadjichristidis, N. *Macromolecules* **2008**, *41*, 6110-6124.

55. Bian, Y.; Pejanovic, S.; Kenny, J.; Mijovic, J. *Macromolecules* **2007**, *40*, 6239-6248.

56. Bian, Y.; Mijovic, J. *Macromolecules* **2008**, *41*, 7122-7130.

57. Serghei, A.; Kremer, F. *Phys. Rev. Lett.* **2003**, *91*, 165702.

58. Mapesa, E. U.; Tress, M.; Schulz, G.; Huth, H.; Schick, C.; Reiche, M.; Kremer, F. *Soft Matter* **2013**, *9*, 10592-10598.

59. Mijovic, J.; Lee, H.; Kenny, J.; Mayes, J. *Macromolecules* **2006**, *39*, 2172-2182.

60. Hernandez, M.; Carretero-Gonzales, J.; Verdejo, R.; Ezquerra, T. A.; Lopez-Manchado, M. A. *Macromolecules* **2010**, *43*, 643-651.

61. Purohit, P. J.; Huacuja-Sanchez, J. E.; Wang, D.; Emmerling, F.; Thunemann, A.; Heinrich, G.; Schonhals, A. *Macromolecules* **2011**, *44*, 4342-4354.

62. Zhang, Q.; Archer, L. A. *Macromolecules* **2003**, *19*, 8094-8101.

63. Alexandris, S.; Sakellariou, G.; Steinhart, M.; Floudas, G. *Macromolecules* **2014**, *47*, 3895-3900.

64. Ding, Y.; Pawlus, S.; Sokolov, A. P.; Douglas, J. F.; Karim, A.; Soles, C. L. *Macromolecules* **2009**, *42*, 3201-3206.

65. Kirst, K. U.; Kremer, F.; Litvinov, V. M. *Macromolecules* **1993**, *26*, 975-980.

66. Bogoslovov, R. B.; Roland, C. M.; Ellis, A. R.; Randall, A. M.; Robertson, C. G. *Macromolecules* **2008**, *41*, 1289-1296.

67. Harton, S. E.; Kumar, S. K.; Yang, H.; Koga, T.; Hicks, K.; Lee, H.; Mijovic, J.; Liu, M.; Vallery, R. S.; Gidley, D. W. *Macromolecules* **2010**, *43*, 3415-3421.

68. Fullbrandt, M.; Purohit, P. J.; Schonhals, A. *Macromolecules* **2013**, *46*, 4626-4632.

69. Agarwal, P.; Kim, A.; Archer, L. A. *Phys. Rev. Lett.* **2012**, *109*, 258301.

70. Quirk, R. P.; Cheong, T.; Yoo, T. *Macromol. Chem. Phys.* **2002**, *203*, 1178-1187.

71. Kim, A.; Archer, L. A. *Macromolecules* **2014**, *47*, 687-694.

72. Agarwal, P.; Qi, H.; Archer, L. A. *Nano Lett.* **2010**, *10*, 111−115.

73. Agarwal, P.; Srivastava, S.; Archer, L. A. *Phys. Rev. Lett.* **2011**, *107*, 268302.

74. Agarwal, P.; Archer, L. A. *Physical Review E* **2011**, *83*, 041402.

75. Sollich, P.; Lequeux, F.; Hebraud, P.; Cates, M. E. *Phys. Rev. Lett.* **1997**, *78*, 2020-2023.

76. Sollich, P. *Phys. Rev. E* **1998**, *58*, 738-759.

77. Ganeriwala, S. N.; Rotz, C. A. *Polym. Eng. and Sci.* **1987**, *27*, 165-178.

78. Dealy, J.; Plazek, D. *Rheology Bulletin*, **2009**, *78*, 16-31.

79. Watanabe, H. *Polymer J.* **2009**, *41*, 929-950.

80. Watanabe, H.; Ishida, S.; Matsumiya, Y.; Inoue, T. *Macromolecules* **2004**, *37*, 1937-1951.

81. Watanabe, H.; Ishida, S.; Matsumiya, Y.; Inoue, T. *Macromolecules* **2004**, *37*, 6619-6631.

82. Samanvaya, S.; Archer, L. A. *Phys. Rev. Lett.* **2013**, *110*, 148302.

83. Boyd, R.; Smith, G. *Polymer Dynamics and Relaxation*; Cambridge University Press: New York, 2010.

84. Yu, L; Cebe, P. *J. Polym. Sci., Part B: Polym. Phys.* **2009**, *47*, 2520-2532.

Table 3.1. Weight average molecular weight (M_w), number average molecular weight (M_n), polydispersity index (PDI), radius of gyration (Rg) of polyisoprene synthesized with anionic living polymerization in the left column. Silica nanoparticle core volume fraction (ϕ), grafting density (Σ), stem length (l), lateral spacing (ξ) of their nanoparticle-tethered polyisoprene in the right column.

Free PI				Silica nanoparticle tethered PI			
M_W	M_N	PDI	Rg (nm)	ϕ (%)	Σ (chains/nm^2)	l (nm)	ξ (nm)
3200	3000	1.07	1.77	5.99	2.84	2.07	0.59
7200	6900	1.04	2.66	4.23	1.68	0.45	0.77
				5.78	1.21	0	0.91
				8.1	0.84	0	1.09
13000	12600	1.03	3.57	2.91	1.35	0	0.86
25100	23300	1.08	4.96	1.11	1.93	0.83	0.72
				1.67	1.27	0	0.89
				2.34	0.91	0	1.05

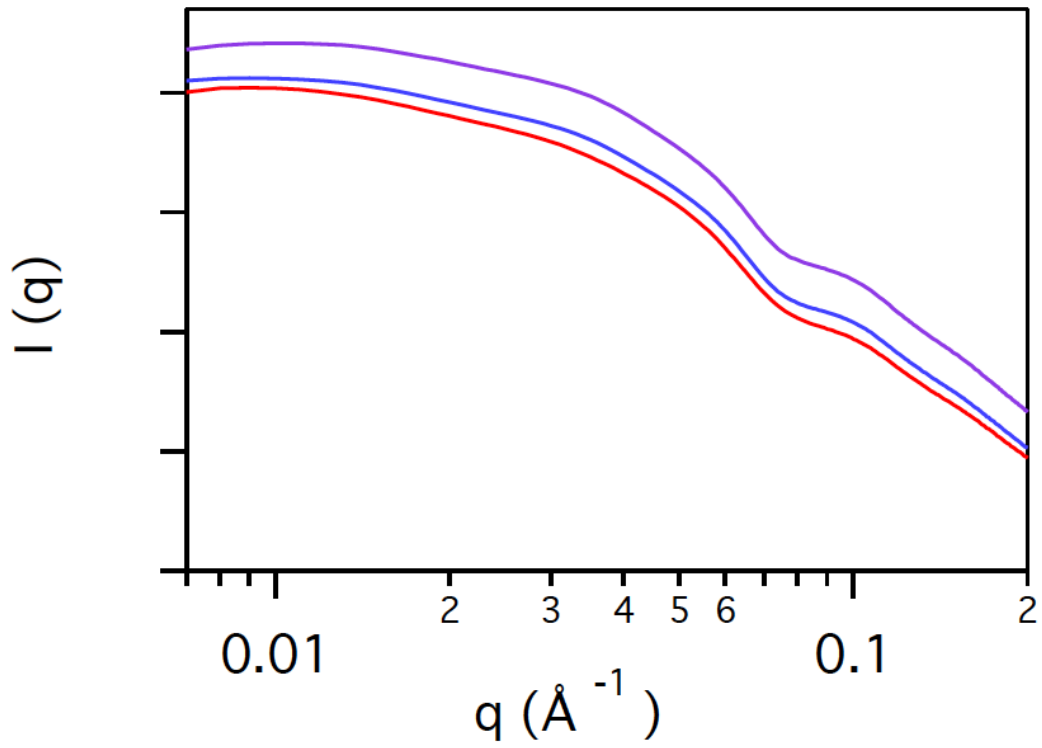

Figure 3.1. *I(q)* vs. *q* determined from Small Angle X-ray Scattering experiments of silica nanoparticle tethered PI with molecular weight of 25.1K Da and grafting densities of 1.93 chains/nm^2 (red line), 1.27 chains/nm^2 (blue line), 0.91 chains/nm^2 (purple line).

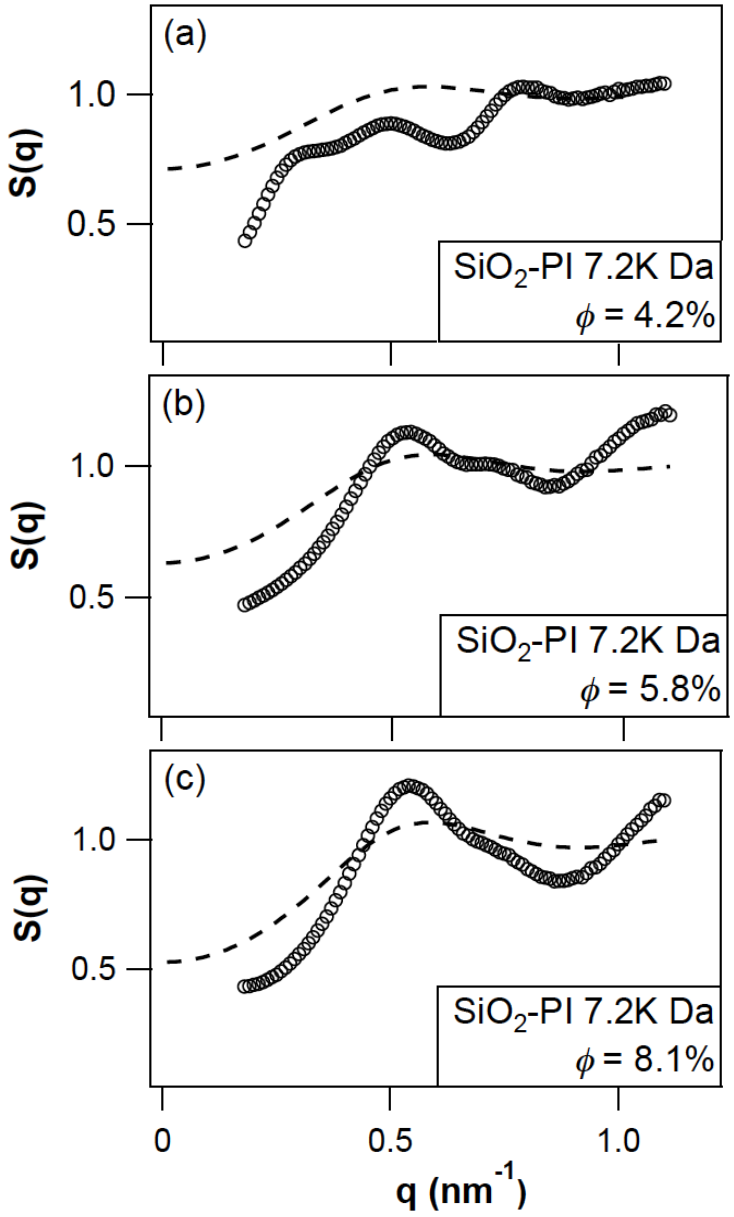

Figure 3.2. Structure factor $S(q)$ vs. q for self–suspended nanoparticle suspensions: (a) SiO_2 tethered PI of 7.2K Da with ϕ =4.2%; (b) SiO_2 tethered PI of 7.2K Da with ϕ =5.8%; and (c) SiO_2 tethered PI of 7.2K Da with ϕ =8.1%. All measurements were carried out at T = 30°C. The corresponding hard sphere suspension $S(q)$ are denoted by dashed lines.

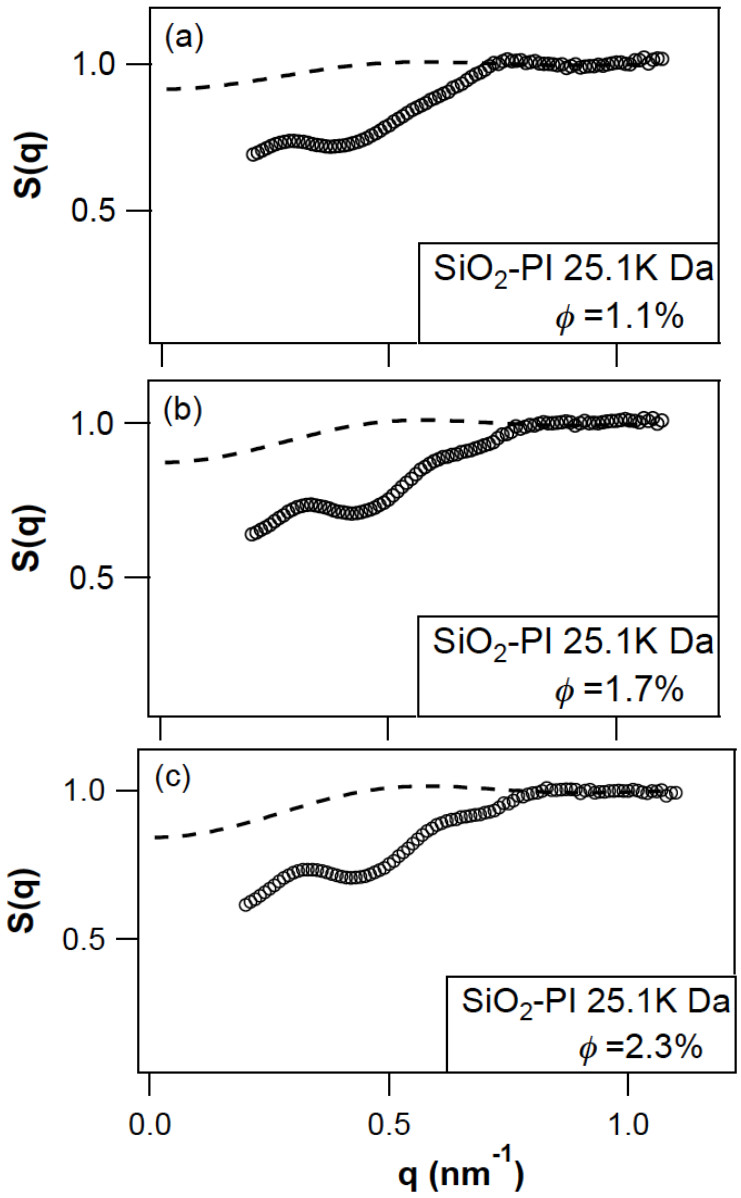

Figure 3.3. Structure factor $S(q)$ vs. q for self–suspended nanoparticle suspensions: (a) SiO_2 tethered PI of 25.1K Da with ϕ =1.1%; (b) SiO_2 tethered PI of 25.1K Da with ϕ =1.7%; and (c) SiO_2 tethered PI of 25.1K Da with ϕ =2.3%. All measurements were carried out at T = 30°C. The corresponding hard sphere suspension $S(q)$ are denoted by dashed lines.

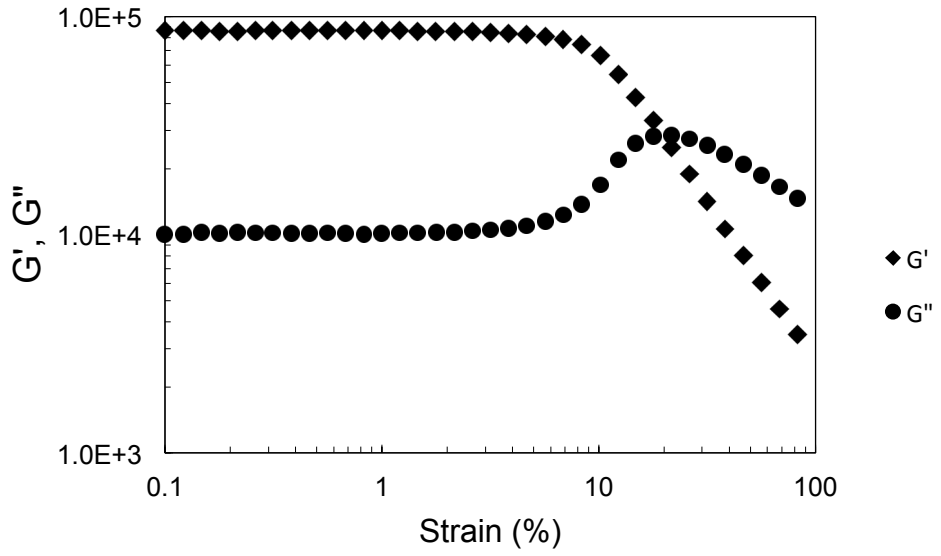

Figure 3.4. Dynamic storage (G') and loss (G") moduli [Pa] versus shear strain [%] for SiO_2 tethered PI with molecular weight of 7.2K Da and grafting density of 1.21 chains/nm^2. Strain sweep measurements were performed at a fixed oscillatory frequency of 10 rad/s at a temperature of 30 °C.

(a)

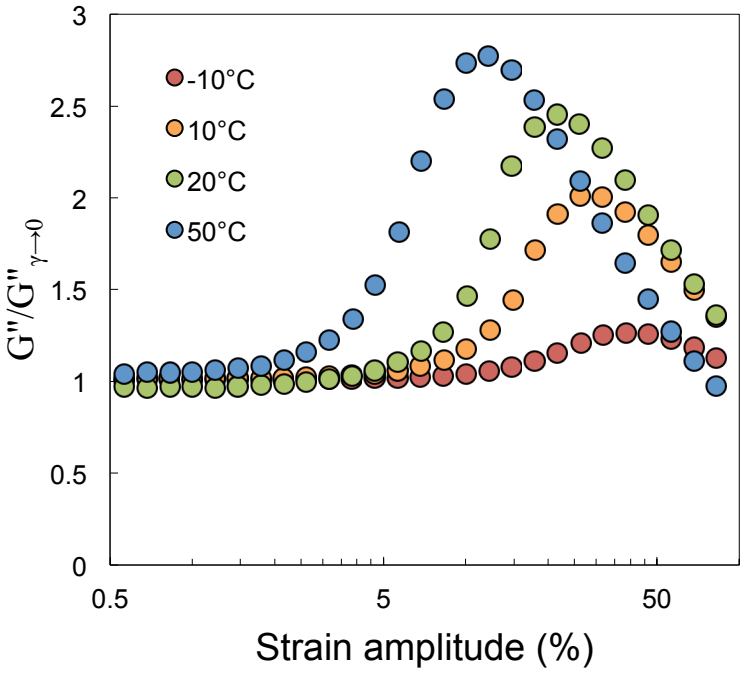
3
2.5
2
1.5
1
0.5
0
-10°C
10°C
20°C
50°C
G"/G"γ→0
0.5
5
50
Strain amplitude (%)

(b)

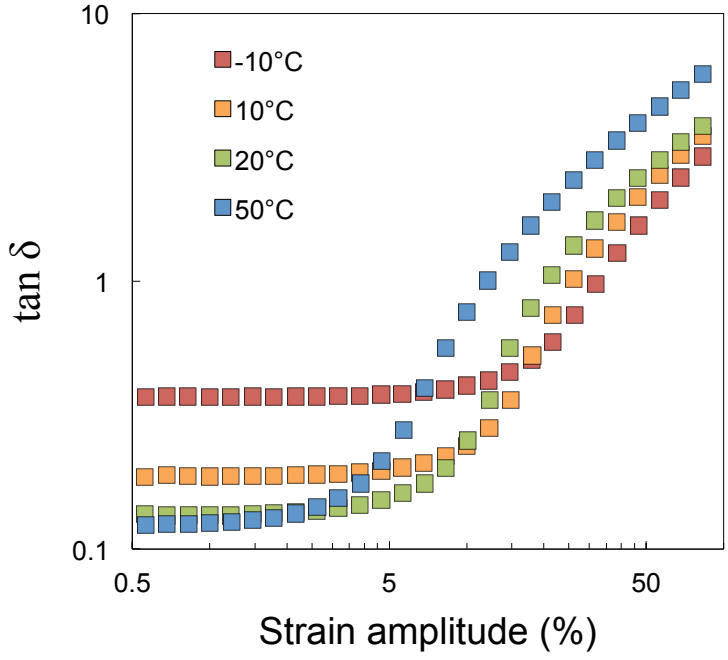
10
1
0.1
-10°C
10°C
20°C
50°C
tan δ
0.5
5
50
Strain amplitude (%)

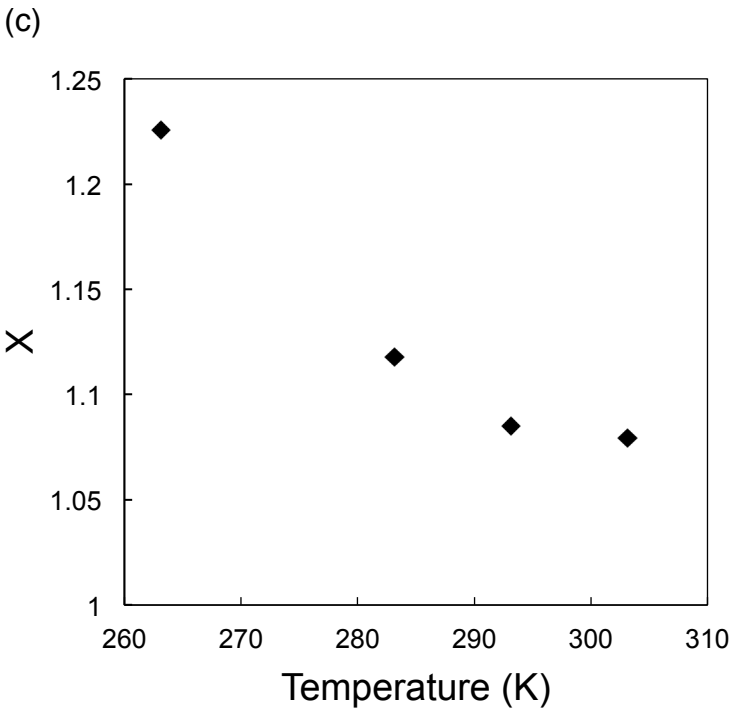

Figure 3.5. (a) Normalized loss maximum vs. strain amplitude [%]; (b) tan δ vs. strain amplitude [%]; and (c) Noise temperature (X) vs. temperature [K] for SiO_2 - PI of M_w 7.2K Da with grafting density of 1.21 chains/nm^2. Strain sweep measurements were performed at a fixed oscillatory frequency of 10 rad/s at different temperatures.

(a)

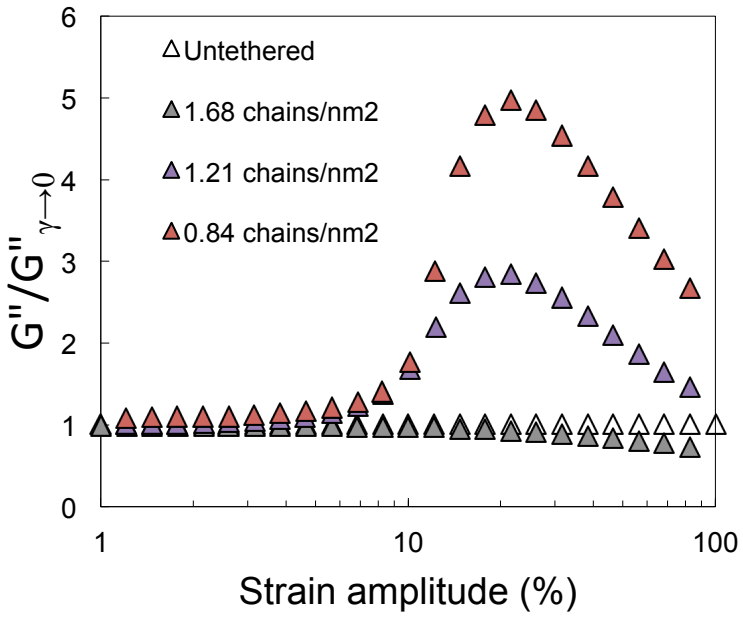
Untethered
1.68 chains/nm2
1.21 chains/nm2
0.84 chains/nm2
G''/G''γ→0
Strain amplitude (%)

(b)

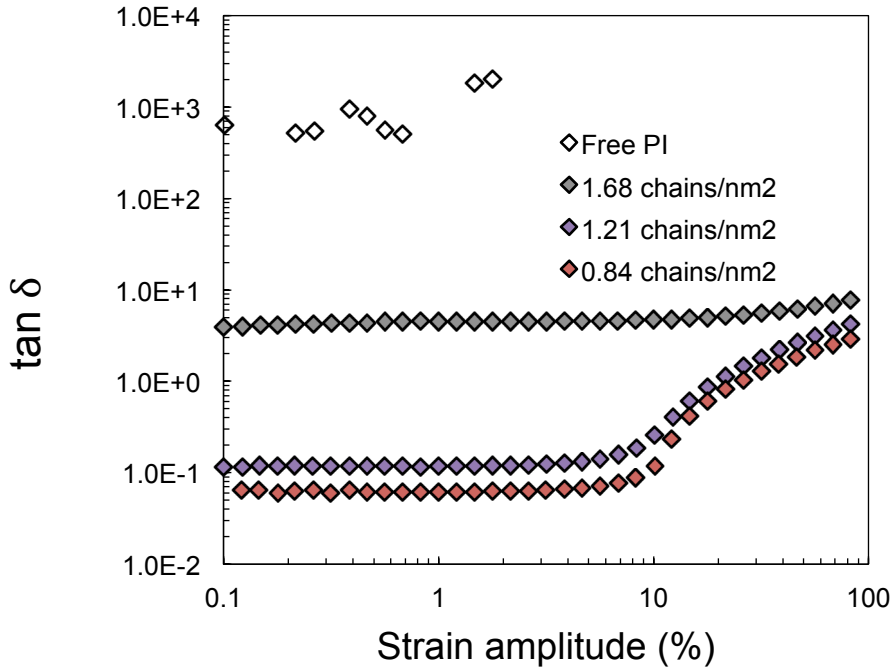
Free PI
1.68 chains/nm2
1.21 chains/nm2
0.84 chains/nm2
tan δ
Strain amplitude (%)

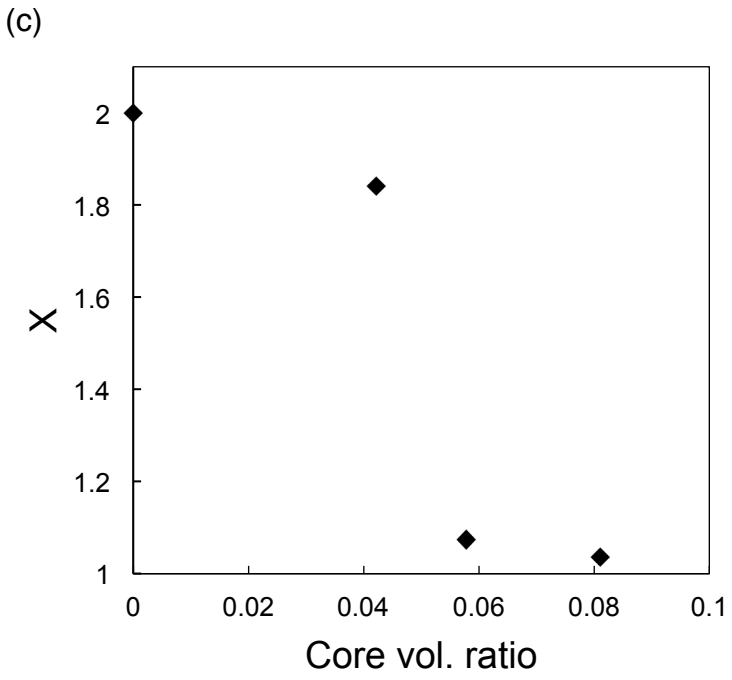

Figure 3.6. (a) Normalized loss maximum vs. strain amplitude [%]; (b) tan δ vs. strain amplitude [%]; and (c) Noise temperature (X) vs. temperature [K] for SiO_2 - PI of M_w 7.2K Da with different grafting densities. Strain sweep measurements were performed at a fixed oscillatory frequency of 10 rad/s at 30 °C.

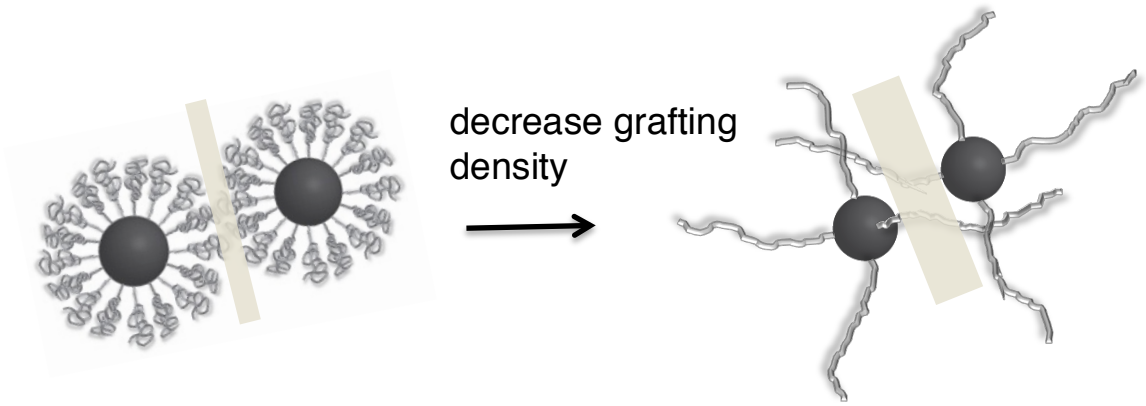

Figure 3.7. Illustration of enhanced jamming of nanoparticle-tethered polymers by decreasing grafting density.

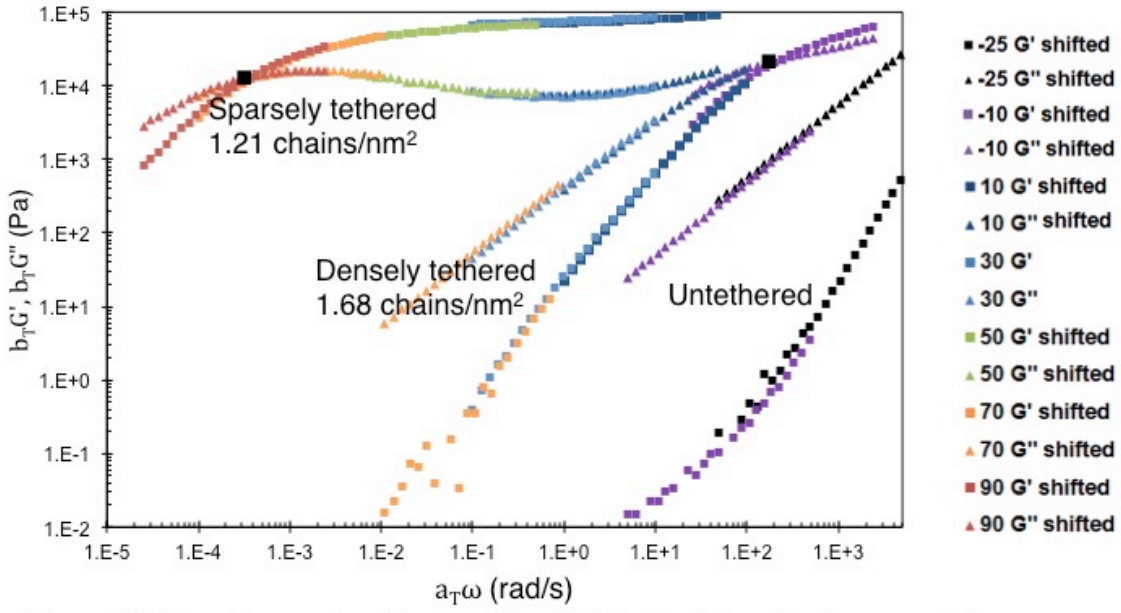

Figure 3.8. Time Temperature Superposition (TTS) for untethered and nanoparticle-tethered PI chains of molecular weight 7.2K Da with different grafting densities. 30 °C moduli data were used as reference.

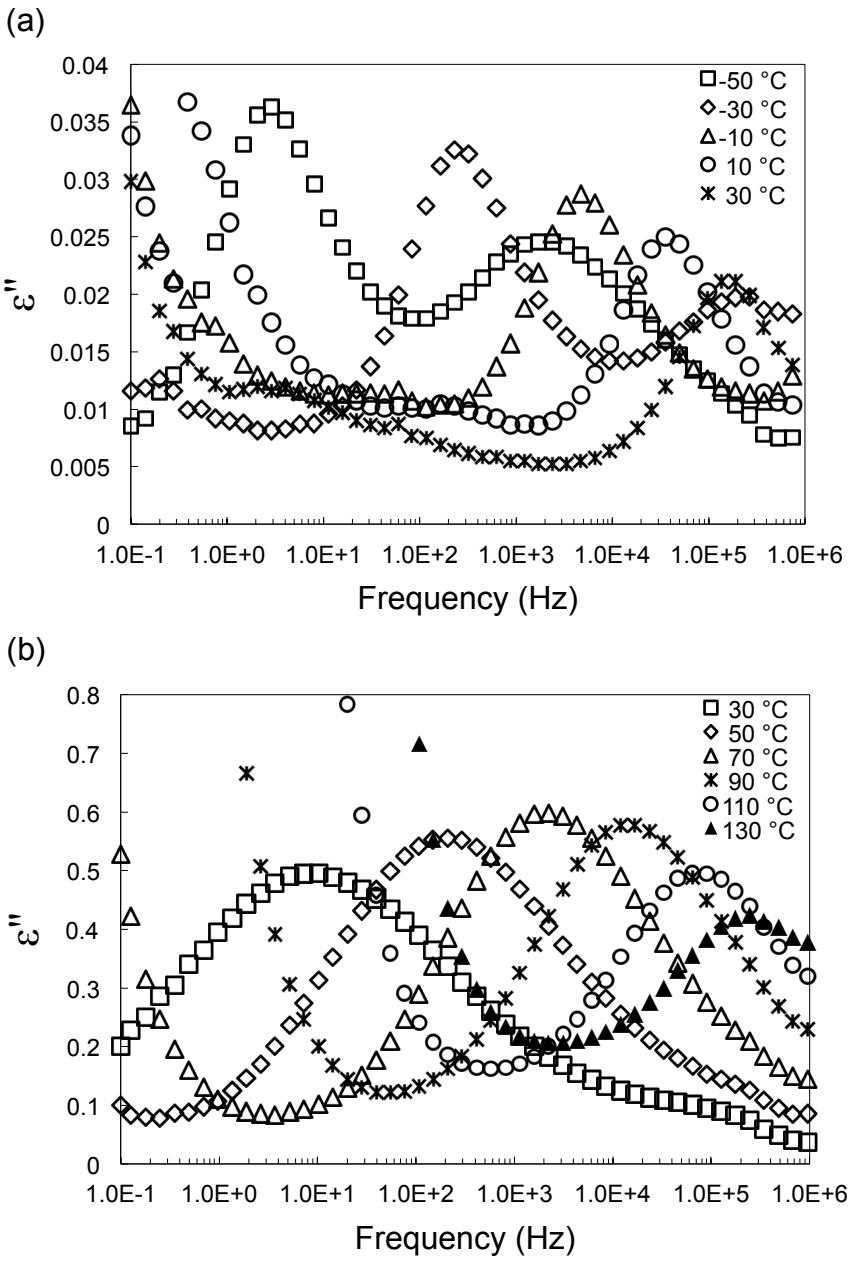

Figure 3.9. (a) Dielectric loss (ε") vs. frequency [Hz] for untethered PI M_W 3,200 g/mol at different temperatures. (b) Dielectric loss (ε") vs. frequency [Hz] for nanoparticle-tethered PI M_W 3.2K Da at different temperatures.

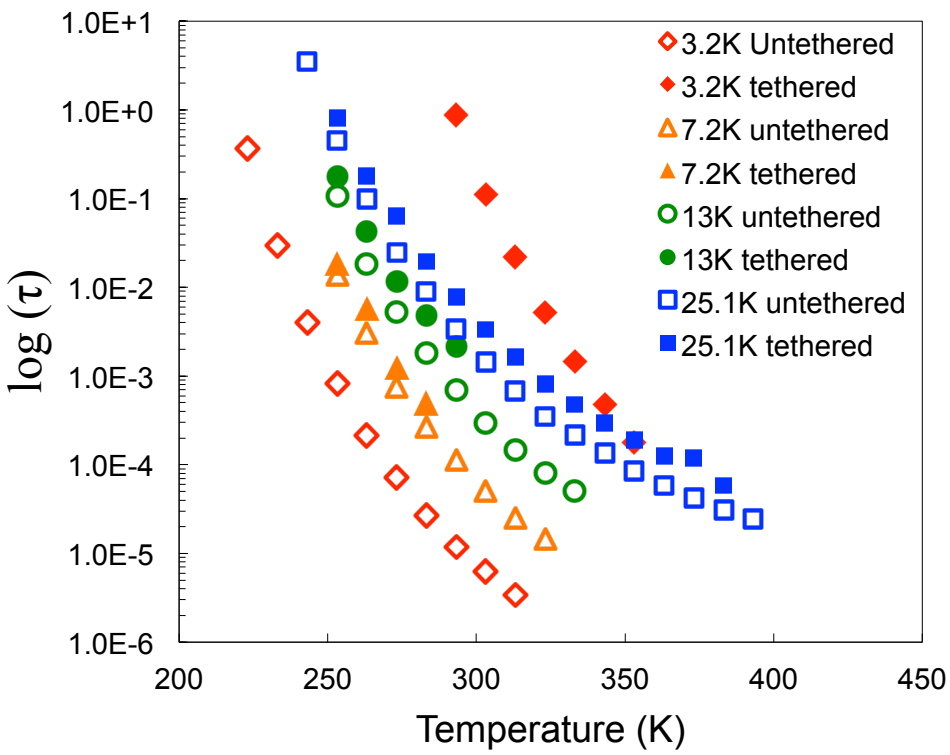

Figure 3.10. Relaxation time of untethered and nanoparticle-tethered polyisoprene of different molecular weights as a function of temperature obtained from H-N fits to the dielectric loss spectra. In this plot, tethered chains are densely tethered PI.

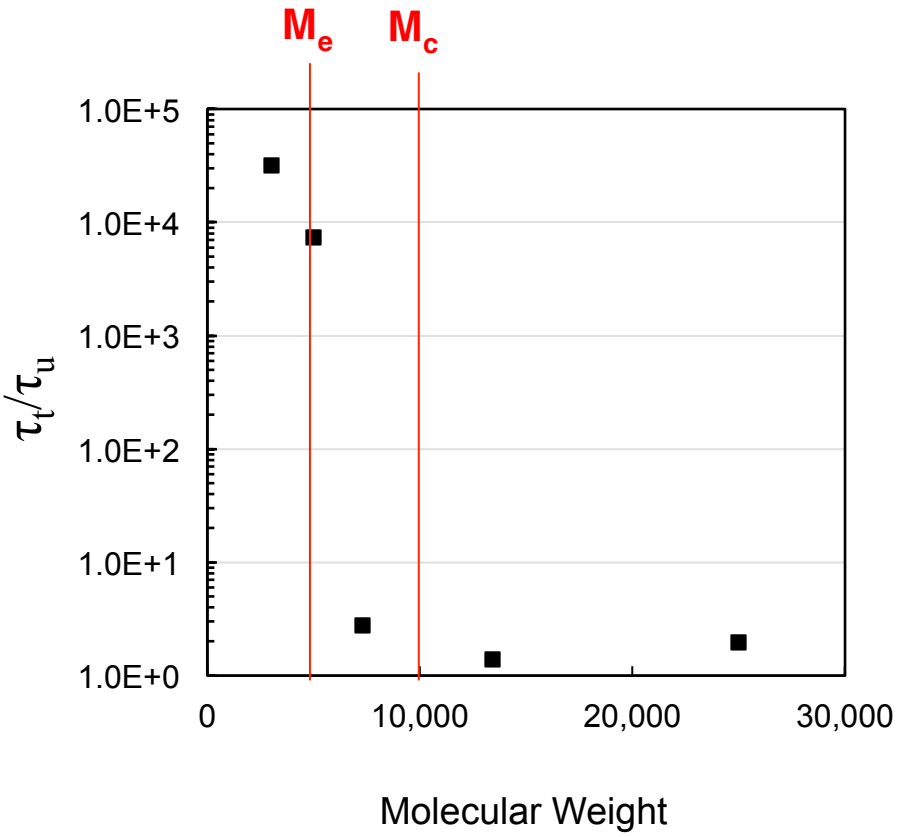

Figure 3.11. Relaxation time ratio between densely tethered and untethered PI with different molecular weights at a fixed temperature of 293.15K. Entanglement molecular weight, M_e, and critical molecular weight, M_c, are indicated by the red lines.

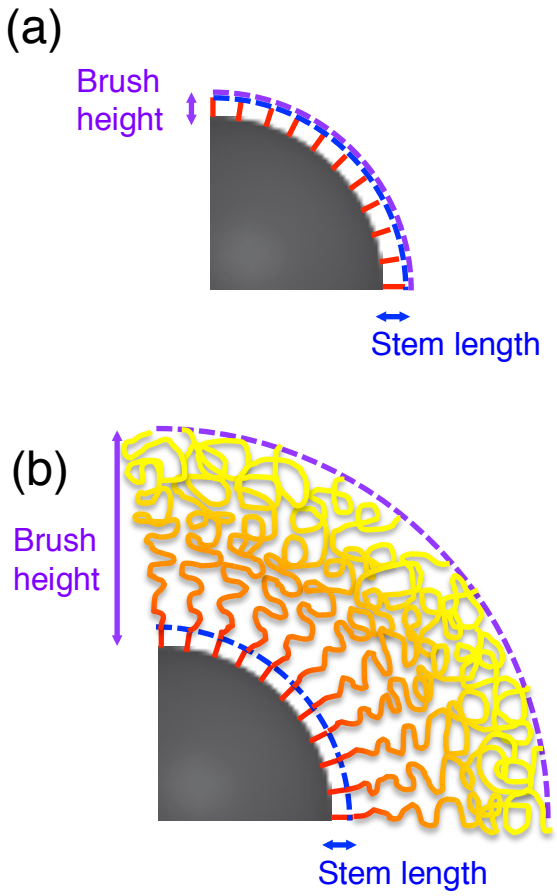

Figure 3.12. Schematic illustration of tethered polymer chain configuration: (a) Low M_w chains; (b) High M_w chains. Stem length (l) is shown with blue dashed line and entire polymer brush height is presented with purple dashed line. The degree of restriction being imposed on chains is expressed by the intensity of the colored lines (red indicating the most confined).

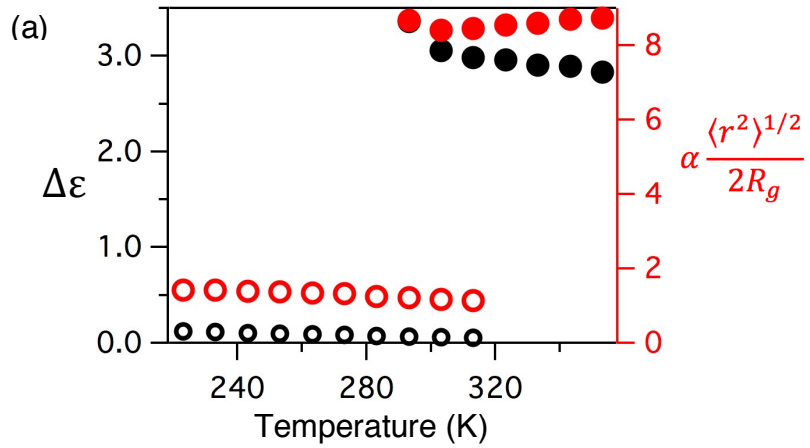
(a)
3.0
2.0
1.0
0.0
Δε
240
280
320
Temperature (K)
8
6
4
2
0
$\alpha \frac{\langle r^2 \rangle^{1/2}}{2R_g}$

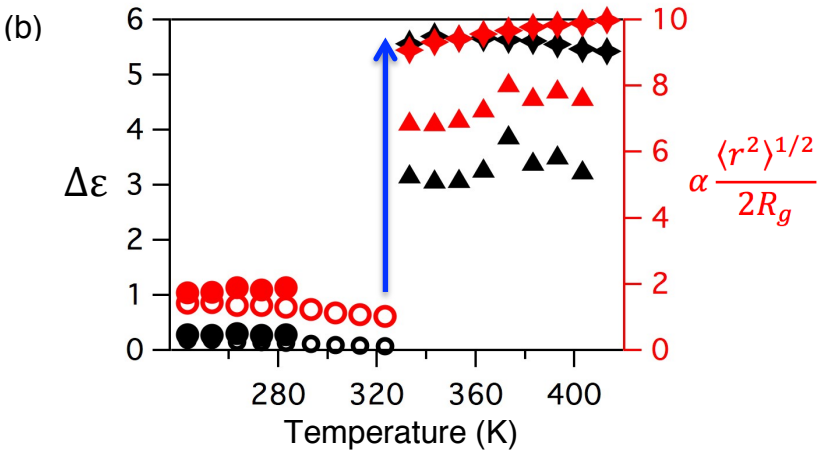
(b)
6
5
4
3
2
1
0
Δε
280
320
360
400
Temperature (K)
10
8
6
4
2
0
$\alpha \frac{\langle r^2 \rangle^{1/2}}{2R_g}$

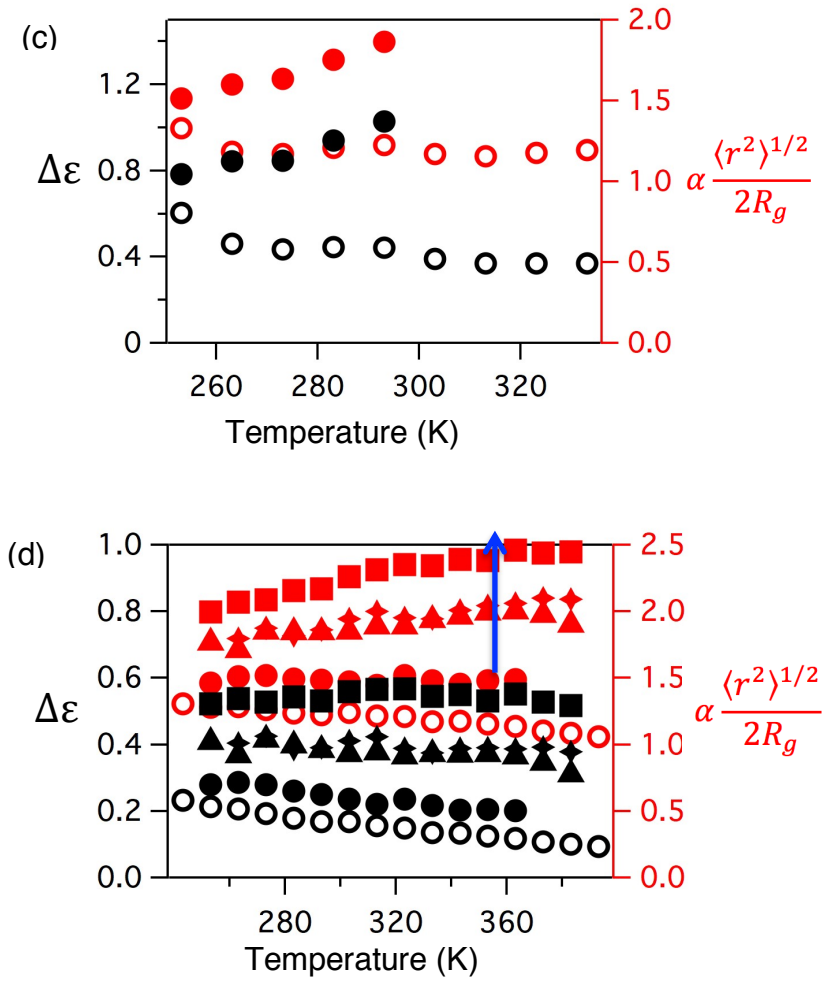

Figure 3.13. Dielectric strength or dielectric intensity, Δε, and characteristic dimensionless length of silica nanoparticle-tethered PI chains with molecular weights of: (a) 3.2K; (b) 7.2K; (c) 13K; and (d) 25.1K with various grafting densities. Black color for Δε (left axis) and red color for characteristic length (right axis) are used. Open circle (o) indicates untethered and closed circle (•) presents densely tethered chains. Arrow direction signifies the decreasing order of grafting density for 7.2K and 25.1K. The grafting densities of 7.2K and 25.1K are summarized in Table 3.1.

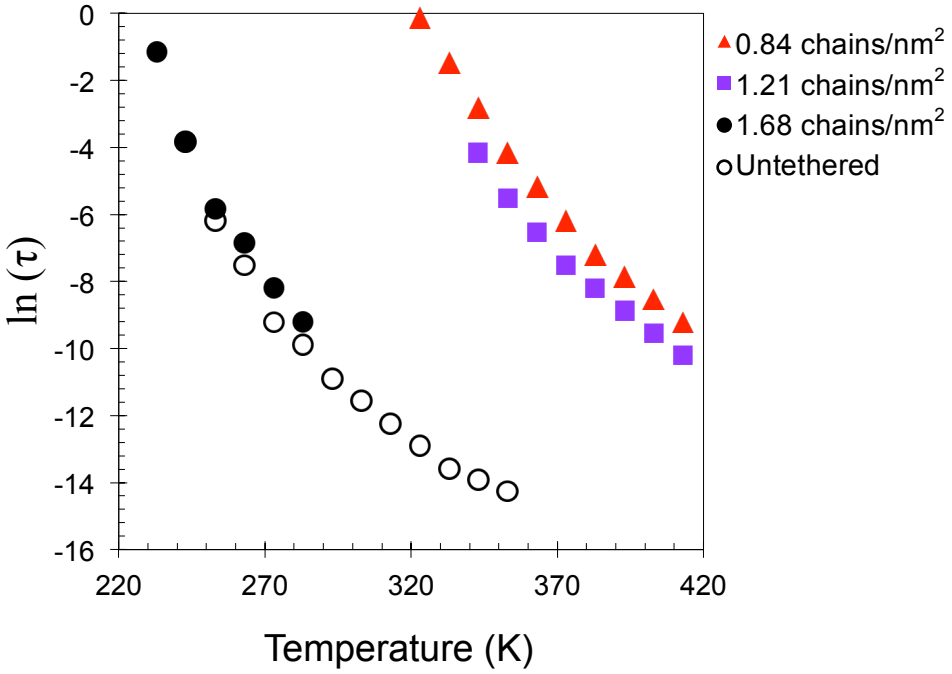

Figure 3.14. Relaxation time of untethered and nanoparticle-tethered PI 7.2K Da at the different grafting densities as a function of temperature.

Table 3.2. Particle distances of silica nanoparticle tethered PI 7.2K Da with different grafting densities (Σ). Interparticle distance (λ) is the distance between the centers of nanoparticles, and the surface-to-surface distance is calculated by subtracting the nanoparticle diameter 10nm from λ.

Σ Grafting density (chains/nm^2)	λ Interparticle distance (nm)	Surface-to-surface distance (nm)
1.68	24.7	14.7
1.21	22.3	12.3
0.84	19.9	9.9

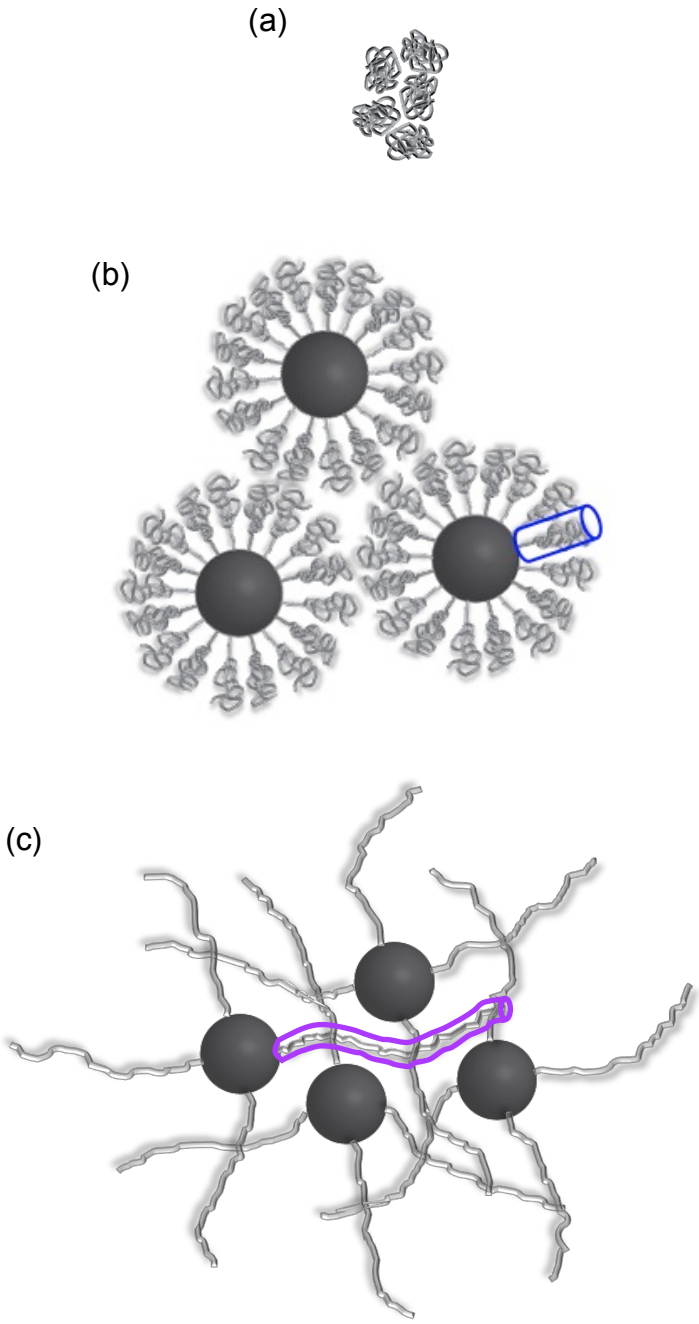

Figure 3.15. Schematic illustrations of: (a) Conformation of free polymer; (b) Proposed relaxation mechanism for densely tethered chains; and (c) Proposed relaxation mechanism for sparsely tethered polymers.

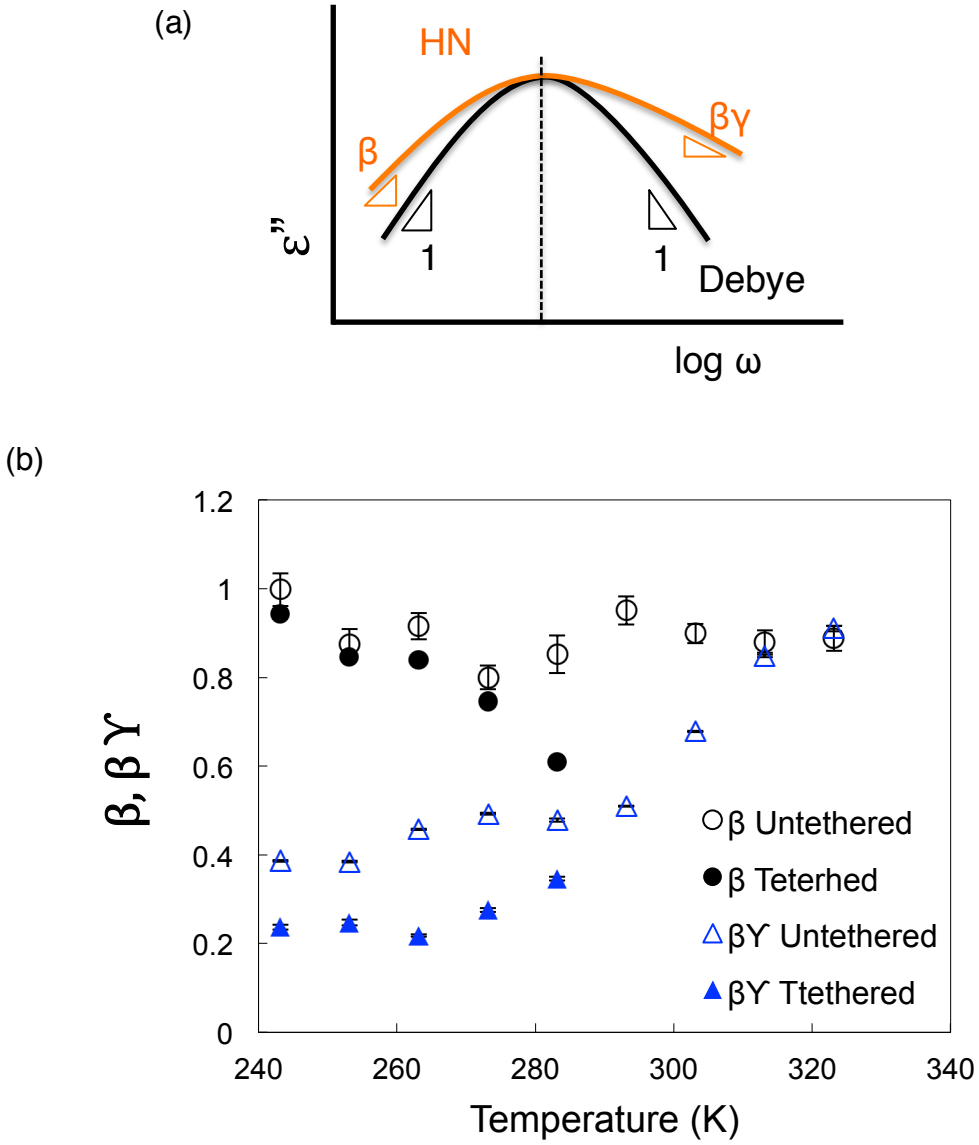

Figure 3.16. (a) Havriliak-Negami fitting parameter β for symmetric broadening and γ for asymmetric broadening above the peak frequency of the dielectric loss spectra. (b) β and βγ values of untethered PI 7.2K Da and tethered PI 7.2K Da with grafting density of 1.68 chains/nm^2.

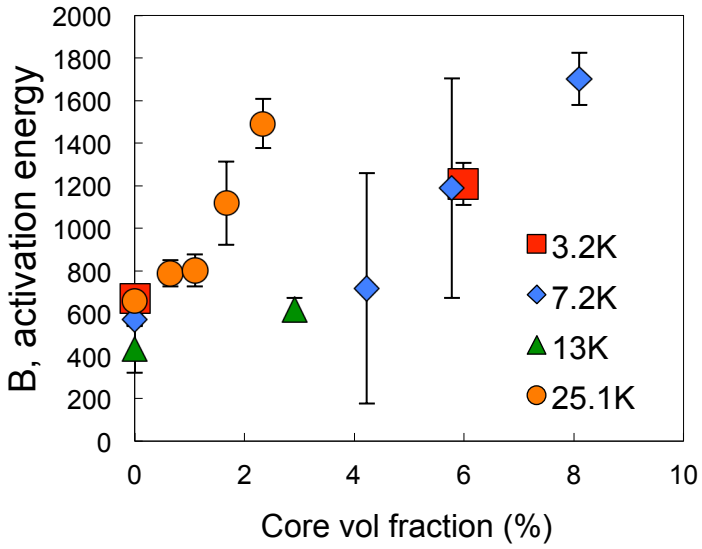

Figure 3.17. Activation energy, derived from fitting relaxation time versus temperature with VFT equation, for untethered and tethered polymer chains versus core volume fraction, or grafting density.

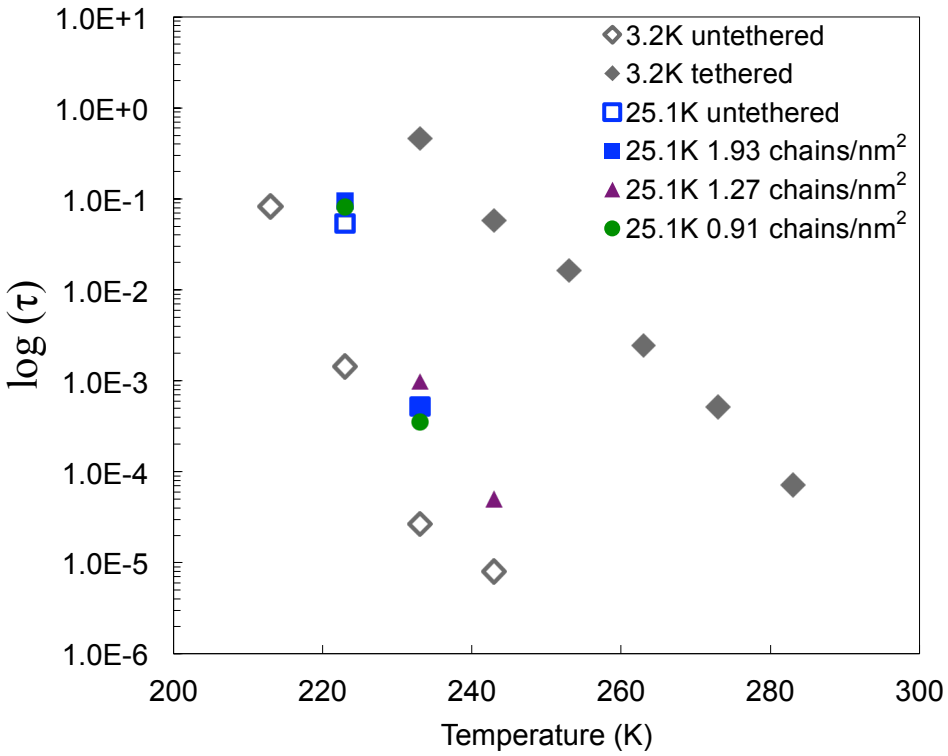

Figure 3.18. Segmental mode relaxation time of untethered and tethered PI Mw 3,200 and 25,100 g/mol. Segmental mode relaxation time of different grafting densities of 25.1K is shown.

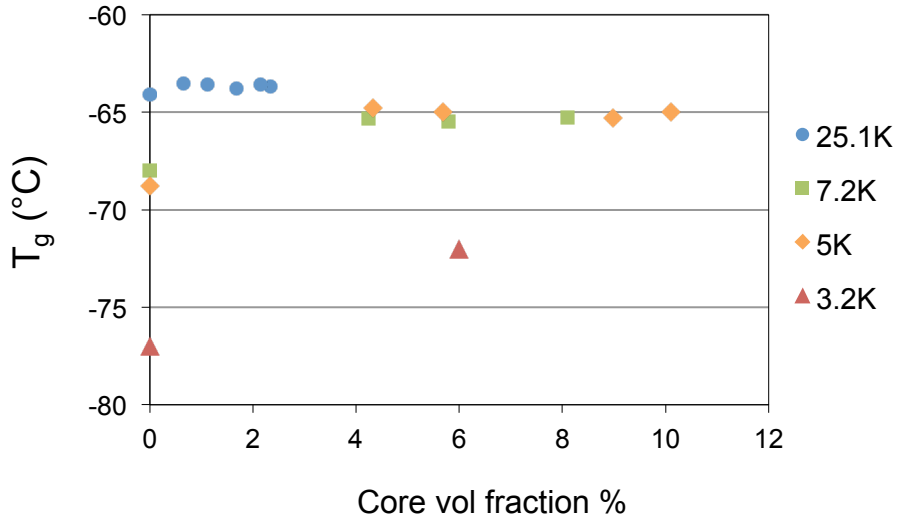

Figure 3.19. Glass transition temperature of untethered and tethered PI chains of different molecular weights vs. silica nanoparticle core volume fraction. Points at core volume fraction of 0 are glass transition temperature of untethered PI. As grafting density decreases the core volume fraction increases.

APPENDIX: Supporting Information for Chapter 3

(a)

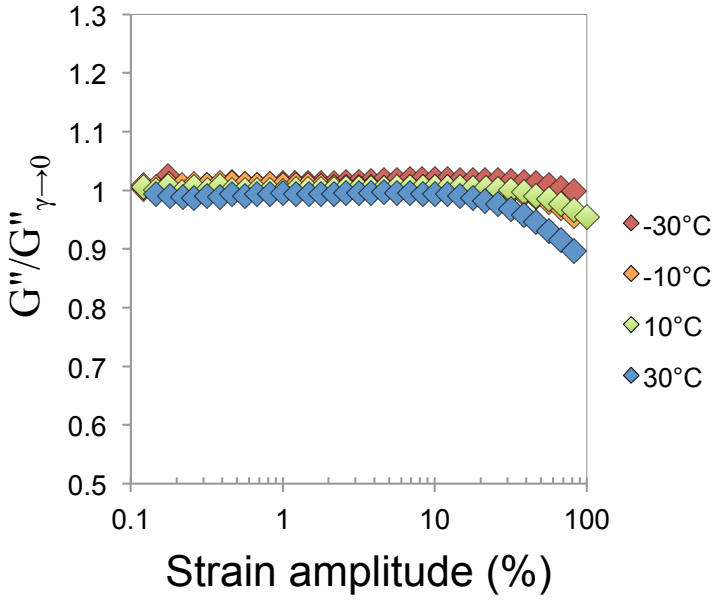

(b)

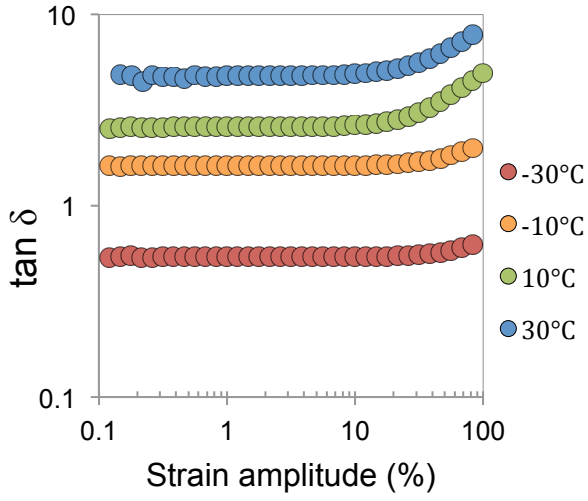

(b)

(c)

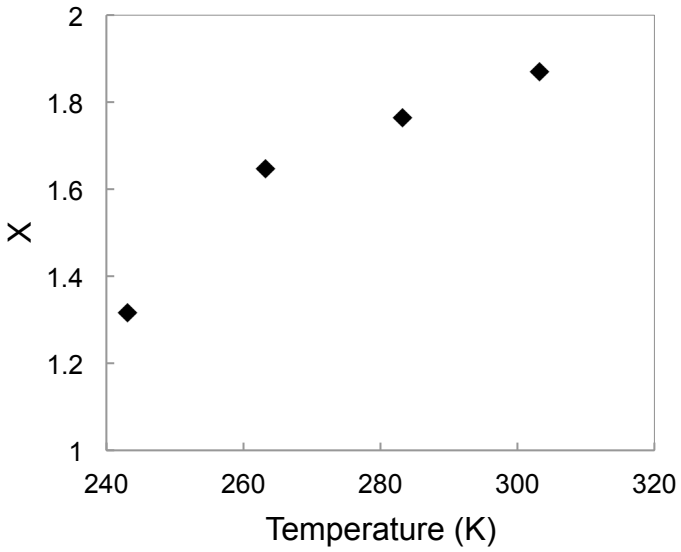

Figure S1. (a) Normalized loss maximum vs. strain amplitude [%]; (b) tan δ vs. strain amplitude [%]; and (c) Noise temperature (X) vs. temperature [K] for SiO_2 - PI of M_w 25.1K Da with grafting density of 1.91 chains/nm^2. Strain sweep measurements were performed at a fixed oscillatory frequency of 10 rad/s at different temperatures.

(a)

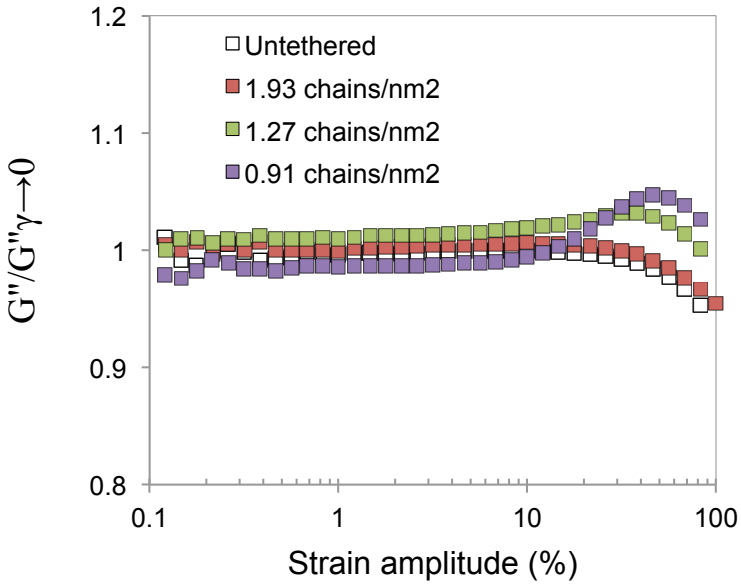
1.2
1.1
1
0.9
0.8
G''/G''γ→0
Untethered
1.93 chains/nm2
1.27 chains/nm2
0.91 chains/nm2
0.1
1
10
100
Strain amplitude (%)

(b)

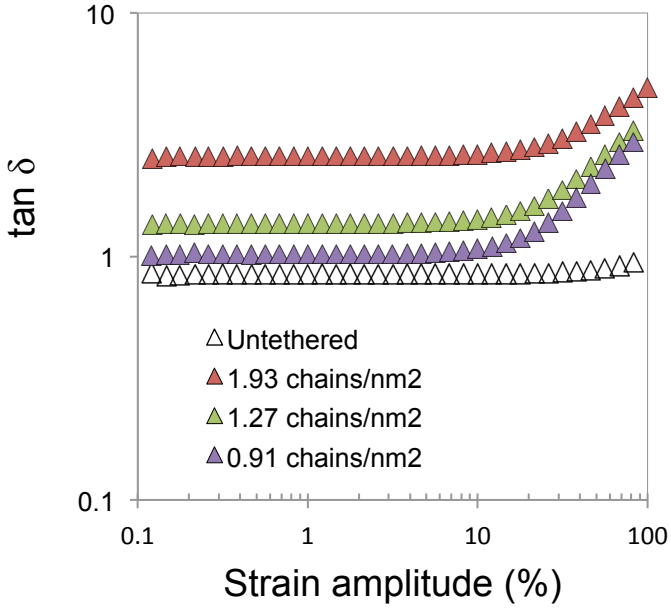
10
1
0.1
tan δ
Untethered
1.93 chains/nm2
1.27 chains/nm2
0.91 chains/nm2
0.1
1
10
100
Strain amplitude (%)

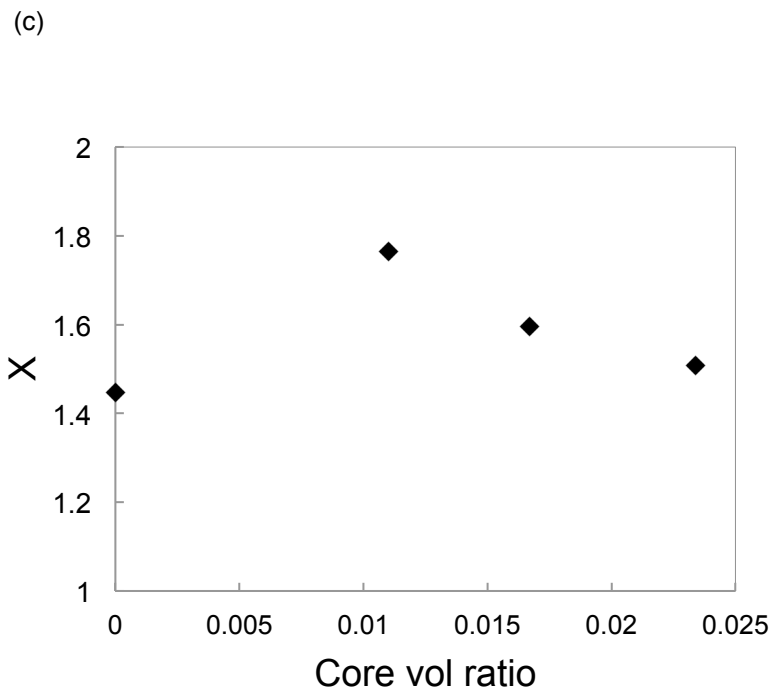

Figure S2. (a) Normalized loss maximum vs. strain amplitude [%]; (b) tan δ vs. strain amplitude [%]; and (c) Noise temperature (X) vs. temperature [K] for SiO_2 - PI of M_w 25.1K Da with different grafting densities. Strain sweep measurements were performed at a fixed oscillatory frequency of 10 rad/s at 30 °C.

(a)

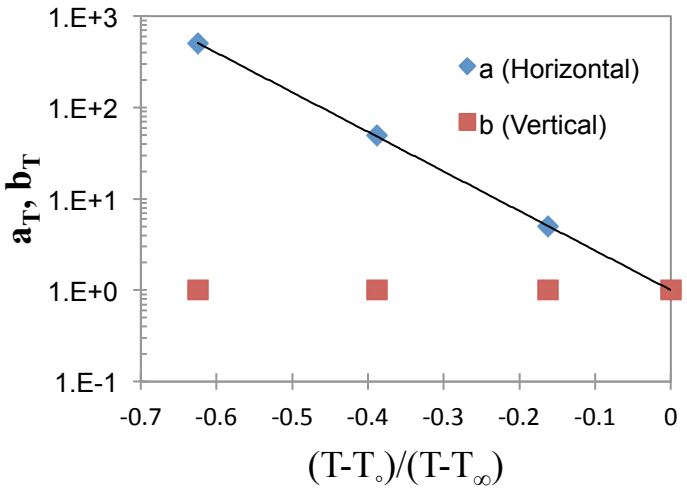

(b)

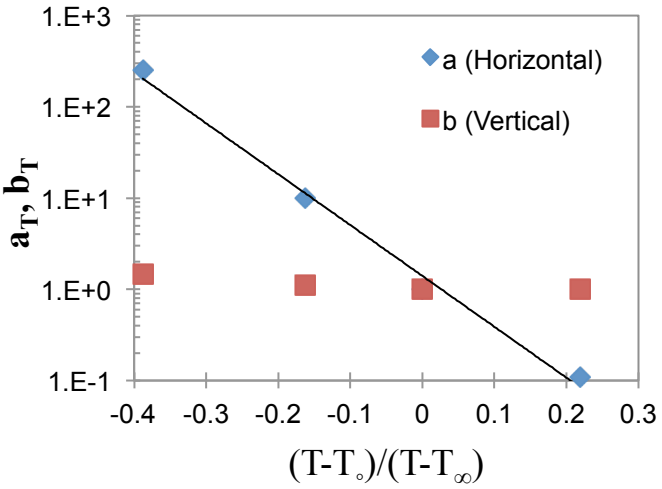

Figure S3. Shift factor for Time Temperature Superposition of (a) untethered and (b) nanoparticle tethered 7.2K PI chains with 1.68 chains/nm^2.

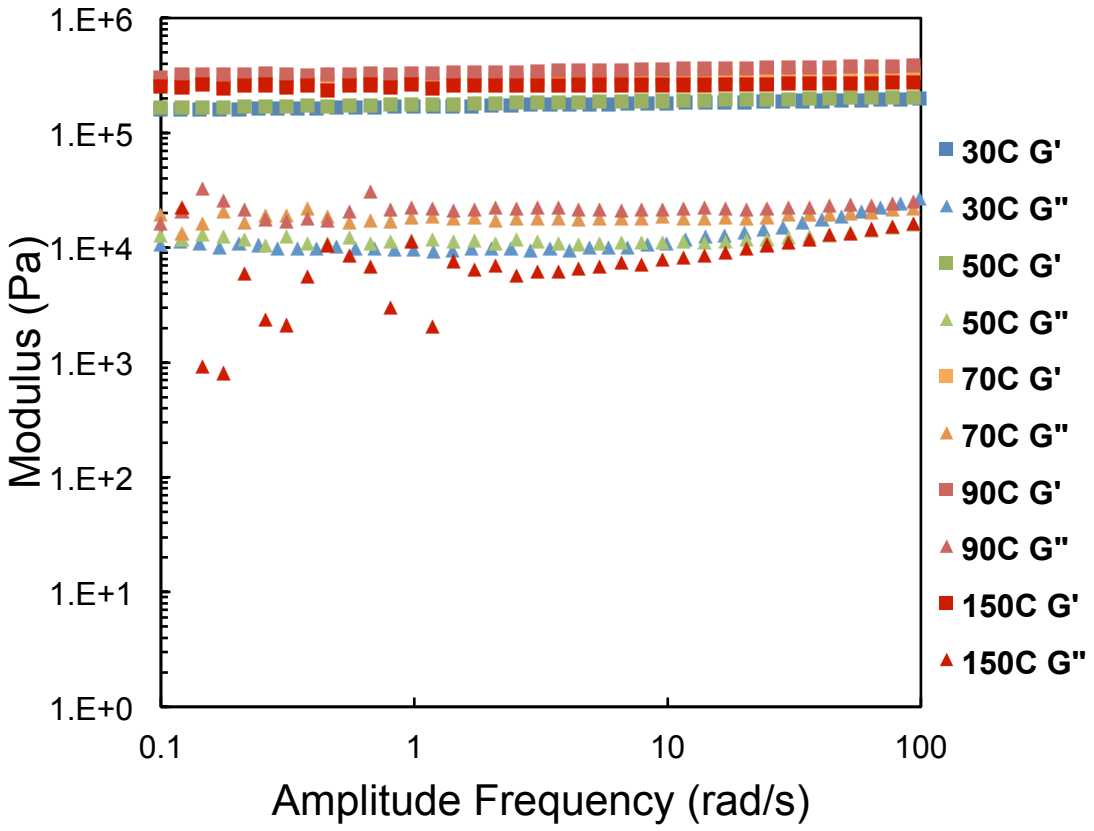

Figure S4. Amplitude sweep rheology results of 0.84 chains/nm^2 grafting density of nanoparticle tethered 7.2K PI chains at each temperature.

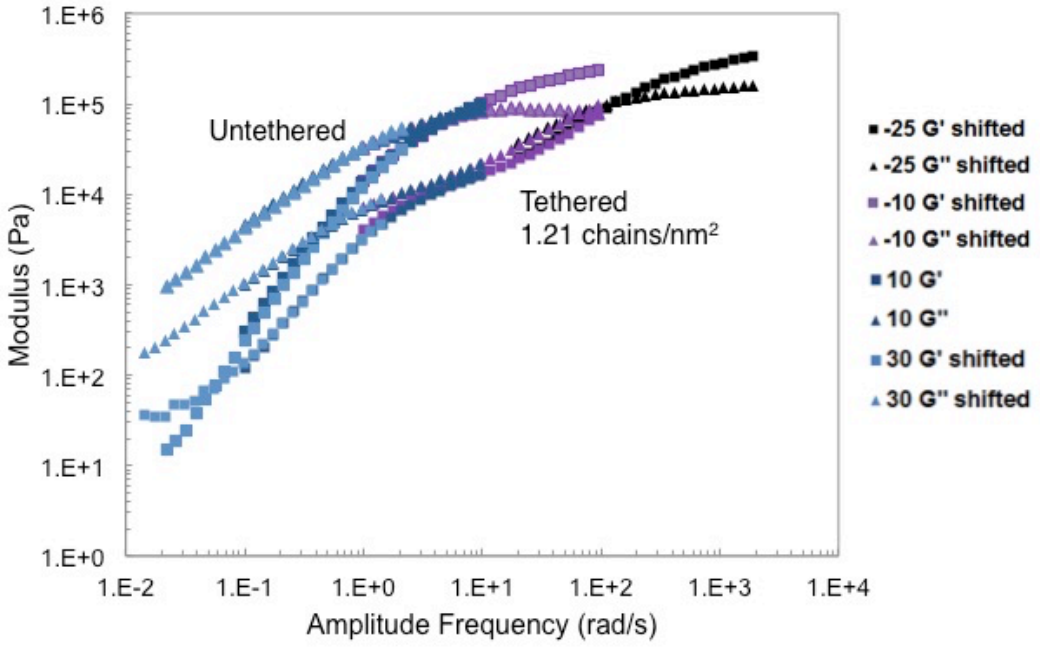

Figure S5. Time Temperature Superposition (TTS) for untethered PI 25.1K Da and nanoparticle-tethered PI chains of molecular weight 25.1K Da with grafting density of 1.21 chains/nm^2. 10 °C moduli data were used as reference.

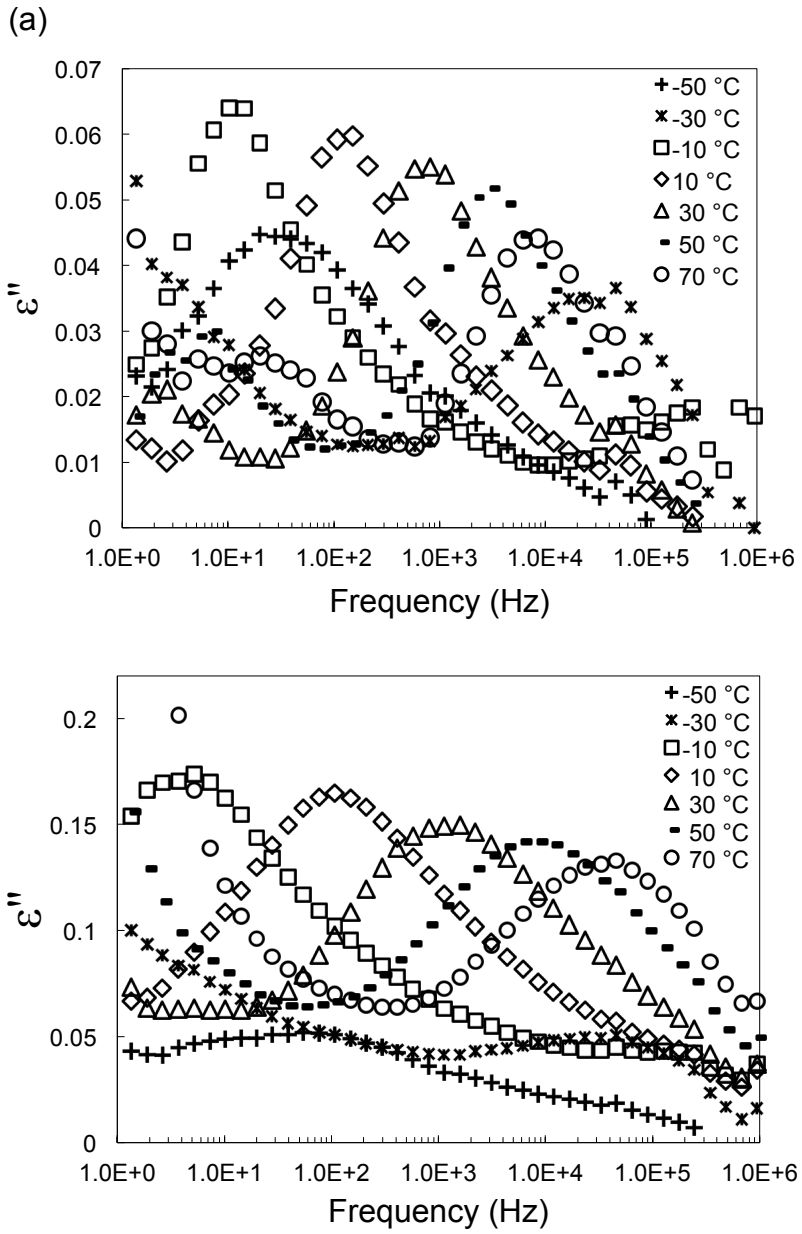

Figure S6. (a) Dielectric loss (ε") vs. frequency [Hz] for untethered PI M_W 25,100 g/mol at different temperatures. (b) Dielectric loss (ε") vs. frequency [Hz] for nanoparticle-tethered PI M_W 25.1K Da at different temperatures.

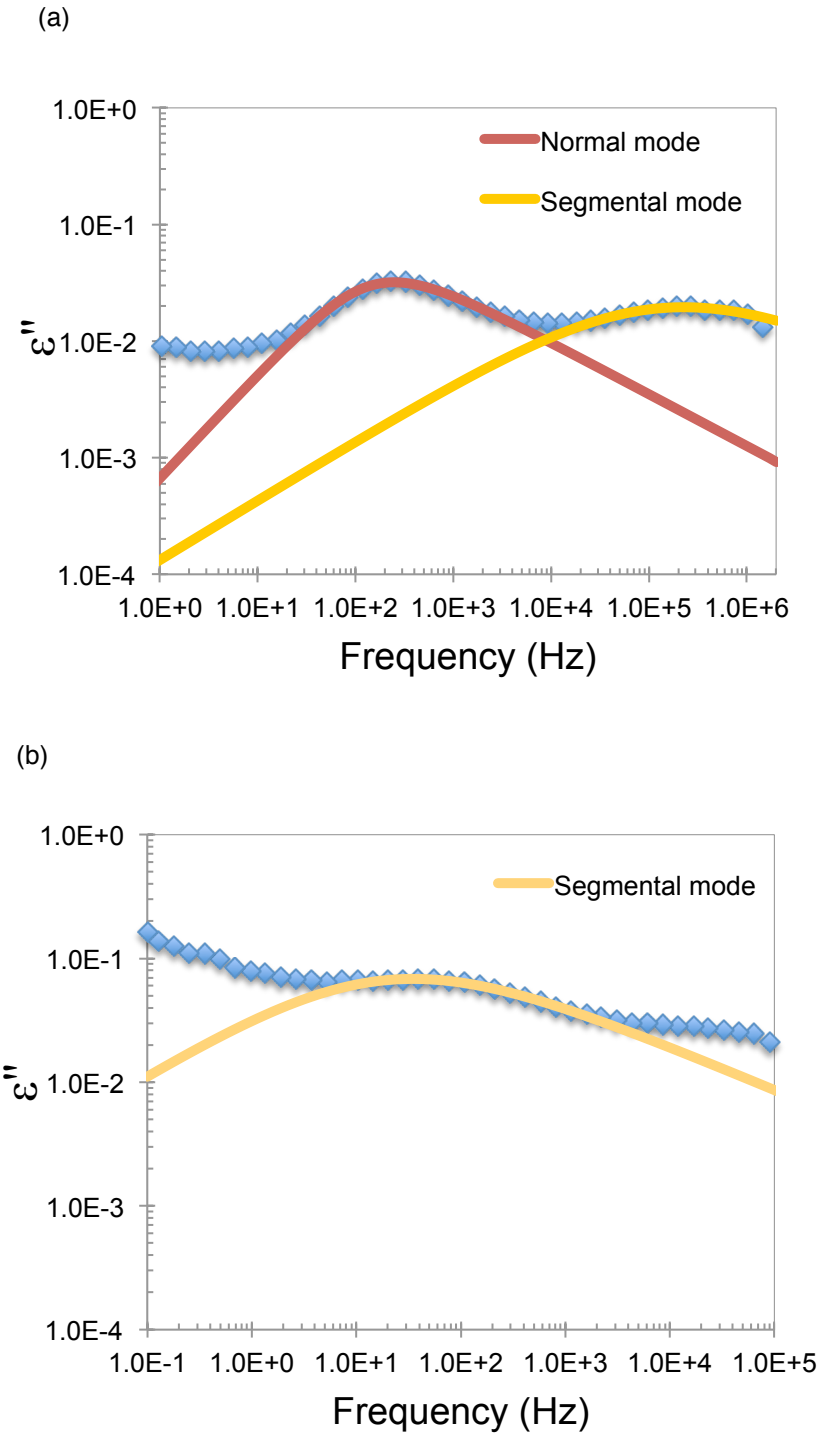

Figure S7. H-N fitting with (a) Dielectric loss spectra of untethered polyisoprene 3.2K Da at -30°C (b) Dielectric loss spectra of tethered polyisoprene 3.2K Da at -30°C.

(a)

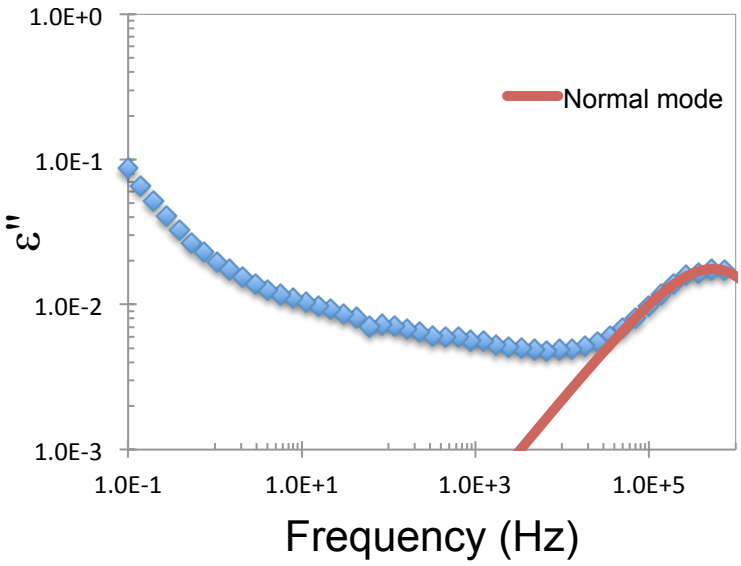

(b)

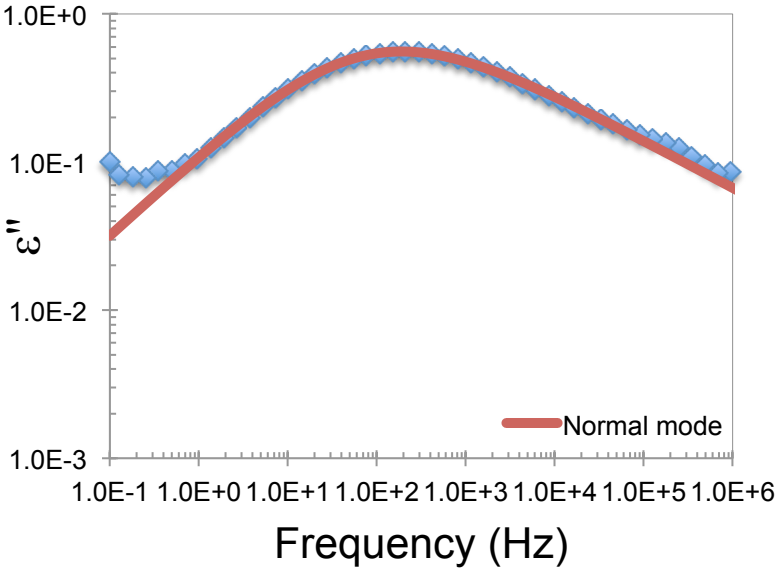

Figure S8. H-N fitting with (a) Dielectric loss spectra of untethered polyisoprene 3.2K Da at 50°C (b) Dielectric loss spectra of tethered polyisoprene 3.2K Da at 50°C .

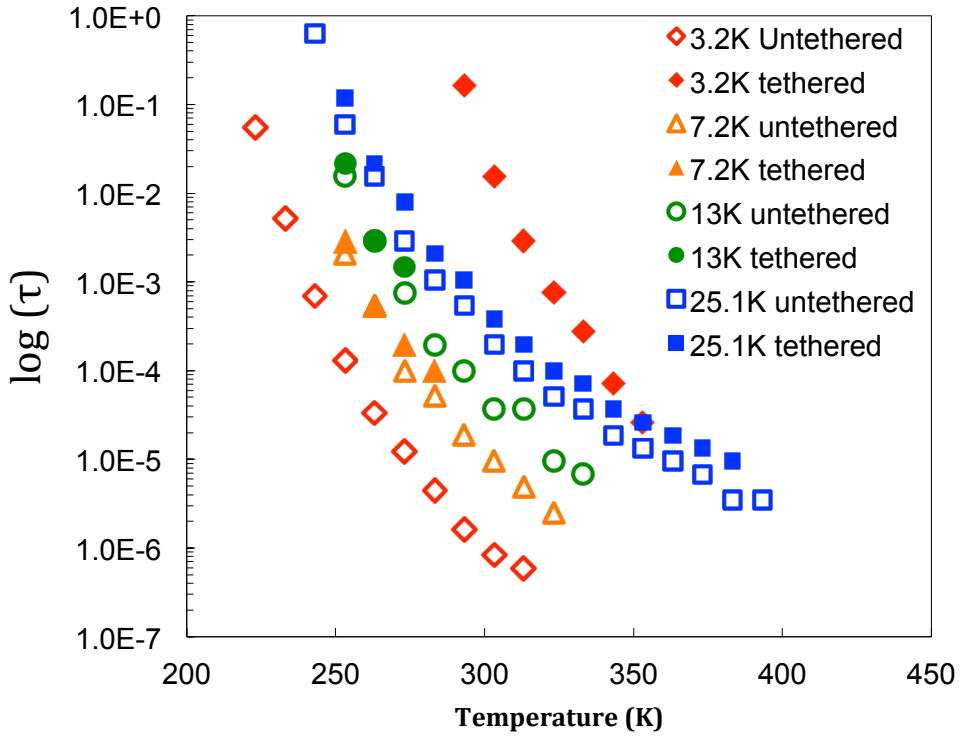

Figure S9. Relaxation time of untethered and nanoparticle-tethered polyisoprene of different molecular weights as a function of temperature calculated from the peak frequency of raw dielectric loss spectra.

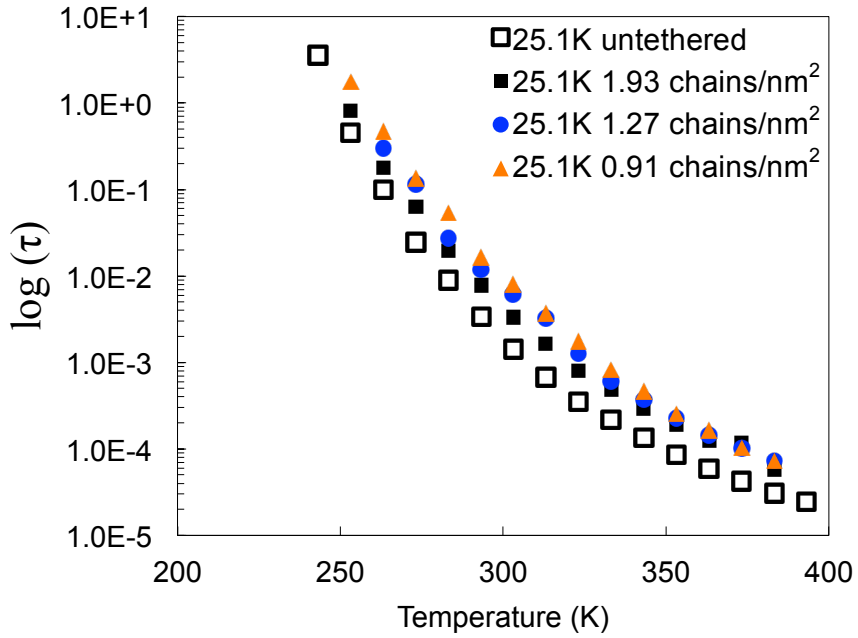

Figure S10. Normal mode relaxation time of untethered and tethered PI 25.1K Da with different grafting density as a function of temperature.

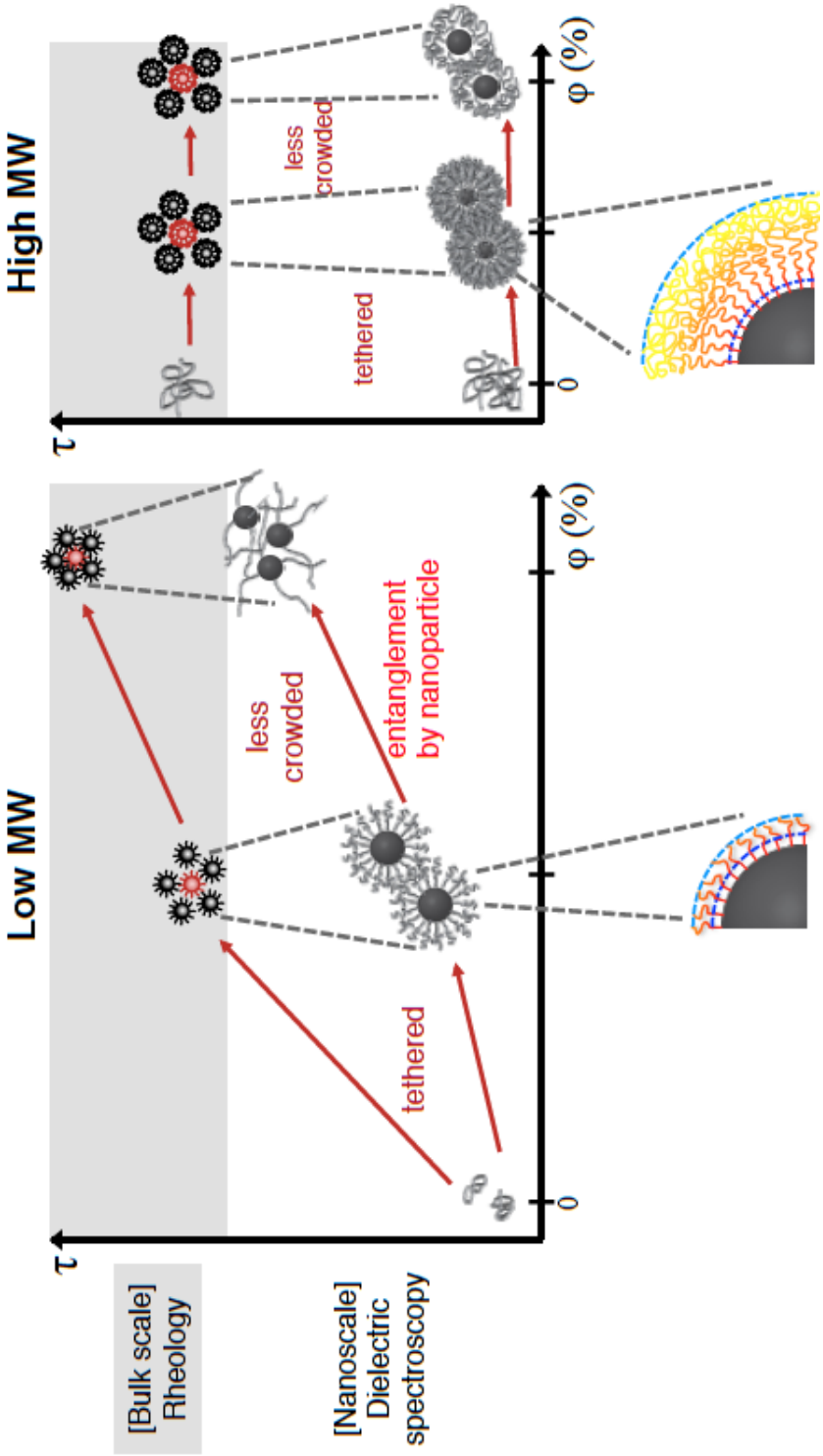

Figure S11. Summary of Chapter 3

CHAPTER 4

CONCLUSION ON THE STRUCTURE, DYNAMICS, AND PROPERTIES OF NANOPARTICLE-TETHERED POLYMERS

The results from Chapter 2 and Chapter 3 apparently look contradictory each other because poly(ethylene glycol) (PEG) chains tend to have more 3D helix crystal unit cell structures, or more coiled conformation, as they are tethered and the grafting density decreases, while polyisoprene (PI) chains are more stretched, or more extended, after tethering and with lower grafting density.

Chapter 2 discusses the solid structures of nanoparticle-tethered polymer chains, how they crystallize around the spherical nanoparticles. As the temperature is lowered, semicrystalline materials crystallize and chains have to find a way to be packed well. PEG is purposely chosen because it is very crystalline polymer and also exhibits dramatic changes in bulk thermal transition after tethering to nanoparticles. The techniques to investigate the static structure of polymer chains are adopted such as FT-IR, XRD, and DSC. Since most materials like to reduce their volume during the liquid to solid transition except water, polymer chains are more coiled, or have more of 3 dimensional helix unit cell structures, to be well packed by tethering and being more sparsely tethered. 3D helix crystal unit cell structure is shorter and is denser than 2D trans zigzag unit cell structure.

Chapter 3 reports the dynamics of amorphous polymers using rheology and dielectric spectroscopy. Amorphous polymers don't crystallize but rather go through glass transition where materials change from glassy state to rubbery state.[1] PI is used for this study because it is a type A dielectric polymer.[2] Nanoparticle-tethered PI chains are perturbed by applying shear with rheometer and by applying voltage with dielectric spectrometer, and their linear responses to those external perturbation are

recorded. It is shown that polymer chains are more jammed and more stretched after tethering and with lowering grafting density. These observations are opposite to those in Chapter 2, because the results in Chapter 3 are chain dynamics responding to disturbances whereas those in Chapter 2 are the equilibrated static structure.

It should be clearly pointed out that PI could not have some TTG/TTT conformations and 3D helix/2D planar zigzag crystal unit cells due to the stiffness of double bond and CH_3 side group perpendicular to the backbone.

In addition, nanoparticle-tethered PEG could not provide global chain relaxation dynamics because PEG is not type A dielectric polymer. However, nanoparticle-tethered PEG could be sheared and it has been formerly reported that nanoparticle-tethered PEG is soft glass[3] and exhibits thermal jamming behaviors.[4]

In conclusion, Chapter 2 is about the packing in solid state and on the other hand, Chapter 3 is about the space filling in soft glass of nanoparticle-tethered polymers.

REFERENCES

1. Gedde, U. W. Polymer Physics; Kluwer Academic Publishers: Norwell, MA, 2001.

2. Stockmayer, W. H. *Pure Appl. Chem.* **1967**, *15*, 539-554.

3. Agarwal, P.; Qi, H.; Archer, L. A. *Nano Lett.* **2010**, *10*, 111−115.

4. Agarwal, P.; Srivastava, S.; Archer, L. A. *Phys. Rev. Lett.* **2011**, *107*, 268302.